

1. Report No. FHWA/TX-82/21+255-1F		2. Government Accession No.		3. Recipient's Catalog No.	
4. Title and Subtitle THE INFLUENCE OF A STEEL CASING ON THE AXIAL CAPACITY OF A DRILLED SHAFT				5. Report Date July 1982	
7. Author(s) Mark J. Owens and Lymon C. Reese				6. Performing Organization Code	
9. Performing Organization Name and Address Center for Transportation Research The University of Texas at Austin Austin, Texas 78712-1075				8. Performing Organization Report No. Research Report 255-1F	
12. Sponsoring Agency Name and Address Texas State Department of Highways and Public Transportation; Transportation Planning Division P. O. Box 5051 Austin, Texas 78763				10. Work Unit No.	
				11. Contract or Grant No. Research Study 3-5-80-255	
13. Type of Report and Period Covered Final				14. Sponsoring Agency Code	
				15. Supplementary Notes Study conducted in cooperation with the U. S. Department of Transportation, Federal Highway Administration. Research Study Title: "The Influence of Steel Casing on the Load Carrying Capacity of Drilled Shafts"	
16. Abstract A series of field load tests were performed to investigate the effects on the axial capacity of drilled shafts when casings could not be pulled. The tests show that leaving casing in place is detrimental, but grouting proved an effective remedial measure when the casing was placed in an oversized excavation. Even though grouting was found to improve the capacity of a shaft where casing was left in place, procedures should be used in the field that will insure that casing will be removed. Shafts cast in the normal manner perform better than do shafts where casing has been grouted. Useful data were obtained on the distribution of axial load from drilled shafts to the supporting soil.					
17. Key Words drilled shaft, axial capacity, steel casing, load test, grouting, vibrating hammer, over-sized excavation			18. Distribution Statement No restrictions. This document is available to the public through the National Technical Information Service, Springfield, Virginia 22161.		
19. Security Classif. (of this report) Unclassified		20. Security Classif. (of this page) Unclassified		21. No. of Pages 228	22. Price

THE INFLUENCE OF A STEEL CASING ON THE AXIAL CAPACITY
OF A DRILLED SHAFT

by

Mark J. Owens
Lymon C. Reese

Research Report Number 255-1F

The Influence of Steel Casing on the Load Carrying
Capacity of a Drilled Shaft

Research Study 3-5-80-255

conducted for

Texas

State Department of Highways and Public Transportation

in cooperation with the
U. S. Department of Transportation
Federal Highway Administration

by

CENTER FOR TRANSPORTATION RESEARCH

THE UNIVERSITY OF TEXAS AT AUSTIN

July 1982

The contents of this report reflect the views of the authors, who are responsible for the facts and the accuracy of the data presented herein. The contents do not necessarily reflect the official views or policies of the Federal Highway Administration. This report does not constitute a standard, specification, or regulation.

There was no invention or discovery conceived or first actually reduced to practice in the course of or under this contract, including any art, method, process, machine, manufacture, design or composition of matter, or any new and useful improvement thereof, or any variety of plant which is or may be patentable under the patent laws of the United States of America or any foreign country.

PREFACE

This report presents the results of field studies of the behavior of drilled shafts under axial load with special reference to the case where casing could not be pulled.

The authors wish to thank the State Department of Highways and Public Transportation for their sponsorship of the work and to express appreciation for the assistance given by many members of their staff. Partial sponsorship of the System of The University of Texas of the tests at Site 1 in Galveston is acknowledged and appreciation is expressed to the staff of Facilities Planning and Construction for their interest and assistance. Appreciation is also expressed to Walter P. Moore and Associates, Inc.; Louis Lloyd Oliver, Architect; and McBride-Ratliff and Associates for their interest and assistance in the Galveston project.

Appreciation is expressed to Farmer Foundation Company who made a financial contribution to the work in Galveston and carried out the construction work in a careful and expeditious manner.

Mark J. Owens

Lymon C. Reese

July 1982

ABSTRACT

A series of field load tests were performed to investigate the effects on the axial capacity of drilled shafts when casings could not be pulled. The tests show that leaving casing in place is detrimental, but grouting proved an effective remedial measure when the casing was placed in an oversized excavation. Even though grouting was found to improve the capacity of a shaft where casing was left in place, procedures should be used in the field that will insure that casing will be removed. Shafts cast in the normal manner perform better than do shafts where casing has been grouted. Useful data were obtained on the distribution of axial load from drilled shafts to the supporting soil.

SUMMARY

The studies reported herein were concerned with evaluating the effects on the axial capacity of drilled shafts when casing could not be pulled and had to be left in place. Two cases were investigated, when casing was placed in an over-sized excavation and when the casing was driven with a vibratory hammer. In both instances, it was learned that the failure to extract the casing had a detrimental effect on the load-carrying capacity of the drilled shaft.

Grouting was found to be an effective method of restoring the capacity of two drilled shafts in this test program when the casing was placed in an over-sized excavation. Even though grouting was found to improve the capacity of a shaft where casing was left in place, procedures should be used in the field that will insure that casing will be removed. Shafts cast in the normal manner perform better than do shafts where casing has been grouted.

A method was suggested for verifying the integrity of drilled shafts when such a remedial measure is employed. Data were obtained and evaluated on the distribution of axial load in skin friction and end bearing. The results from the analysis of these data will prove useful to designers.

IMPLEMENTATION STATEMENT

The information presented in this report is recommended for consideration by the Bridge Division of the State Department of Highways and Public Transportation. The results of the research on the behavior of drilled shafts when casing is left in place provides positive information to allow the engineering staff of SDHPT to take appropriate action when the occasion arises. Data that were acquired on the behavior of instrumented drilled shafts under axial load will provide additional information related to procedures for design. This new information, along with similar data acquired in the past, will provide useful guidance to the designer.

Even though grouting was found to improve the capacity of a shaft where casing was left in place, procedures should be used in the field that will insure that casing will be removed. Shafts cast in the normal manner perform better than do shafts where casing has been grouted.

TABLE OF CONTENTS

	Page
PREFACE	iii
ABSTRACT	v
SUMMARY	vii
IMPLEMENTATION STATEMENT	ix
CHAPTER 1. INTRODUCTION	1
CHAPTER 2. SITE CONDITIONS	7
Site 1 - Galveston, Texas	7
Site Location	7
Soil Profile	7
Site 2 - Galveston, Texas	15
Site Location	15
Soil Profile	15
Site 3 - Eastern Site	19
Site Location	19
Soil Profile	19
CHAPTER 3. INSTRUMENTATION	23
Measurement of Axial Load at the Top of the Shaft	23
Measurement of Movements at the Top of the Shaft	26
Measurement of Loads at Selected Locations within the Shaft	26
Testing of Mustran Cells	33
Readout System	36
CHAPTER 4. SHAFT INSTALLATION AND CONSTRUCTION PROCEDURES	39
Test Site 1 - Galveston, Texas	39
Test Shafts	39
Grouting of Test Shafts	44
Reaction Shafts	45
Test Site 2 - Galveston, Texas	47
Test Shaft	47
Reaction Shafts	48

	Page
Test Site 3 - Eastern Site	48
Test Shafts	48
Reaction Shafts	51
 CHAPTER 5. LOAD TESTS	 53
Test Procedure	53
Test Site 1 - Galveston, Texas	54
Test Arrangement	54
Test Results	54
Test Shaft G-1	54
Test Shaft G-2	56
Test Shaft G-3	58
Test Site 2 - Galveston, Texas	60
Test Arrangement	60
Test Results	60
Test Site 3 - Eastern Site	64
Test Arrangement	64
Test Results	64
Test Shaft E-1	64
Test Shaft E-2	67
 CHAPTER 6. ANALYSIS AND DISCUSSION OF LOAD TESTS	 71
Method of Analysis	71
Mustran Cell Behavior	71
Calibration of Mustran Cells	71
Load Distribution Curves	73
Tip Load	73
Side Resistance	75
Shaft Movement	76
Analysis of Load Tests	78
Test Shaft G-1	78
Test Shaft G-3, Test 1	82
Test Shaft G-3, Test 2	82
Test Shaft G-4	82
Test Shaft E-1	90
Test Shaft E-2	90

	Page
Discussion of Load Tests	97
Tip Resistance in Clay	97
Tip Resistance in Sand	102
Side Resistance in Sand	104
Side Resistance in Clay	114
Influence of Construction Methods	119
 CHAPTER 7. SUGGESTIONS CONCERNING MODIFICATIONS OF CONSTRUCTION SPECIFICATIONS	129
 CHAPTER 8. CONCLUSIONS AND RECOMMENDATIONS	133
Conclusions	133
Recommendations	134
APPENDIX A. LOGS OF BORINGS	139
APPENDIX B. PREPARATION AND INSTALLATION OF MUSTRAN CELLS	169
APPENDIX C. TYPES OF INTERNAL INSTRUMENTATION FOR USE IN DRILLED SHAFTS FOR MEASUREMENT OF AXIAL LOAD AS A FUNCTION OF DEPTH	195
APPENDIX D. CONSTRUCTION SITUATIONS WHERE CASING WOULD BE DIFFICULT TO REMOVE	201
REFERENCES	203

LIST OF TABLES

Table		Page
6.1	Tabulation of theoretical values of bearing capacity in sand	103
6.2	Tabulation of theoretical values for skin friction of drilled shafts in sand	105
6.3	Tabulation of theoretical values for skin friction of drilled shafts in sand	109
6.4	Comparison of measured and theoretical values of K and x for test site 1	112
6.5	Comparison of measured and theoretical values of K and x for test site 3	113
6.6	Comparison of measured and theoretical values of α	118
6.7	Tabulation of theoretical values for skin friction of driven piles in sand	124

LIST OF FIGURES

Figure		Page
1.1	Casing method of construction	2
1.1	(Cont'd) Casing method of construction	3
2.1	Location of test site 1 and test site 2	8
2.2	Test site 1, soil boring locations	9
2.3	Soil profile, test site 1	10
2.4	Penetration resistance as a function of depth for test site 1	13
2.5	Undrained shear strength as a function of depth test site 1	14
2.6	Soil boring locations, test site 2	16
2.7	Soil profile, test site 2	17
2.8	Penetration resistance and undrained shear strength as a function of depth, test site 2	18
2.9	Soil profile, test site 3	20
2.10	Penetration resistance as a function of depth, test site 3	21
3.1	Schematic of loading system arrangement	24
3.2	Photographs of instrumentation at top of shaft	25
3.3	Components of mustran cell	28
3.4	Schematic arrangement of mustran cell pressurization system	29
3.5	Photographs of installed mustran cells	31
3.6	Relative positions of soil layers and mustran cells	32
3.7	Terminal strips and connectors in manifold	34

Figure		Page
3.8	Mustran cell in triaxial type set up	35
3.9	Collapsed radiator hose on mustran cell	35
3.10	Vishay automatic data logging system	37
3.11	Portable strain indicator and switch and balance units .	37
4.1	Method of construction of test shaft G-2 at test site 1	41
4.1	Method of construction of test shaft G-2 at test site 1	42
4.2	Elevation of test shafts at test site 1, Galveston . . .	46
5.1	Testing arrangement, test site 1	55
5.2	Load settlement curve, test shaft G-1	57
5.3	Load settlement curves, test shaft G-2	59
5.4	Load settlement curves, test shaft G-3	61
5.5	Testing arrangement, test site 2	62
5.6	Load settlement curve, test shaft G-3	63
5.7	Testing arrangement, test site 4	65
5.8	Load settlement curve, test site E-1	66
5.9	Load settlement curve, test shaft E-2	69
5.10	Load uplift curves for reaction shafts, test site E-2	70
6.1	Variation of concrete strength as a function of depth .	74
6.2	Load distribution curves, test shaft G-1	79
6.3	Load transfer in skin friction versus movement, test shaft G-1	80

Figure		Page
6.4	Unit end bearing versus tip movement, test shaft G-1	81
6.5	Load distribution curves, test shaft G-3, test 1	83
6.6	Load transfer in skin friction versus movement, test shaft G-3, test 1	84
6.7	Unit end bearing versus tip movement, test shaft G-3, test 1	85
6.8	Load distribution curves, test shaft G-3, test 2	86
6.9	Load transfer in skin friction versus movement, test shaft G-3, test 2	87
6.10	Unit end bearing versus tip movement, test shaft G-3, test 2	88
6.11	Load distribution curves, test shaft G-4	89
6.12	Load transfer in skin friction versus movement, test shaft G-4	91
6.13	Unit end bearing versus tip movement, test shaft G-4	92
6.14	Load distribution curves, test shaft E-1	93
6.15	Load transfer in skin friction versus movement, test shaft E-1	94
6.16	Unit end bearing versus tip movement, test shaft E-1	95
6.17	Load distribution curves, test shaft E-2	96
6.18	Load transfer in skin friction versus movement test shaft E-2	98
6.19	Unit end bearing versus tip movement, test shaft E-2	99

Figure		Page
6.20	Unit end bearing versus tip movement for clay	101
6.21	Theoretical and measured unit skin friction in sand, test site 1	107
6.22	Theoretical and measured unit skin friction in sand	110
6.23	Theoretical and measured unit skin friction in caly, test sites 1 & 2	116
6.24	Load transfer in skin friction versus depth, test shafts G-1 and G-3	120
6.25	Load transfer in skin friction versus depth for test shafts E-1 and E-2	123
6.26	Theoretical and measured load transfer, test shaft E-1	125
6.27	Load transfer versus depth, test shaft G-1 and G-4	127
7.1	Schematic of TNO testing arrangement	131
B.1	Top cap	171
B.2	Bottom cap	172
B.3	Centerpiece	173
B.4	Mounting angles	174
B.5	Cleaned and scribed centerpiece	177
B.6	Alignment of strain gauge	177
B.7	Strain gauge and centerpiece ready for application of M-Bond 600	178
B.8	Application of M-Bond 600 to strain gauge	180

Figure		Page
B.9	Application of M-Bond 600 to centerpiece	180
B.10	Laying of strain gauge	181
B.11	Placement of teflon pads	182
B.12	Clamp and pressure pads	182
B.13a	Strain gauge on back of centerpiece	183
B.13b	Strain gauge and tab on front of centerpiece	183
B.14	Wiring between gauges	184
B.15	Wiring between gauges, front and back of centerpiece shown	186
B.16	M-coat D applied to centerpiece	186
B.17	M-coat applied to centerpiece	188
B.18	Assembled mustran cell	188
B.19	Mounting of mustran cells , ,	190

CHAPTER 1. INTRODUCTION

INTRODUCTION

During the past few decades the use of drilled shafts in foundations has increased greatly. There are two principal reasons for the increased usage: drilled shafts have proved economical on the basis of the cost per ton of sustained load, and acceptable design and construction procedures have been developed. The procedures for the design of drilled shafts permit the use of frictional resistance along the sides of a shaft (skin friction) in determining the total load-carrying capacity of the shaft. Research has shown that skin friction can constitute an important fraction of the load and that the amount of skin friction that can be developed is not only dependent upon the soil conditions but also upon the construction.

The casing method of construction of drilled shafts is a common procedure and is applicable to sites where soil conditions are such that caving or excessive deformation will occur when a hole is excavated. Examples of such sites are clean sand below the water table or a sand layer between layers of cohesive soils. If it is assumed that some dry soil of sufficient stiffness to prevent caving exists near the ground surface, as shown in Fig. 1.1a, the construction procedure can be initiated with the dry method. When the caving soil is encountered, a slurry is introduced to the hole and the excavation proceeds, as shown in Fig. 1.1b. The slurry is frequently manufactured on the job, using sacks of dry bentonite. Depending on the condition

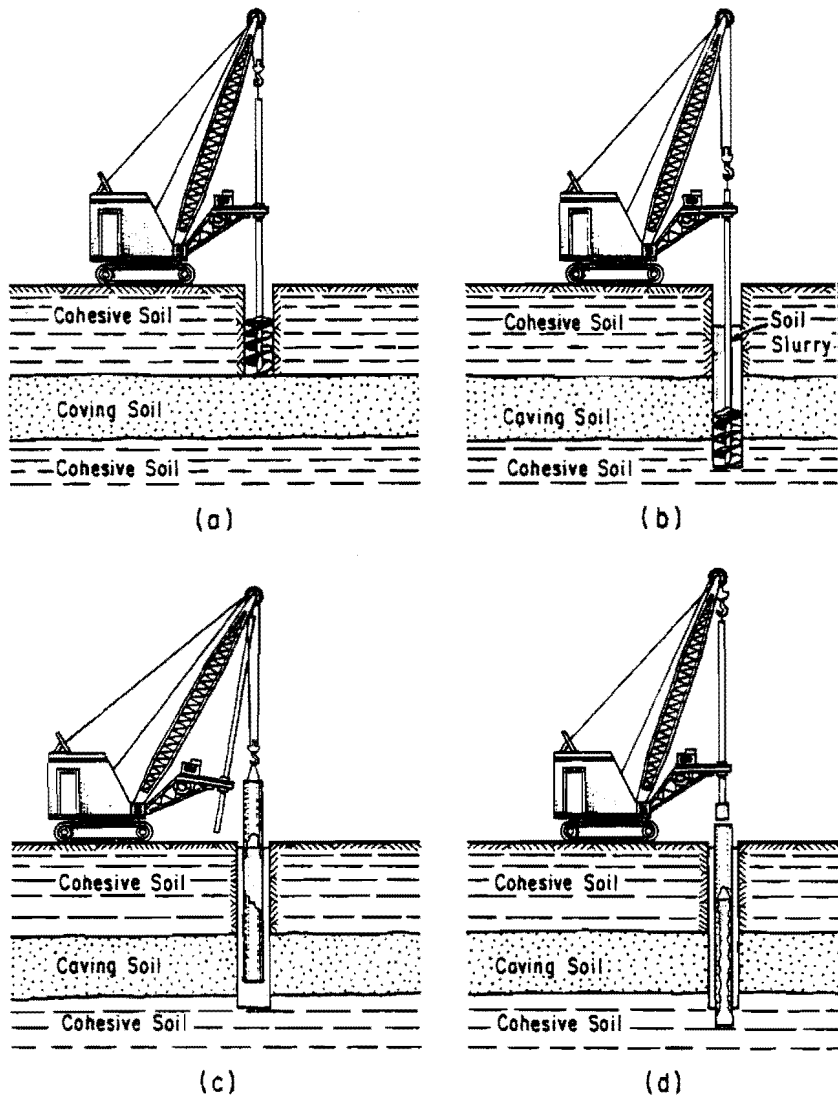


Fig. 1.1 Casing Method of Construction. (a) Initiating drilling; (b) Drilling with slurry; (c) Introducing casing; (d) Casing is sealed and slurry is being removed from interior of casing.

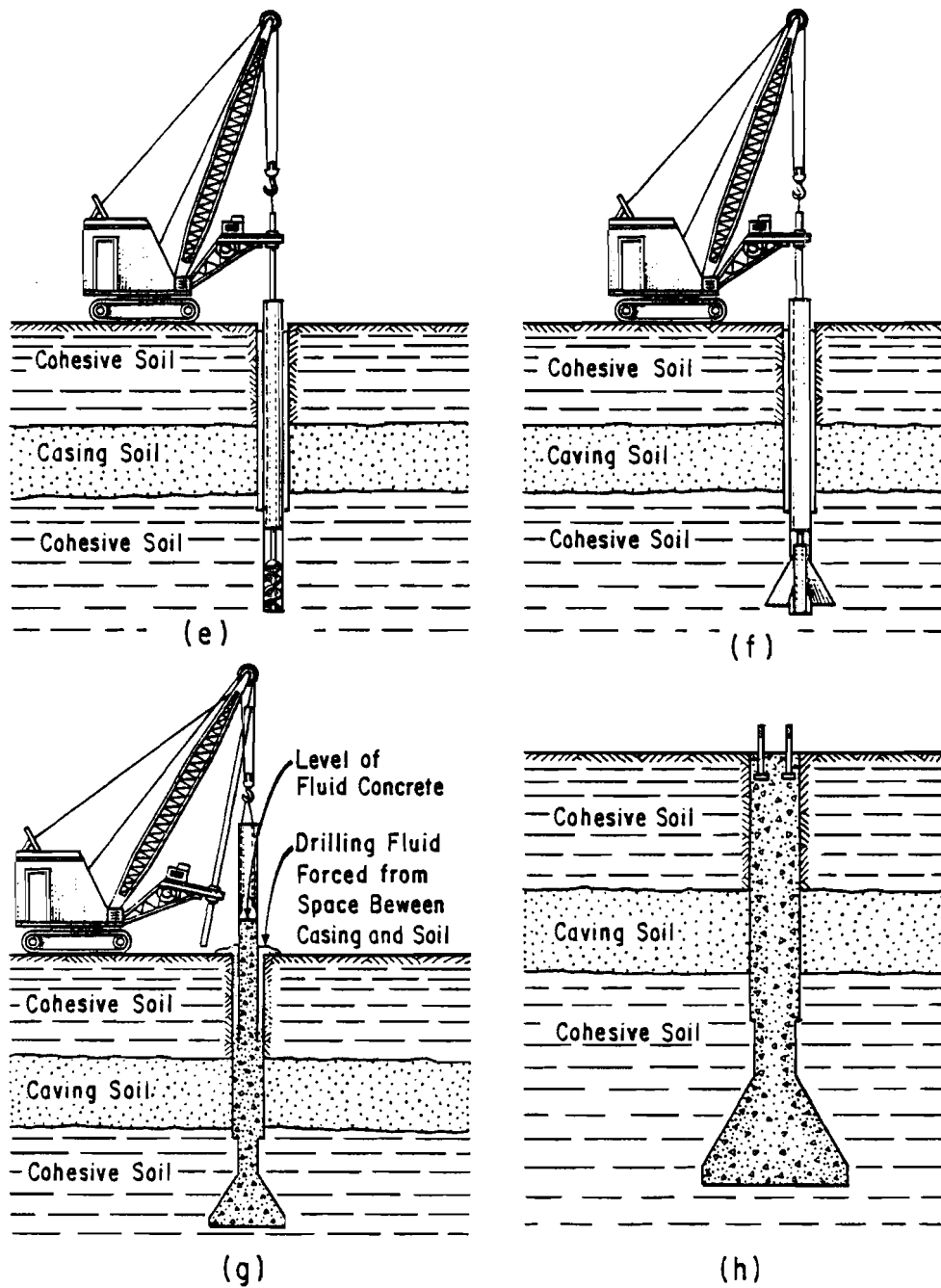


Fig. 1.1 (con'd) Casing Method of Construction. (e) Drilling below casing; (f) Underreaming; (g) Removing casing; (h) Completed shaft.

of surface soil, the elevation of the top of the slurry column may be just above the caving soil, or it may be brought near the ground surface, as shown in Fig. 1.1b.

Drilling is continued until the stratum of caving soil is pierced and a stratum of impermeable soil is encountered. As shown in Fig. 1.1c, a casing is introduced at this point, a "twister" or "spinner" is placed on the kelly of the drill rig, and the casing is rotated and pushed into the impermeable soil a distance sufficient to effect a seal.

A bailing bucket is placed on the kelly and the slurry is bailed from the casing, as shown in Fig. 1.1d. A smaller drill is introduced into the hole, one that will just pass through the casing, and the drilling is carried to the projected depth, as shown in Fig. 1.1e. A bellig tool can be placed on the kelly, as shown in Fig. 1.1f, and the base of the drilled shaft can be enlarged. During this operation, slurry is contained in the annular space between the outside of the casing and the inside of the upper drilled hole. Therefore, it is extremely important that the casing be sealed in the impermeable formation in sufficient amount to prevent the slurry from flowing past the casing. It is sometimes necessary to place teeth on the bottom of the casing in order to be able to twist or core the casing a sufficient depth into the impermeable formation to produce a seal. As may be understood, the casing method cannot be employed if a seal is impossible to obtain, or if there is no impermeable formation into which the lower portion of the hole can be drilled.

If reinforcing steel is to be used with drilled shafts constructed by the casing method, the rebar cage must extend to the full depth of the excavation. After any reinforcing steel has been placed, the hole should be completely

filled with fresh concrete with good flow characteristics (see Fig. 1.1g). Under no circumstances should the seal at the bottom of the casing be broken until the concrete is brought above the level of the external fluid. The casing may be pulled when there is sufficient hydrostatic pressure in the column of concrete to force the slurry that has been trapped behind the casing from the hole (see Fig. 1.1g).

The slurry in the excavation is designed to prevent the collapse of the drilled hole and usually is effective, but on a number of occasions it has been found that the casing is "seized" by the surrounding soil and cannot be recovered. It should be noted that the resistance to pulling the casing comes not only from soil resistance along the sides of the excavation but from the soil resistance at the seal and from the friction between the concrete and the inside of the casing.

In the event the casing cannot be pulled, it is critical that the design and specifications be such that the field engineer has clear and unequivocal directions. He must immediately be able to decide whether or not the drilled shaft, with casing in place, will be adequate. However, because the performance of a drilled shaft where a casing has been left in place is adversely affected, every effort should be made to withdraw a casing. Some additional discussion on this point is presented later in the report.

The objective of this study has been to develop information of the load-carrying capacity of drilled shafts where the casing is left in place and to develop possible solutions to the problem. Information has also been gained on the importance of using concrete of good flow characteristics.

CHAPTER 2. SITE CONDITIONS

Site 1 - Galveston, Texas

Site Location. As mentioned earlier, this research program was conducted to deal with problems that are sometimes encountered when constructing drilled shafts by the casing method. The site for the tests needed to be one where there were relatively homogeneous strata of sand or clay. Fortunately, a site was found where it was possible to obtain information on the behavior of a drilled shaft with the casing in place in sand and in clay. The site was at The University of Texas Galveston Medical Branch, Galveston, Texas. The load tests were performed in conjunction with the construction of the new Physical Plant Building for the Medical Branch. The location of the proposed building and test site is shown in Fig. 2.1.

Soil Profile. The soil profile was determined from three borings, designated as CB-1, CB-2, and SDHPT-1. The location of these borings relative to the proposed structure is shown in Fig. 2.2. Borings CB-1 and CB-2 were performed by McBride-Ratcliff and Associates, Inc., a geotechnical consulting firm located in Houston. Boring SDHPT-1 was sampled and logged by personnel of the State Department of Highways and Public Transportation. The general soil profile is shown in Fig. 2.3, and the boring logs are given in Appendix A.

At borings CB-1 and CB-2 the standard penetration test was performed. The SDHPT cone test was performed at boring SDHPT-1. The standard penetration test is a dynamic penetration test used to obtain the approximate

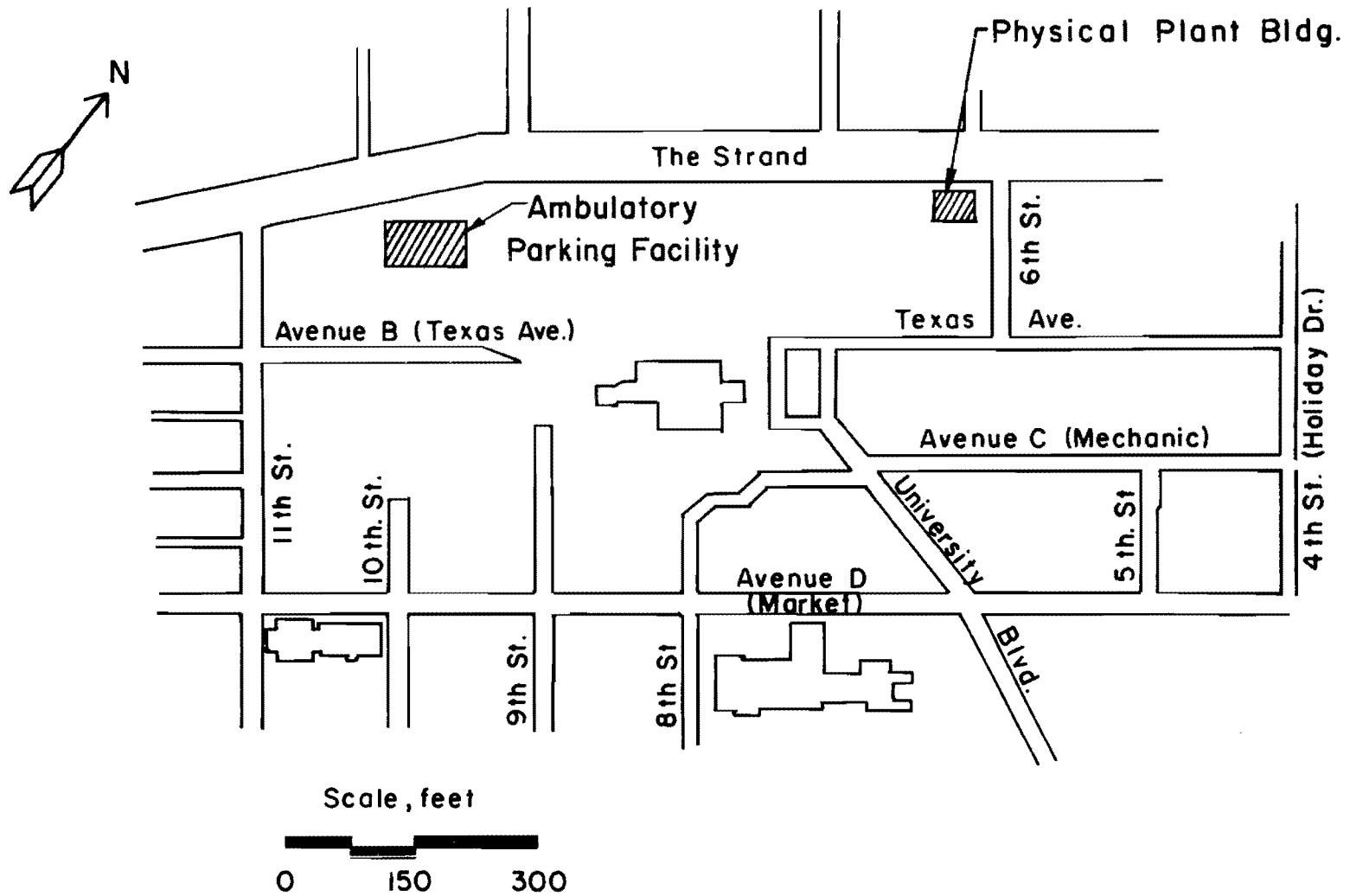


Fig. 2.1 Location of Test Site 1 and Test Site 2

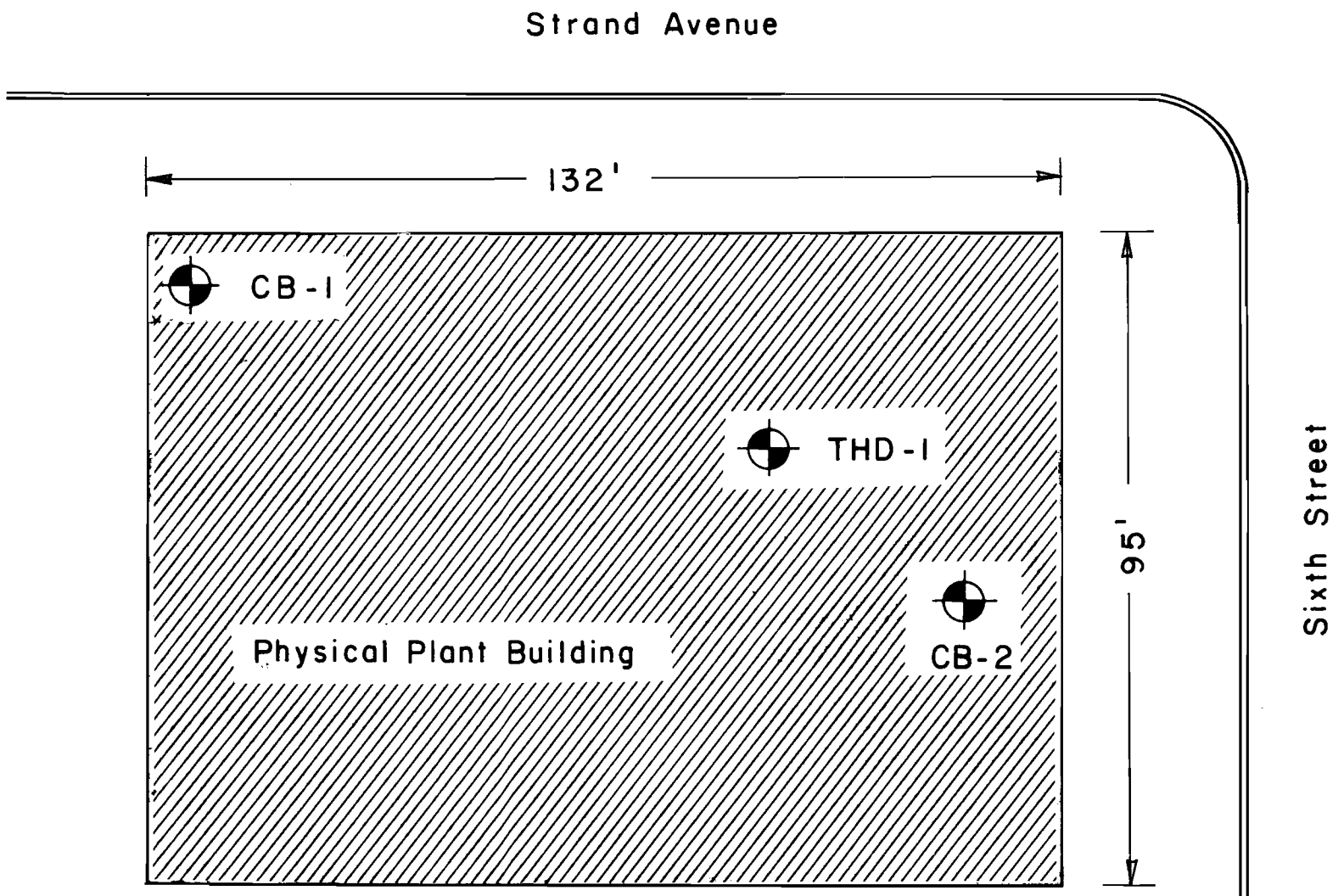


Fig. 2.2 Test Site 1, Soil Boring Locations

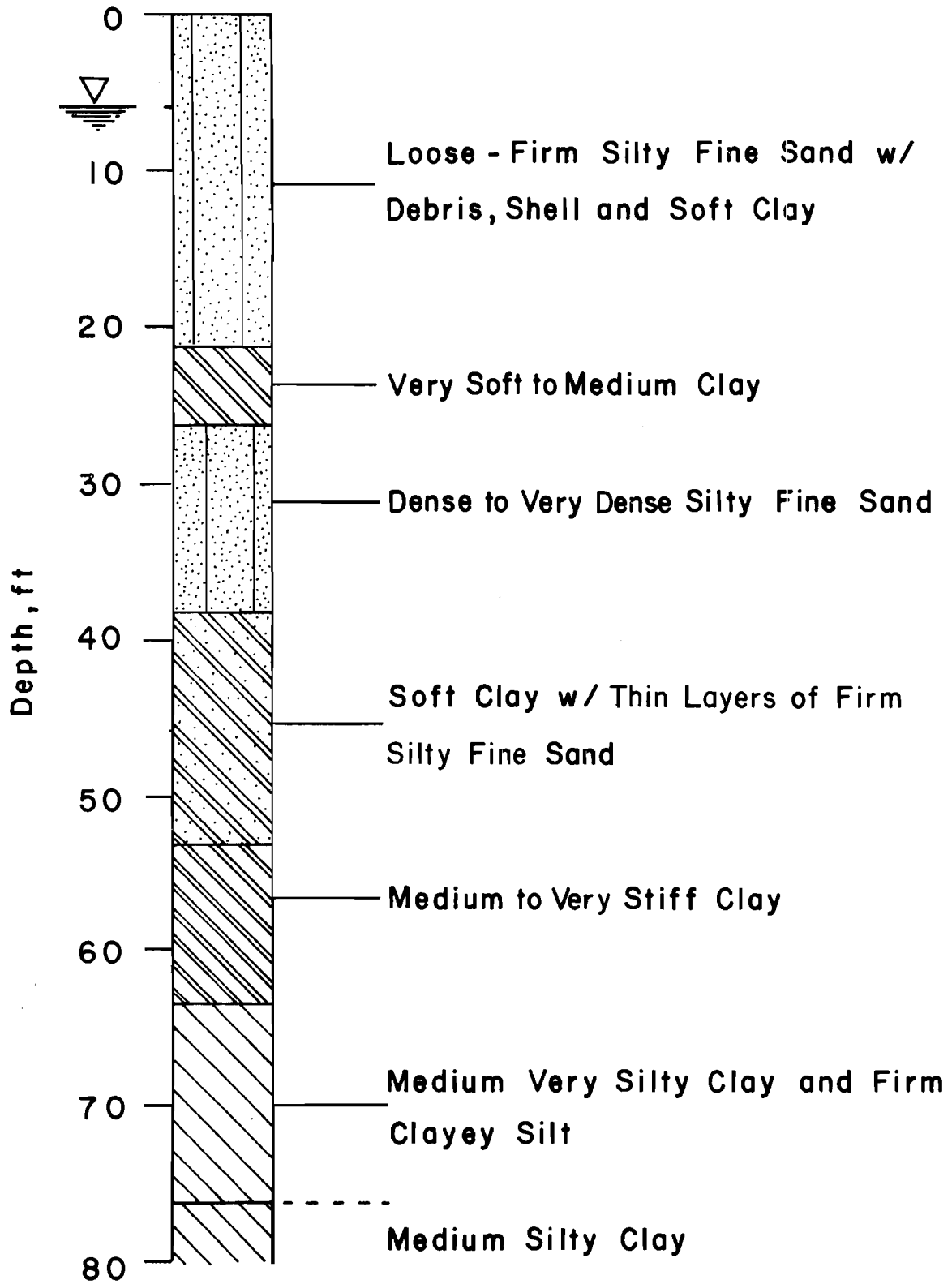


Fig. 2.3 Soil Profile, Test Site 1

in-situ density or consistency of soils. A standard split spoon sampler is driven with a 140-lb hammer that is dropped 30 in. The number of blows needed to drive the sampler 6 in. is recorded for three consecutive 6-in. increments. The blows required to drive the sampler the last two 6-in. increments constitute the N_{SPT} -value.

The SDHPT cone test is also a dynamic penetration test. In this test a "standard" cone is driven by a 170-lb hammer that is dropped 24 in. The number of blows required to drive the cone 6 in. into the soil is recorded for two consecutive 6-in. increments. The total number of blows for the two consecutive 6-in. increments constitute the N_{SDHPT} -value.

Correlations between the standard penetration test and the dynamic SDHPT cone penetrometer tests are given by Touma and Reese (1972) and are as follows.

In clay:

$$N_{SDHPT} \approx 0.7 N_{SPT} \quad (2.1)$$

In sand:

$$N_{SDHPT} \approx 0.5 N_{SPT} \quad (2.2)$$

The variation of N_{SPT} and N_{SDHPT} with depth for the three borings is shown in Fig. 2.4.

Besides performing the standard penetration test, McBride-Ratcliff also performed the pocket penetrometer test and various laboratory tests on the clay. The laboratory tests performed included consolidation tests, Atterberg limits, moisture contents, unconfined compression tests, and unconsolidated-undrained triaxle tests (Q-test).

Consolidation tests showed that the clay from 40 to 48 ft was normally consolidated and the clays below the 53-ft depth were normally consolidated to slightly overconsolidated. Atterberg limits and moisture contents were determined at various depths. The results of the index tests can be found in the boring logs (CB-1 and CB-2 in Appendix A). The results of the tests run to estimate the undrained shear strengths are shown in Fig. 2.5. Included in this figure are values of the undrained shear strength determined from N_{SDHPT} AND N_{SPT} values. Correlations between N_{SDHPT} and N_{SPT} values and undrained shear strength are given by Quiros and Reese (1976) and are as follows.

For homogenous clays (CH):

$$s_u \approx 0.07 N_{SDHPT} \quad (2.3)$$

or

$$s_u \approx 0.10 N_{SPT} \quad (2.4)$$

For silty clays (CL):

$$s_u \approx 0.063 N_{SDHPT} \quad (2.5)$$

and/or

$$s_u \approx 0.09 N_{SPT} \quad (2.6)$$

For sandy clays (CL):

$$s_u \approx 0.053 N_{SDHPT} \quad (2.7)$$

and/or

$$s_u \approx 0.076 N_{SPT} \quad (2.8)$$

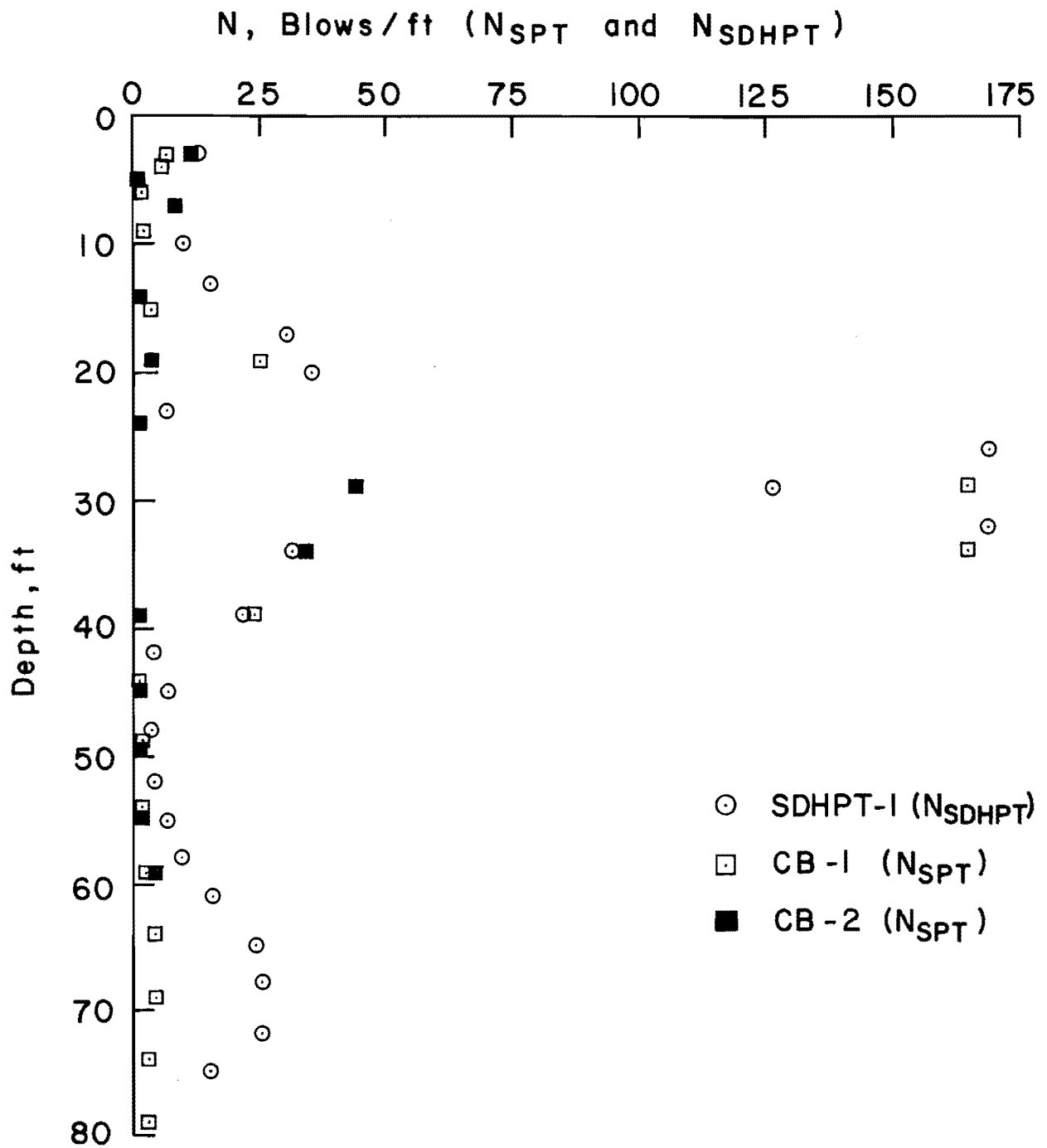


Fig. 2.4 Penetration Resistance as a Function of Depth for Test Site 1

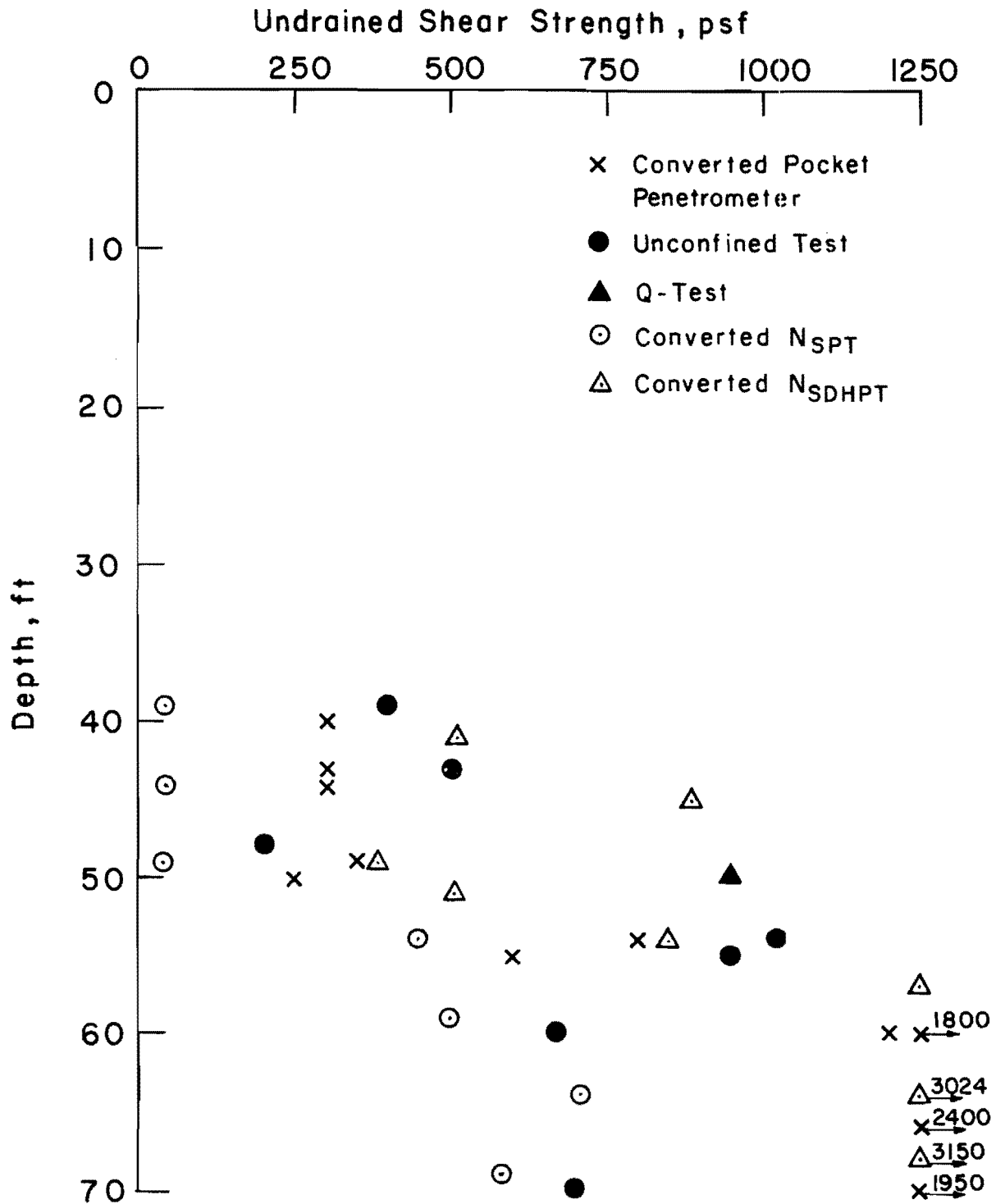


Fig. 2.5 Undrained Shear Strength as a Function of Depth, Test Site 1

These equations give the values of the undrained shear strength in tons per square foot.

Site 2 - Galveston, Texas

Site Location. The test at site 2 was also done at The University of Texas Galveston Medical Branch, Galveston, Texas. This test was done in June of 1978. The load test was performed in conjunction with the construction of a parking facility for the Ambulatory Care Center. The location of the proposed structure and test site is shown in Fig. 2.1.

Soil Profile. The soil profile at site 2 was determined from two borings, designated as B-1 and B-2. The location of these borings relative to the proposed structure is shown in Fig. 2.6. The borings were sampled and logged by personnel of McClelland Engineers, Inc., a geotechnical engineering consulting firm. The general soil profile is shown in Fig. 2.7. The boring logs are given in Appendix A.

At both borings the standard penetration test was done to approximately a depth of 40 ft. Below a depth of 40 ft samples were taken and pocket penetrometer and torvane tests were performed, along with various laboratory tests. Laboratory tests that were performed include Atterberg limits, moisture contents, unconfined compression tests, and unconsolidated-undrained triaxle tests (Q tests). Atterberg limits and moisture contents were determined at various depths and the results can be found in the boring logs in Appendix A. The results of the tests run to estimate the undrained shear strength are shown in Fig. 2.8, along with the variation of N_{SPT} with depth. It should be noted that the N_{SPT} values were not converted to undrained shear strength because the standard penetration test was run only in the sand layers.

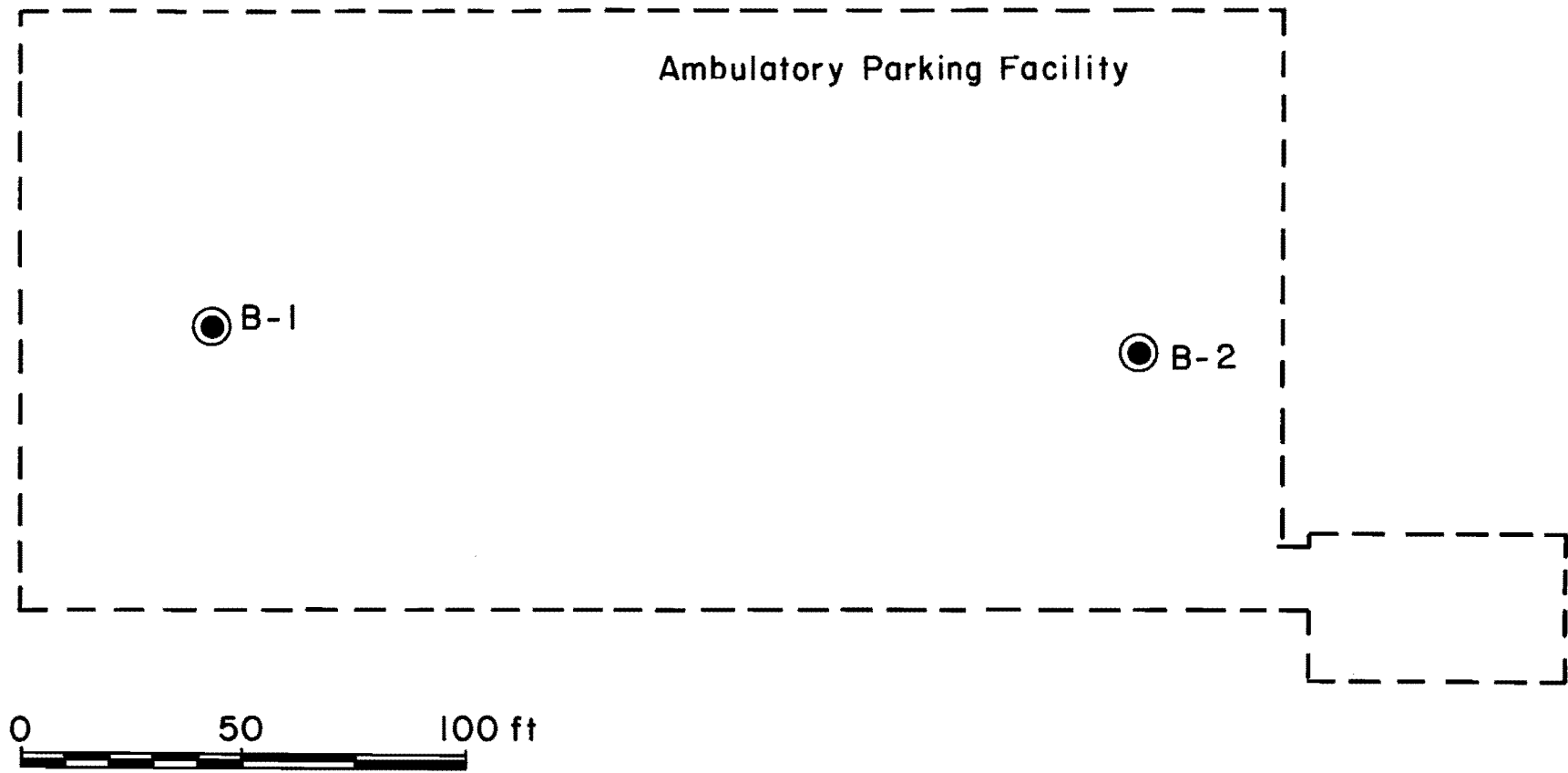


Fig. 2.6 Soil Boring Locations, Test Site 2

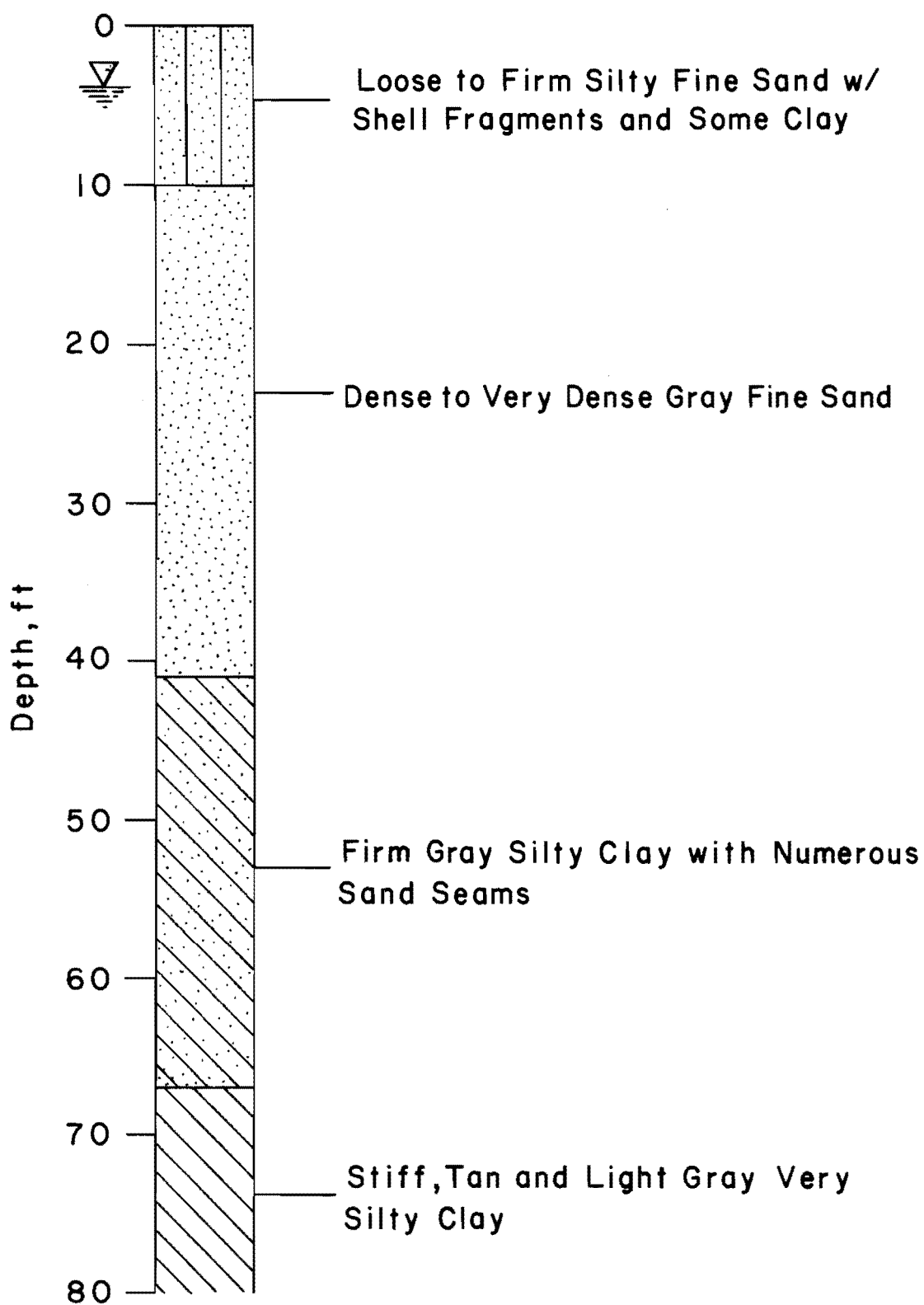


Fig. 2.7 Soil Profile, Test Site 2

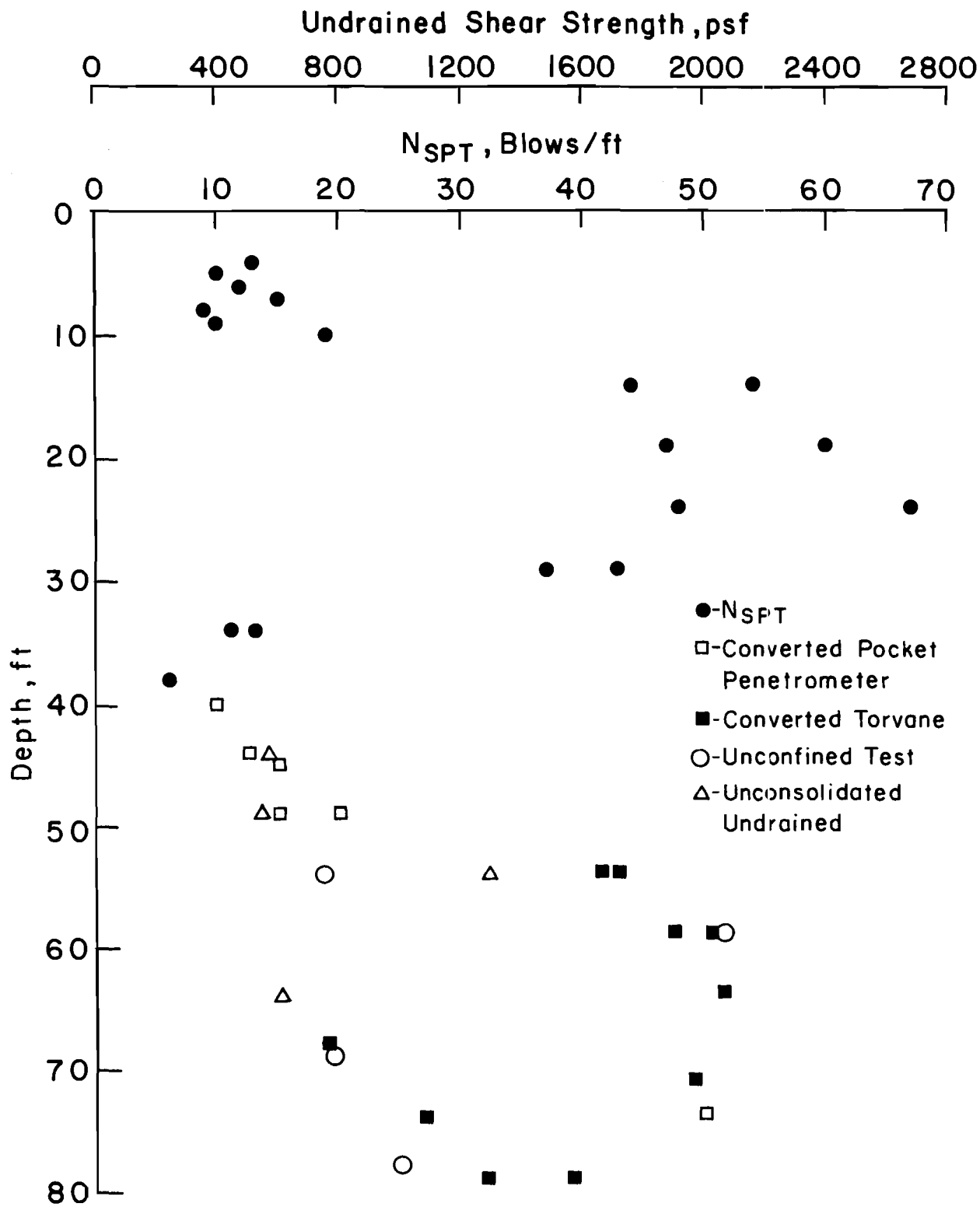


Fig. 2.8 Penetration Resistance and Undrained Shear Strength as a Function of Depth, Test Site 2

Site 3 - Eastern Site

Site Location. The only information about the location of this site that can be disclosed is that the test site was in an eastern state. The two load tests were done in conjunction with the building of three nine-story structures. The results from these load tests were to be presented to the designers so that a foundation type could be selected and a final design could be made.

Soil Profile. The soil profile was determined from three borings, designated as E-1, E-2, and E-3. The borings were done by a testing and engineering company from the same area. Boring E-1 was located exactly where the first test shaft was to be installed. Borings E-2 and E-3 were nearby and within the perimeter of the proposed building. The second load test was also located within the perimeter of this building. The standard penetration test was done at all three borings. The general soil profile is shown in Fig. 2.9 and the variation of N_{SPT} with depth is shown in Fig. 2.10. The boring logs are given in Appendix A.

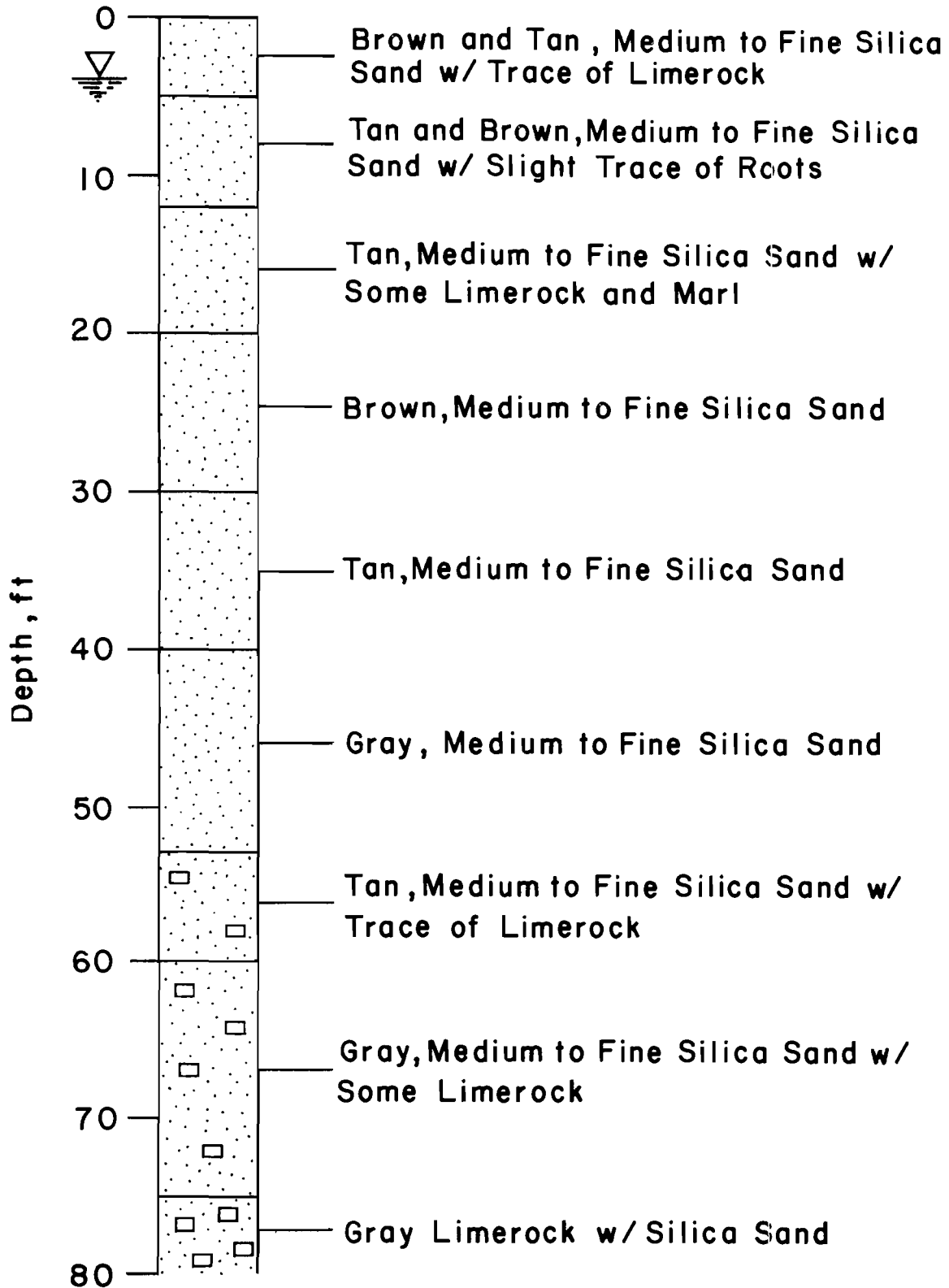


Fig. 2.9 Soil Profile, Test Site 3

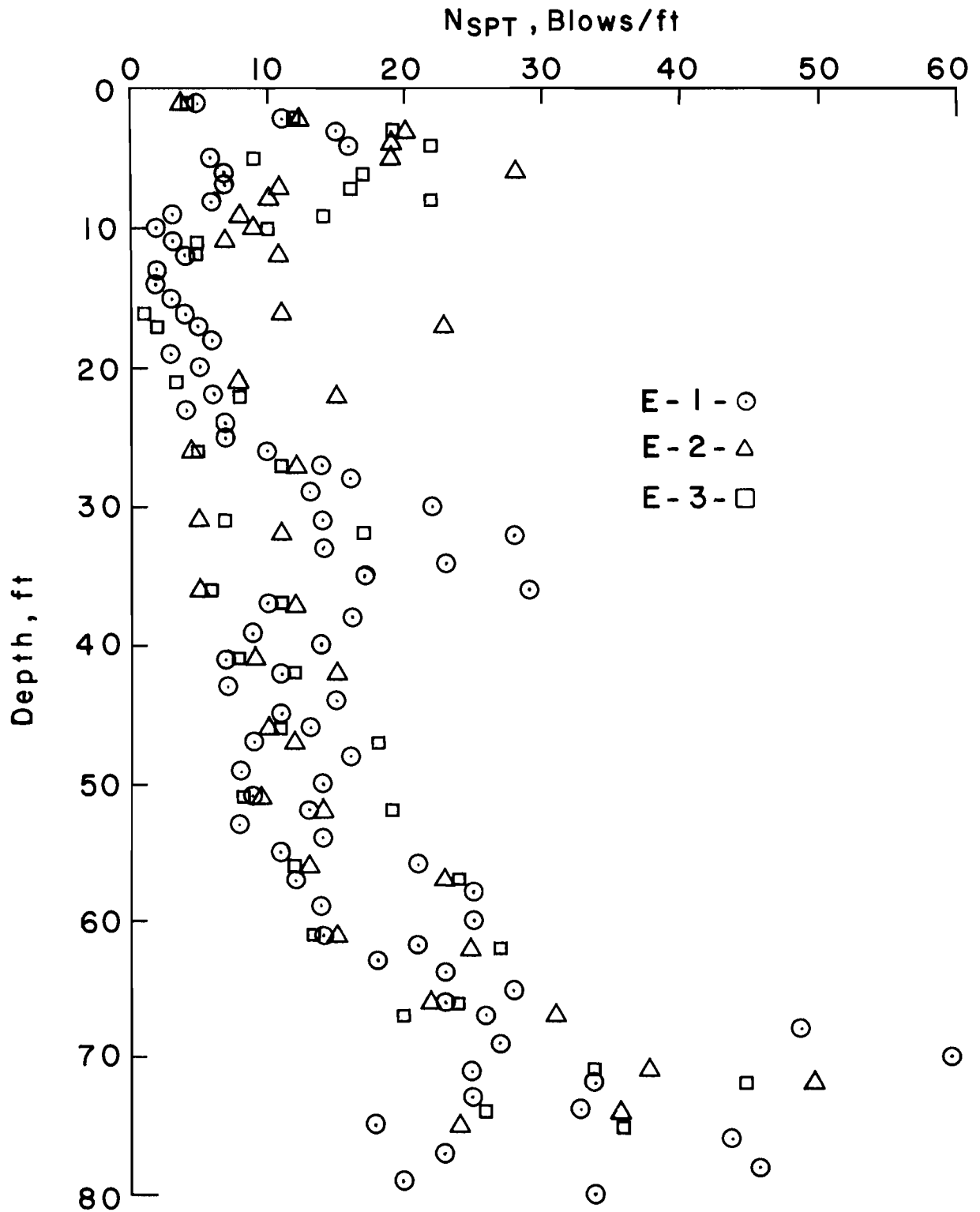


Fig. 2.10 Penetration Resistance as a Function of Depth, Test Site 3

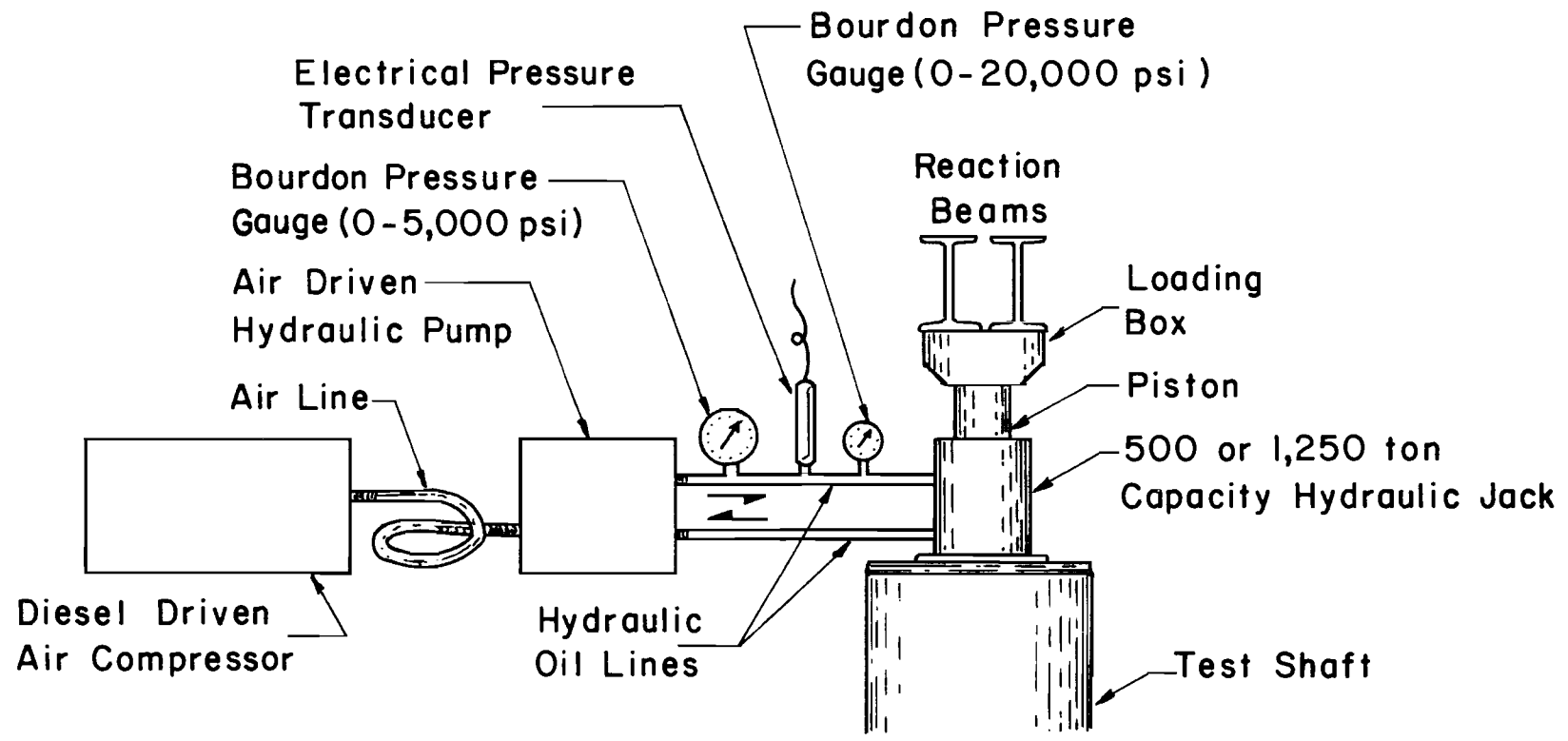
CHAPTER 3. INSTRUMENTATION

Measurement of Axial Load at the Top of the Shaft

Axial loads were applied to the top of the test shafts by means of hydraulic jacks supplied by Farmer Foundation Company and the Texas State Department of Highways and Public Transportation. The hydraulic jack supplied by Farmer Foundation Company has a maximum load capacity of 1,250 tons and was used for load tests at site 1 and site 3. Each of the two jacks supplied by the SDHPT had a maximum capacity of 500 tons and both were used at test sites 1 and 2. Exactly which jacks were used for a load test will be given in a later chapter. The loading-system arrangement is shown schematically in Fig. 3.1. This is the same system that was employed for all the tests, both at Galveston, Texas and at the eastern site.

The hydraulic jacks that are used in these load tests are not ordinary jacks, but jacks specifically designed for load tests. For further information on these hydraulic jacks and their special characteristics, a report by Engeling and Reese (1974) may be consulted.

The axial load at the top of the shaft was obtained by measuring the pressure of the hydraulic fluid going to the jack. Measurement of the pressure was accomplished with both a Bourdon-tube pressure gauge and an electrical pressure transducer (model BLH GP-CG). Both the Bourdon pressure gauge and pressure transducer can be seen in the photographs in Fig 3.2. The transducer allows measurement of pressures to a sensitivity of 10 psi. The jack pressure is then converted into applied axial load by the use of a calibration curve.



(After Barker and Reese , 1969)

Fig. 3.1 Arrangement of Loading System



Fig. 3.2 Photographs of Instrumentation at Top of Shaft

Measurement of Movements at the Top of the Shaft

Vertical movements at the top of the shaft were measured by three dial gauges. The gauges were located approximately at third points around the shaft. The dial gauges were mounted on a stationary reference frame as seen in Fig. 3.2. A typical reference frame is composed of two 1 x 6 timber beams, each 18 ft. in length. The beams are braced to prevent lateral movement and supported at each end. Mounted on the reference frame were aluminum gauge stands (Fig. 3.2) which were used to hold and position the dial gauges over the top of the test shaft. The dial indicators used were Starrett No. 655-2041, which have a sensitivity of 0.001 in. and a maximum travel of 2.0 in.

Measurements of Loads at Selected Locations within the Shaft

There are a few different instrumentation systems that are capable of measuring axial loads in drilled shafts. These systems have been discussed in detail by Barker and Reese (1969) and O'Neill and Reese (1970). During the past ten years, because of research done at The University of Texas at Austin, the Mustran-cell system has been used almost exclusively in instrumenting drilled shafts to be subjected to axial loads. The term Mustran is an abbreviation for "Multiplying Strain Transducer." The successful use of the Mustran cell system has been reported by Barker and Reese (1970), O'Neill and Reese (1970), Touma and Reese (1972), Engeling and Reese (1974), Wooley and Reese (1974), and Aurora and Reese (1976). Because of the proven performance of the Mustran-cell system, it was used as the only system for measurement of loads at selected locations within the shafts for this study.

The Mustran-cell system has undergone a few changes since its first use in 1969, but the theory of its use, as reported by Barker and Reese (1969),

is still the same. The Mustran cells used for these tests were a modification of the Type-2 Mustran cell. The components of a typical Mustran cell used in this study are shown in Fig. 3.3. The cell is composed of a 1/2-in. square, steel bar which is tightly screwed at each end into cell caps. Bonded to the cell column are two 90° rosette strain gauges. The gauges are of the foil type. A rubber hose with an inside diameter of 1-3/8 in. fits over the 1/2-in. square, steel bar and is clamped tightly at each end to the cell caps. Between the cell cap and rubber hose there is silicone rubber glue that is used as a sealant and helps to make the system air-tight. The interior of the Mustran cell needs to be kept dry because the electrical resistance of the strain gauges change erratically in the presence of moisture. The cells are kept moisture-free by pressurizing the cells with dry nitrogen. The lead cable of each cell is connected to a sealed manifold. The manifold is then pressurized with dry nitrogen and the nitrogen is distributed to each cell through the lead cables. The schematic arrangement of pressurizing Mustran cells through the manifold is shown in Fig. 3.4. The materials needed and the construction procedure for a Mustran cell are given in Appendix B. In Appendix C a brief presentation is given of some of the types of instrumentation that can be employed in drilled shafts to measure the distribution of axial load with depth.

In the field, before the cells were attached to the reinforcement cage, each cell was connected to a portable strain indicator to check electrical continuity, and the resistance-to-ground of each cell was checked with an ohmmeter. These checks were made to insure that each Mustran cell was functioning properly before installation.

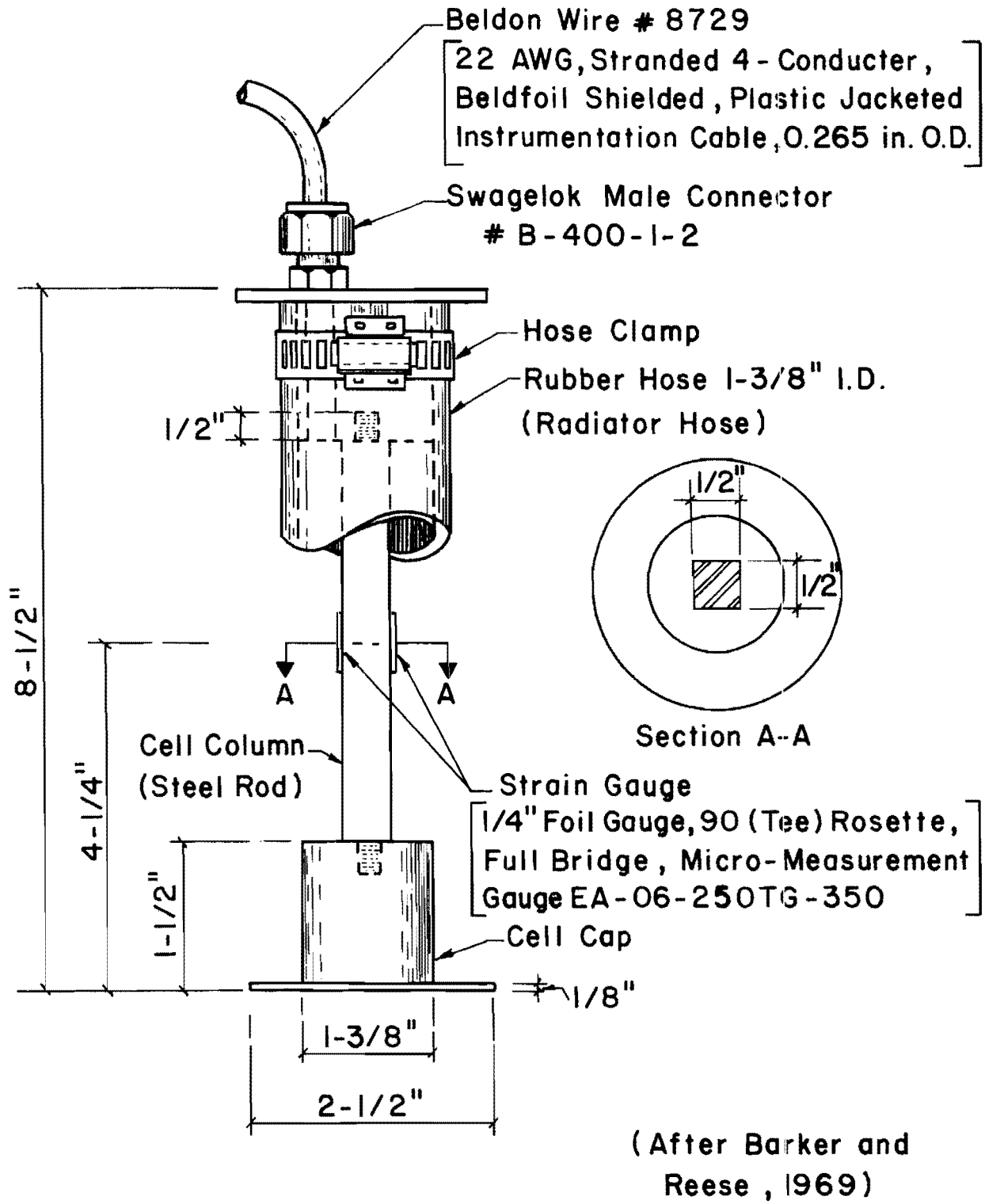
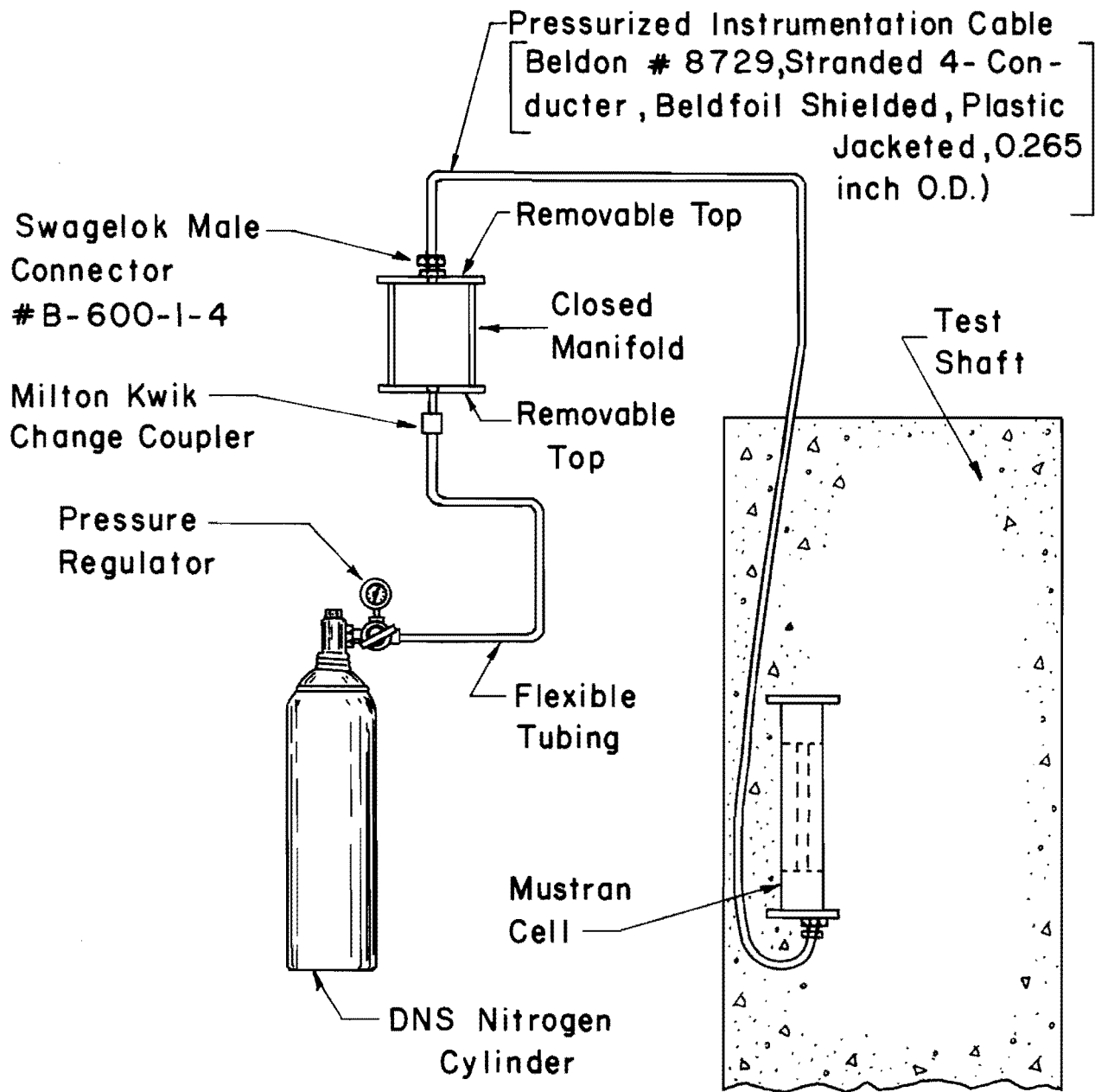


Fig. 3.3 Components of Mustran Cell



(After Barker and Reese, 1970)

Fig. 3.4 Schematic Arrangement of Mustran Cell Pressurization System

After the cells were checked, the cells were installed in the following manner. Attached to each cell cap was a steel angle made from 1/2-in.-wide and 1/8-in.-thick steel strap. The angles were used to mount the cells on the reinforcing steel using radiator-hose clamps. The cells were mounted at predetermined depths (distance from top of rebar cage) with two cells at each depth (level), except the top and bottom levels which had four cells each. The axes of the Mustran cells were parallel to the axis of the shaft. At each level the cells were placed on opposite sides of the reinforcing cage. This was done so that if any bending occurred in the shaft, averaging the cell readings at a level should eliminate the effect of bending. Therefore, at any level, the cells were spaced 180 or 90 degrees apart, depending on whether there were two or four cells. The cells were attached with the Swagelok fitting facing the bottom of the shaft. The lead cable was then made into a small loop and taped to the reinforcing steel. The cable was then run along the length of and taped to the reinforcing bar and out the top of the reinforcing cage. The procedure for installing Mustran cells is given in Appendix B. Photographs in Fig. 3.5 show Mustran cells installed on a rebar cage. The relative positions of soil layers and Mustran cells are shown in Fig. 3.6 for the Galveston tests and for the Eastern tests.

After all the cells were mounted on the reinforcement cage and the lead wires taped to the reinforcing bars, the lead cables were connected to the manifold and pressurized. The reasons for pressurizing the system and how it was done were given earlier in this section. At test site 1 in

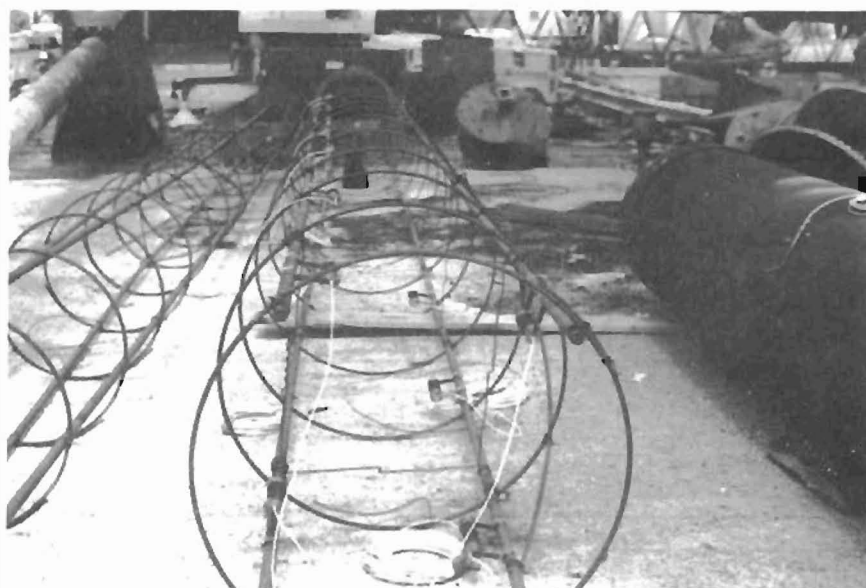
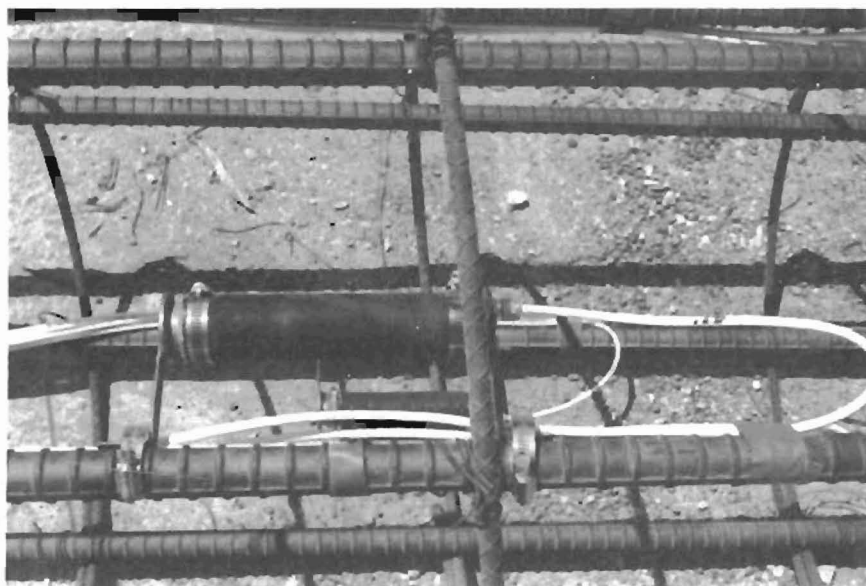


Fig. 3.5 Photographs of Installed Mustran Cells

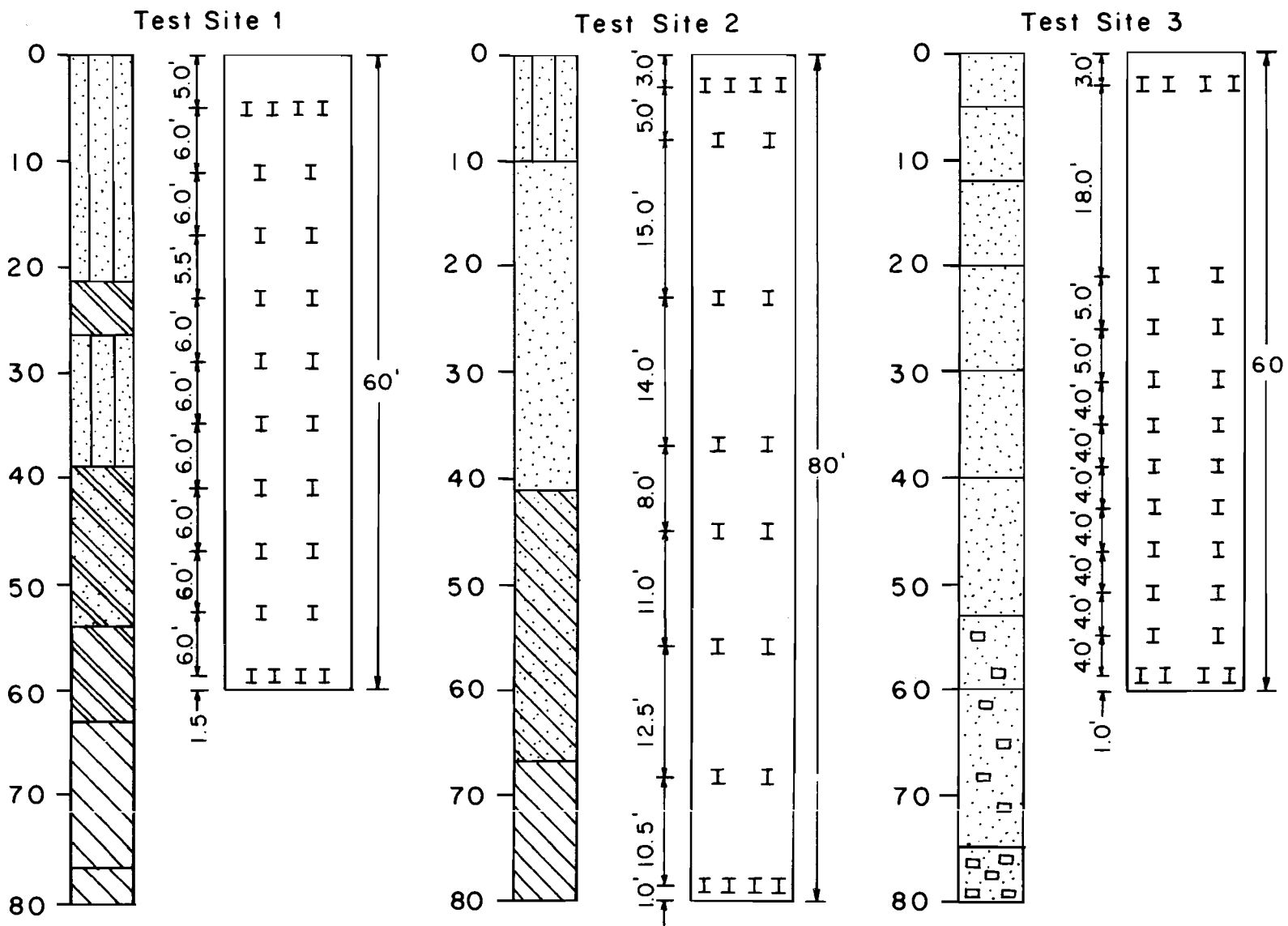


Fig. 3.6 Relative Positions of Soil Layers and Mustran Cells

Galveston, before the manifold was sealed, the wires coming from the lead cable were soldered to a terminal strip. The terminal strip was then connected to a 51-pin, Bendix environmentally sealed female connector, which was in the end plates of the manifold, as shown in Fig. 3.7. The special manifold was used in order to keep nitrogen pressure on the Mustran cells during the load tests.

After pressurizing the Mustran cells, a soap solution was used to check for leaks in the system.

Testing of Mustran Cells. Tests were done on the Mustran cells prior to the load tests at test site 1 in Galveston to study the nitrogen pressure that should be maintained. Prior to the Galveston tests the pressure had always been set at 20 psi. Earlier that year a load test on a 100-ft-deep shaft was performed and many of the Mustran cells at the bottom did not respond. This led to the investigation dealing with the internal pressure of the cells. The Mustran cells were put inside a triaxial-type set-up, as shown in Fig. 3.8, so that both the internal pressure of the Mustran cell and the external pressure around the Mustran cell could be controlled. The tests showed that the radiator hose used for the Mustran cell started to collapse inward when the external pressure was 5 psi greater than the internal pressure, as shown in Fig. 3.9. When the external pressure was 20 psi or greater than the internal pressure, the Mustran cell would short out. Also, the collapsing of the rubber hose on the Mustran cell will change the stiffness of the cell, making it impossible to compare directly the output from the various cells. As a result of these tests, it was decided that the

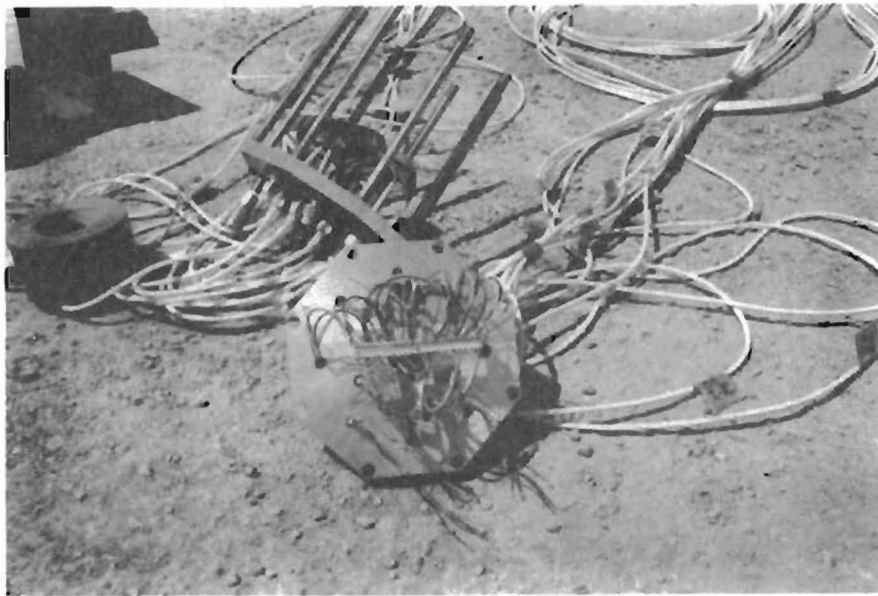


Fig. 3.7 Terminal Strips and Connectors in Manifold

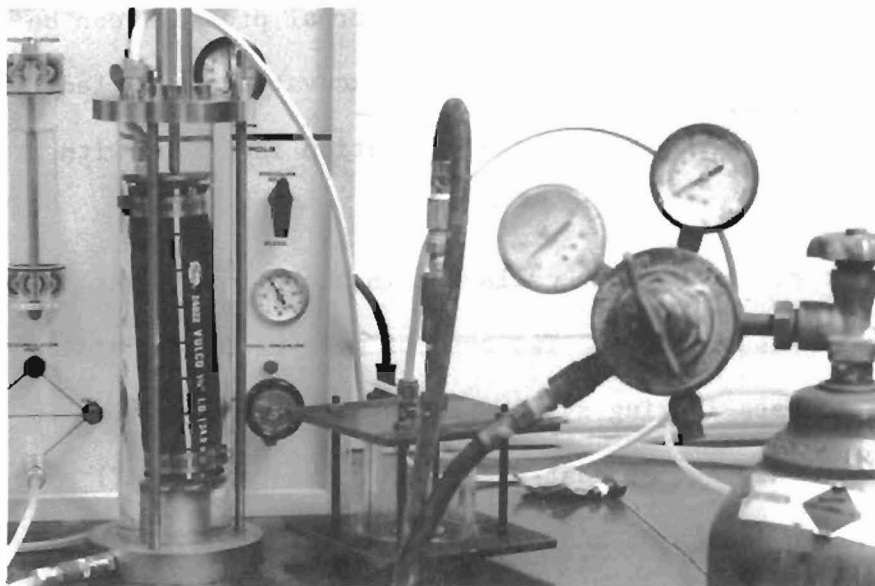


Fig. 3.8 Mustran Cell in Test Setup

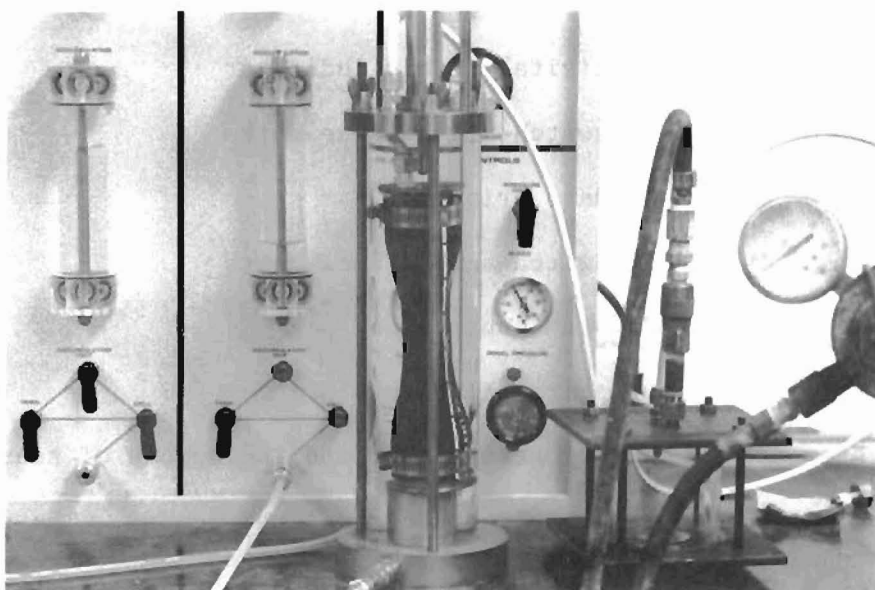


Fig. 3.9 Collapsed Radiator Hose on Mustran Cell

internal pressure of the Mustran cell should be kept greater than or equal to the external pressure on the cell. The external pressure can be assumed to be about 1/2 psi per ft of depth when the excavation is filled with slurry and about 1 psi per ft of depth when the excavation is filled with fluid concrete.

Readout System

The output of the Mustran cells was in micro inches per inch as indicated by the recording instruments. Two systems were used for reading the gauges: 1) an automatic data-logging system manufactured by Vishay-Ellis (See Fig. 3.10), used for the test at test site 1 in Galveston; and 2) a system employing a portable strain indicator and switch-and-balance units (See Fig. 3.11), used at the Eastern site. It is not known what system was used at test site 2 in Galveston.

The Vishay-Ellis Data Recording System consists of the following components.

- o one VE-20 digital strain indicator
- o one VE-21 switch-and-balance unit
- o one VE-22 data printer
- o two VE-24 switch-and-balance units
- o one VE-25 scan controller
- o five gauge terminal blocks

This system requires only one operator and is capable of scanning 40 channels at a rate of approximately one channel per second. The system also has an automatic printer which records the readings on a paper tape.

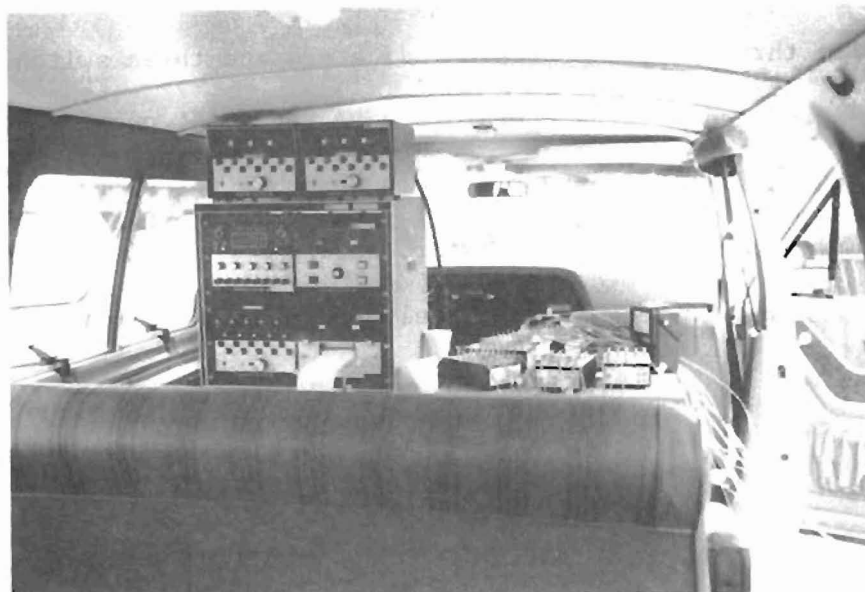


Fig. 3.10 Vishay Automatic Data-logging System

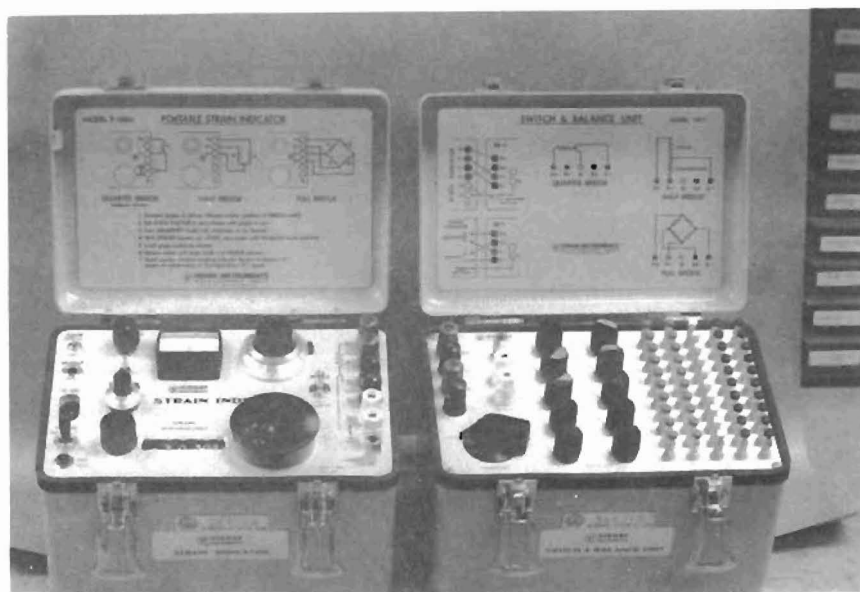


Fig. 3.11 Portable Strain Indicator and Switch and Balance Unit

The second system, consisting of a portable strain indicator and switch-and-balance units, is a manually operated system. For the tests at the Eastern site three portable strain indicators and three switch-and-balance units were used. Three operators were required, one for each set. The operator had to switch to a channel (10 channels per switch-and-balance unit), balance it on the strain indicator, record the readings, and switch to the next channel. It took approximately one minute to read and record the ten channels.

CHAPTER 4. SHAFT INSTALLATION AND CONSTRUCTION PROCEDURES

Test Site 1 - Galveston, Texas

Test Shafts. Three test shafts were constructed at test site 1 in Galveston between August 5, 1980 and August 15, 1980. A 48-in.-diameter by 60-ft-long test shaft, G-1, was constructed by the casing method. The following procedure was employed. The first step was to drive a 48-in.-diameter casing with a vibratory hammer to a depth of 52 ft. Then a 46-in.-diameter auger was used to excavate the soil inside the casing and to advance the hole to its final depth of 60 ft. At this time it was noticed that water was seeping into the hole, so a slurry was added to the excavation. A cleaning bucket was then fitted to the kelly and used to clean the bottom of the hole.

The steel cage for the 48-in.-diameter shaft consisted of eight number 10 bars to 18 ft and four number 10 bars from 18 to 60 ft. The cage, instrumented with Mustran cells, was lifted with a crane and carefully placed into the hole. Nitrogen pressure was maintained on the Mustran cells to prevent any seepage of moisture into the cells.

Concreting of this shaft was done with the help of a tremie which was lifted and positioned inside the steel cage by means of a crane. The tremie was filled with concrete by means of a steel hopper. Because of the high temperatures, between 90 and 100 degrees Fahrenheit, it was decided to add 300 lb of ice to each 8-yd load to keep the temperature of the concrete down. This worked quite well; the temperature of the concrete was around 85 degrees Fahrenheit when it was poured. A slump test was also done and the concrete

slump was found to range from 9 1/2 to 10 in., which was considered acceptable.

Concrete was tremied into the shaft until the level of the concrete was within a few feet of the top of the shaft. At this time the manifold for the Mustran cells was placed inside the rebar cage and tied to the cage. The vibratory hammer was then connected to the steel casing and the casing was pulled out. The manifold was removed from inside the shaft and more concrete was added to complete the construction.

The next shaft constructed was 36 in. in diameter by 65 ft in length, test shaft G-2. The construction procedure used for this shaft was as follows. A 48-in.-diameter casing was driven to a depth of 50 ft with a vibratory hammer, as shown in Fig. 4.1a. A 46-in. auger was then used to excavate the casing to its full depth. Slurry was introduced and a 36-in. auger was then used to excavate the hole to its final depth of 65 ft, as shown in Fig. 4.1b. After the excavation was at its final depth, a 36-in.-diameter casing was placed in the hole, with the slurry still in the hole as shown in Fig. 4.1c. The casing went the full length of the hole.

At this time a problem occurred in that sand and water blew into the hole and the casing started to settle. The sand that was encountered was not indicated on the original soils report. To overcome this problem, cables from the crane were hooked to the casing and the casing pulled plumb and to its original position. Then the bottom 6 ft of the shaft was filled with concrete, as shown in Fig. 4.1d. With the crane still supporting the casing, the concrete was left to set overnight. The next day, with the slurry still in the hole, the concrete in the casing was augered out to a depth of 60 ft.

A reinforcing cage consisting of eight number 10 bars to 18 ft and four number 10 bars to 60 ft was placed into the hole. This cage was

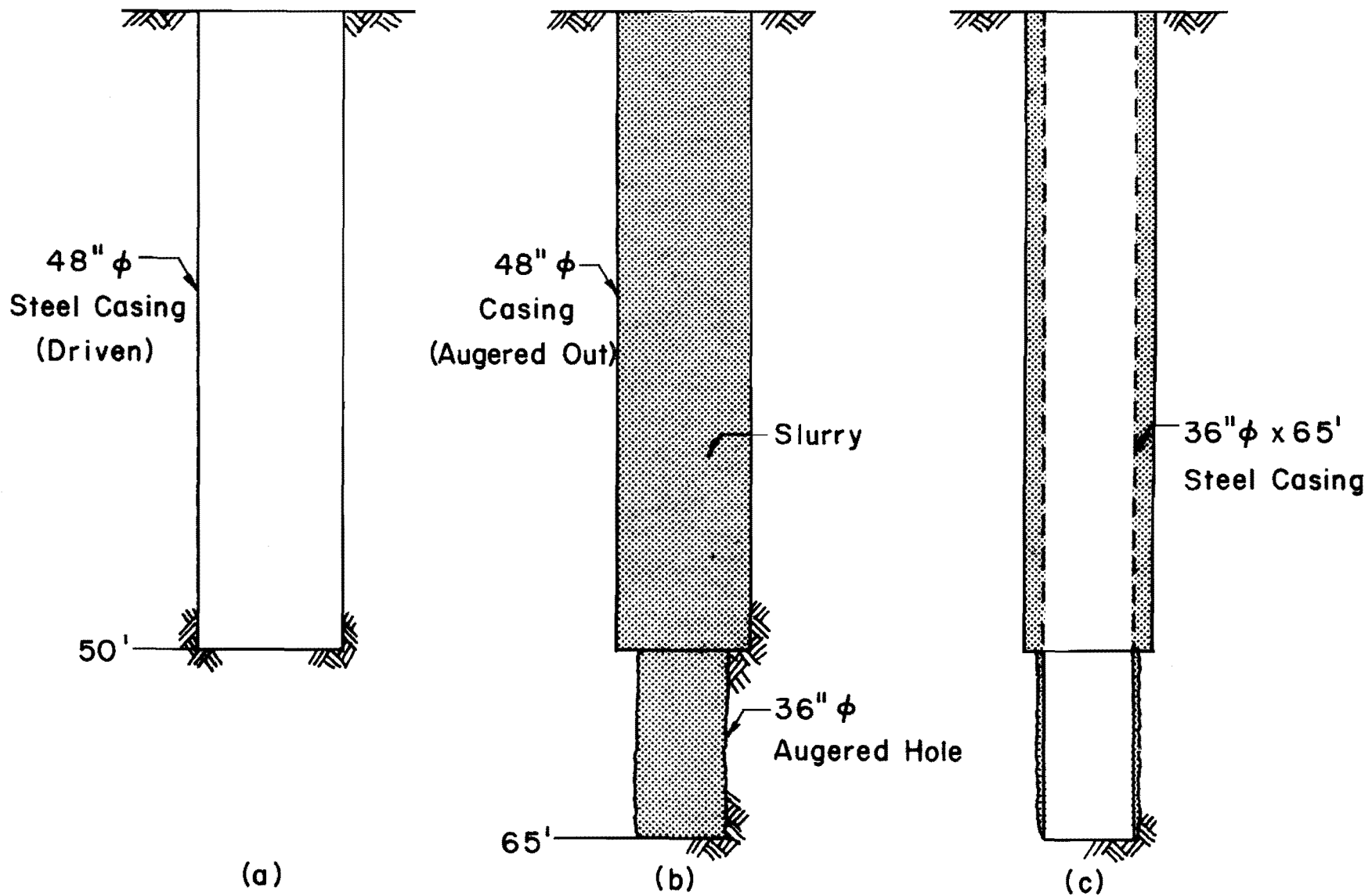


Fig. 4.1 Method of Construction of Test Shaft G-2 at Test Site 1 (a) Driven Casing; (b) Drilling Below Casing with Slurry; (c) Placement of Inner Casing

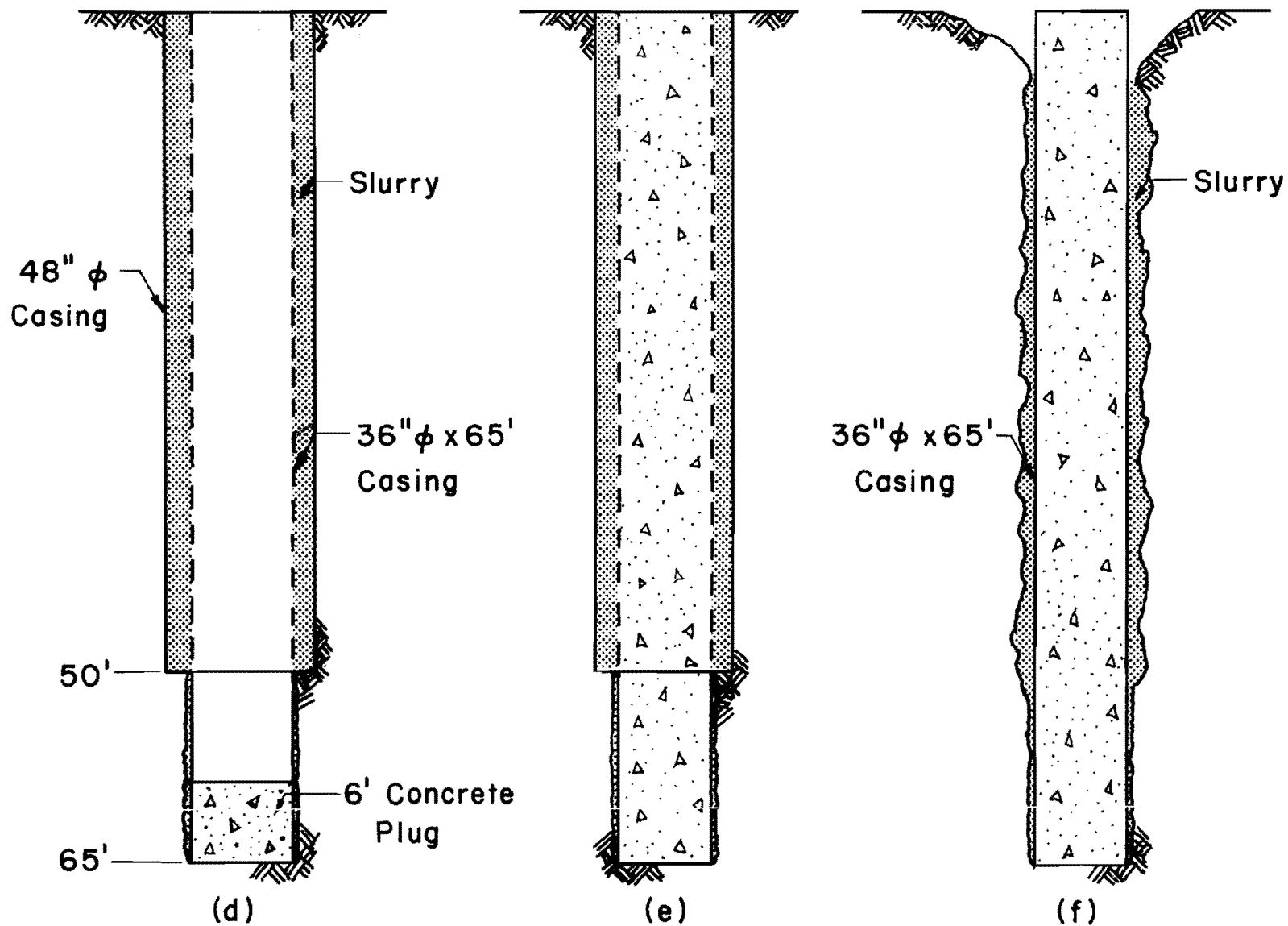


Fig. 4.1 Method of Construction of Test Shaft G-2 at Test Site 1 (con'd)
 (d) Concrete Plug Poured; (e) Placement of Concrete; (f) Completed Shaft

uninstrumented. With the 48-in.-diameter casing still in place, the concrete for this shaft was placed with the aid of a tremie, as shown in Fig. 4.1e. As with the 48-in.-diameter shaft, 300 lb of ice were added to each 8 yd of concrete. Slump tests were done and the concrete slump was found to range from 9 1/2 to 10 in. The 36-in., steel casing was left in place on this shaft, but the 48-in. casing was removed and the slurry was left between the casing and the soil. By the next day the soil at the ground surface had moved inward toward the casing. Figure 4.1f presents an estimate of the final configuration of the casing, slurry, and excavation.

The third test shaft, G-3, constructed was 36 in. in diameter by 60 ft in length. The following construction procedure was used. A 42-in.-diameter surface casing was driven to a depth of 10 ft. Then a 36-in.-diameter hole was augered, with the use of slurry, to a depth of 35 ft. At this time a 36-in.-diameter casing was screwed in to a depth of 40 ft. The excavation was then continued, with a 34-in. auger and slurry, to a final depth of 60 ft.

The steel-reinforcing cage for this shaft consisted of eight number 10 bars to 18 ft and four number 10 bars from 18 to 60 ft. The cage, fully instrumented, was lifted by a crane and carefully placed into the hole. Nitrogen pressure of approximately 55 psi was maintained on the Mustran cells to prevent any seepage of moisture into the cells.

Concrete was placed in the shaft with the aid of a tremie and steel hopper. The shaft was filled completely with concrete and the casing was left in place. As in the previous shafts, 300 lb of ice were added to each 8 yd of concrete. Slump tests were performed and the concrete slump was found to range from 9 1/2 to 10 in. The last step was to remove the 42-in. surface casing.

Grouting of Test Shafts. The two 36-in.-diameter test shafts were tested on September 4 and 5, 1980. The instrumented, 36-in.-diameter shaft (G-3) was tested on September 5. As expected, because of the casings being left in place, the shafts failed at relatively low loads. The results of these tests will be discussed in a later chapter. In an attempt to increase the load-carrying capacity of the shafts, it had been previously decided to grout around sections of each of the 36-in.-diameter shafts.

The grout that was used for both shafts was supplied by Sullivan Enterprises in Galveston (quality control no. 740-1271). The mixture for one cubic yard of grout consisted of 750 lb of sand, 846 lb of cement, 40 lb of water, 27 oz of normal-set water reducer. Water was then added on the job site to get a workable fluid mix. A single-cylinder grout pump was used to inject the grout. Although the grout pressure was not measured, it is assumed that it was low.

Grouting of the 36-in.-diameter shaft, (G-3) with a casing to 40 ft was as follows. Six grout tubes were jetted into place, three to a depth of 40 ft and three to a depth of 30 ft. Grout was then pumped into the tubes, and pumping was continued as the grout tubes were removed. A total of 8 cu yd of grout were used to grout the shaft from the ground surface to a depth of 40 ft. Assuming that the excavation in the top 40 ft, using the 36-in.-diameter auger, had a diameter of 37 in., the volume of the annular space around the casing was 0.6 cu yd. Therefore, the volume of grout was about 13 times greater than the annular space.

The grouting of the 36-in.-diameter shaft (G-2) with a casing to 65 ft was done in the following manner. Three grout tubes were jetted to a depth of 65 ft. Then a total of 6 cu yd of grout was pumped into the grout tubes, pumping was stopped, and the grout tubes withdrawn. After the grout had been

allowed to set, a steel rod was used to learn the extent of the grouting. It was determined that the lower 15 ft of the shaft had been grouted. The volume of the annular space around the casing of the lower 15 ft, using the same assumptions indicated above, was about 0.3 cu ft. Therefore, the volume of grout was about 27 times greater than the annular space.

The amount of grout used around the drilled shafts, 8 and 6 cu yd, is considered to be quite large for the area that was grouted. No information is available about what happened to the excess grout that was used. It is unlikely that the diameter of the annular space around the shaft was increased uniformly. The most likely possibility is that the soil was fractured and that the grout flowed into a weak zone in the soil. Elevations of the three test shafts prior to grouting, but showing the area to be grouted, are shown in Fig. 4.2.

Reaction Shafts. Four reaction shafts were constructed at test site 1 in Galveston. All four reaction shafts were 48-in. in diameter by 60 ft in length with a 96-in. underream. Each shaft contained twelve 1 in. by 60 ft dywidag bars. The following general procedure was employed for the construction of the four reaction shafts. The first step was to drive a 48-in.-diameter casing with a vibratory hammer to a depth of 52 ft. A 46-in.-diameter auger was then used to excavate the soil inside the casing. When the excavation reached the bottom of the casing, water began to seep in, so a slurry was added to the excavation. The excavation was then advanced to its final depth of 60 ft. At this time a bellig tool was used to add a 96-in. underream to the bottom of the shaft. The dywidag bars were then lifted with a crane and placed into the hole.

Concreting of the reaction shafts was done with the aid of a tremie and steel hopper. The tremie was lifted and placed inside the excavation with a

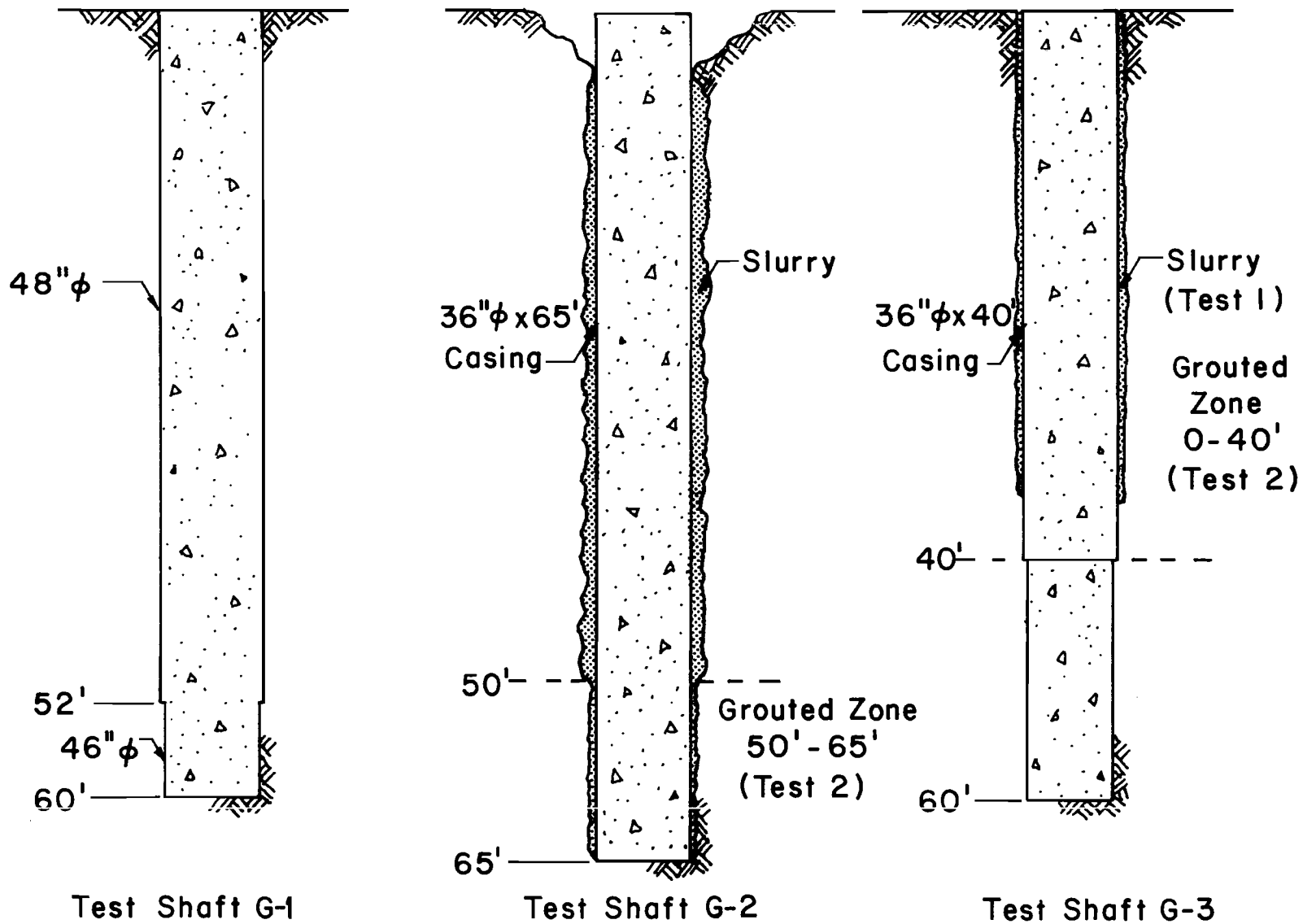


Fig. 4.2 Elevation of Test Shafts at Test Site 1, Galveston

crane. The concrete, which had a slump of 9 in., was tremied into the shaft until the level of the concrete was at the top of the shaft. At this time, the 48-in.-diameter casing was pulled with the vibratory hammer. Then more concrete was added to complete the construction.

Test Site 2 - Galveston, Texas

Test Shaft. A single test shaft, G-4, was constructed at test site 2 in Galveston. The shaft was constructed on June 7, 1978 with the following procedure. First, a 24-in.-diameter by 40-ft-long casing was driven to a depth of 40 ft with a vibratory hammer. Excavation of the soil within the casing was then done with a 22-in.-diameter auger. The excavation was then flooded with slurry and the hole was advanced to its final depth of 80 ft. A cleaning bucket was then fitted to the kelly and used to clean the bottom of the excavation.

The steel cage for the shaft consisted of six number 6 bars extending the complete length of the shaft. The cage, instrumented with Mustran cells, was lifted with a crane and carefully placed into the hole. Nitrogen pressure was maintained on the Mustran cells to prevent any seepage of the moisture into the cells.

Concrete for the shaft arrived at the site and a slump test was performed, with the slump being approximately 4 to 5 in. It was decided that this slump was too low, so more water was added, producing a high slump. Concrete was then placed in the shaft with the aid of a tremie. In order to prevent contamination of the concrete in the tremie with drilling mud, a plywood plate was loosely fastened to the bottom of the tremie. The hydrostatic pressure of the concrete in the tremie was not sufficient to push this plate from the end of the tremie. In order to free the plate and initiate concrete

placement, it was necessary to "yo-yo" the tremie several times. This may have damaged some of the Mustran cells.

When the level of the concrete had reached the top of the shaft, it was noticed that the concrete again had a very low slump, possibly 3 in. This low slump may have been a result of time or possibly bad cement. After the concrete level was at the top of the shaft, the casing was vibrated out a distance of 5 ft. At this time the casing was filled with concrete and pulled completely out.

After the casing was pulled, it was found that the lead wires to two Mustran cells had been pulled from the manifold. Thus, the nitrogen pressure in the system was temporarily lost until the two lead wires were reconnected to the manifold.

Reaction Shafts. The construction procedure for the two reaction shafts at this site is not known. It can be assumed that it was similar to the procedure used for the test shaft. The reaction shafts at this site were 30 in. in diameter by 80 ft in length with a small diameter bell at the end. The size of the bell is not known.

Test Site 3 - Eastern Site

Test Shafts. Two test shafts, E-1 and E-2, were constructed at test site 3 between January 11, 1981 and January 29, 1981. A 36-in.-diameter by 60-ft-long shaft, E-1, was the first test shaft constructed. The following procedure was employed. First, a 36-in.-diameter by 60-ft casing was driven to a depth of 60 ft but, due to densification of the sand and side resistance (skin friction), the casing could only be driven to 40 ft at this time. The 20 ft of casing that was above the ground surface was then cut off and a 34-in. auger was used to excavate the soil inside the 40 ft of casing in the

ground. The excavation of the soil on the inside of the casing was done to eliminate some of the skin friction. The 20 ft of casing that was cut off was then welded back on to the rest of the casing, the vibratory hammer attached, and the casing driven to the final depth of 60 ft. The 34-in.-diameter auger was then used to excavate the remaining 20 ft of soil inside the casing. When augering at the bottom of this shaft, limestone cobbles (8 to 10 in. in diameter) were encountered.

The reinforcing cage, instrumented with Mustran cells, was then lifted with a crane and carefully placed in the hole. The steel reinforcing cage for this 36-in.-diameter shaft consisted of eight number 8 bars and eight number 6 bars. All the reinforcing bars went the complete length of the shaft.

Concreting of this shaft was done with the aid of a tremie, which was lifted with a crane and positioned inside the steel cage. A concrete pump was then used to get the concrete inside the tremie. A slump test was done and the concrete slump was found to range from 8 1/2 to 9 3/4 in., which was acceptable.

Concrete was tremied into the shaft until the level of the concrete was within a few feet of the top of the shaft. At this time, the tremie was removed and the manifold for the Mustran cells was placed inside the rebar cage and tied to the cage. The vibratory hammer was then connected to the steel casing and an attempt was made to pull the casing. This first attempt failed so a 50-ton crane and a 25-ton cherrypicker were added to the 50-ton crane already being used to pull on the vibratory hammer and casing. This second attempt also failed. At this time the engineer on the project decided that they would try to recover the instrumentation so an attempt was made to

pull the reinforcing cage out. This also failed. The casing and instrumentation were both left in place.

The next shaft constructed, E-2, was also 36 in. in diameter by 60 ft in length. This shaft was constructed because the company for which the test was being done would not accept a test on a cased shaft. The construction procedure used for this shaft was as follows. A 36-in.-diameter by 60-ft long casing was driven with a vibratory hammer until the casing broke at a weld. Information is not available about the exact depth at which the casing broke, but it was within a few feet of the final depth of 60 ft. The inside of the casing was then excavated with a 34-in.-diameter auger. The casing was then welded back together and driven to the final depth of 60 ft. The remainder of the soil was then excavated.

The reinforcing cage, instrumented with Mustran cells, was then lifted with a crane and carefully placed inside the casing. The steel cage for this shaft consisted of eight number 8 bars. Before concreting of the shaft began, the vibratory hammer was attached to the casing and it was pulled up a foot or so just to make sure they would be able to pull this casing. Concrete was placed in this shaft in the same manner as the first test shaft at this site, with a tremie and concrete pump. The slump of the concrete used for this shaft ranged from 9 1/2 to 10 inches.

Concrete was tremied into the shaft until the level of the concrete was within a few feet of the top of the shaft. The tremie was then removed and the manifold was tied to the reinforcing steel inside the casing. The vibratory hammer was then connected to the casing and the casing was pulled up approximately 10 ft. More concrete was then pumped into the casing and the casing was then pulled completely out. The manifold was then removed from inside the shaft.

Reaction Shafts. At test site 3 four reaction shafts were constructed. All four of the reaction shafts were 36 in. in diameter by 65 ft in length. Each reaction shaft had twelve 1 in. by 60 ft dywidag bars in them. The following general procedure was used in constructing the reaction shafts. The first step was to drive, with a vibratory hammer, a 36-in.-diameter casing to refusal, which usually occurred at a depth of approximately 55 ft. The interior of the casing was then excavated with a 34-in. auger. After the inside of the casing was excavated, the casing was driven to the final depth of 65 ft. The inside of the casing was then excavated to the final depth. Limestone cobbles (8 to 10 in. in diameter) mentioned earlier were encountered when excavating almost all the reaction shafts, usually between depths of 55 and 65 ft. The dywidag bars were then lifted with a crane and placed into the hole.

Concreting of the reaction shafts was accomplished with the aid of a tremie and concrete pump. The concrete was tremied into the shaft until the level of the concrete was near the top of the shaft. At this time the vibratory hammer was attached to the casing and the casing was pulled out approximately 10 ft. More concrete was added and the casing was pulled completely out.

CHAPTER 5. LOAD TESTS

Test Procedure

The method used to apply the axial loads to the test shafts was essentially the State Department of Highways and Public Transportation "quick load" procedure. Fuller and Hoy (1970) reported that results from tests performed using the "quick-load" procedure, in most instances, agree closely with results from tests using the more common "maintained-load" procedure. Essentially, the "quick-load" test requires that loads be applied in equal increments with gross settlement, loads, and Mustran cell readings recorded immediately before and after the application of each increment of load. Each increment of load is held for the same amount of time and then the next load is applied.

When the load-settlement curve obtained during the test shows that the shaft has been failed, that is, that the load on the shaft can only be held by continuous pumping of the hydraulic jack and the shaft is being driven into the ground, a final set of readings is taken and pumping is stopped. After the shaft has come to equilibrium, the shaft is unloaded in equal decrements of loads with settlement readings being taken when movement on the dial gauges is negligible. When all the load is removed and the shaft has been allowed to recover, net settlement readings are taken.

The procedure described above follows the SDHPT procedure closely, but there are a few minor exceptions. The SDHPT procedure states that the time interval be two and one-half minutes between application of load increments.

At test site 1 in Galveston the interval was three minutes, and at the Eastern site it was four-minutes. There is no information of the time interval used at test site 2 in Galveston. Also, the SDHPT procedure recommends readings immediately before and after the application of each load. At the Eastern site only one set of readings was taken. These were started 30 seconds after the load was applied. Only one set was taken because the readings were being taken manually with switch-and balance units. The SDHPT procedure recommends that unloading be done in one step (i.e., all of the load removed at once); for these tests the unloading was done in decrements.

Test Site 1 - Galveston, Texas

Test Arrangement. The testing arrangement at this site consisted of four reaction shafts and three test shafts. The reaction shafts were all 48 in. in diameter by 60 ft in length, with a 96-in. underream. These shafts were to be incorporated into the foundation of the building.

The three test shafts consisted of two instrumented shafts and one uninstrumented shaft. The first test shaft, which will be designated G-1, was 48 in. in diameter by 60 ft in length. This shaft was instrumented. Test shaft 2, designated as G-2, was an uninstrumented shaft that was 36 in. in diameter by 65 ft in length, with a casing extending the full length of the shaft. Test shaft 3, designated as G-3, was 36 in. in diameter by 60 ft in length, with a casing extending from the ground surface to a depth of 40 ft. This shaft was also instrumented. The arrangement of the test shafts with respect to the reaction shafts is shown in Fig. 5.1.

Test Results

Test Shaft G-1. The load test of test shaft G-1 was performed on August 26, 1980, nineteen days after construction of the shaft. The test was begun

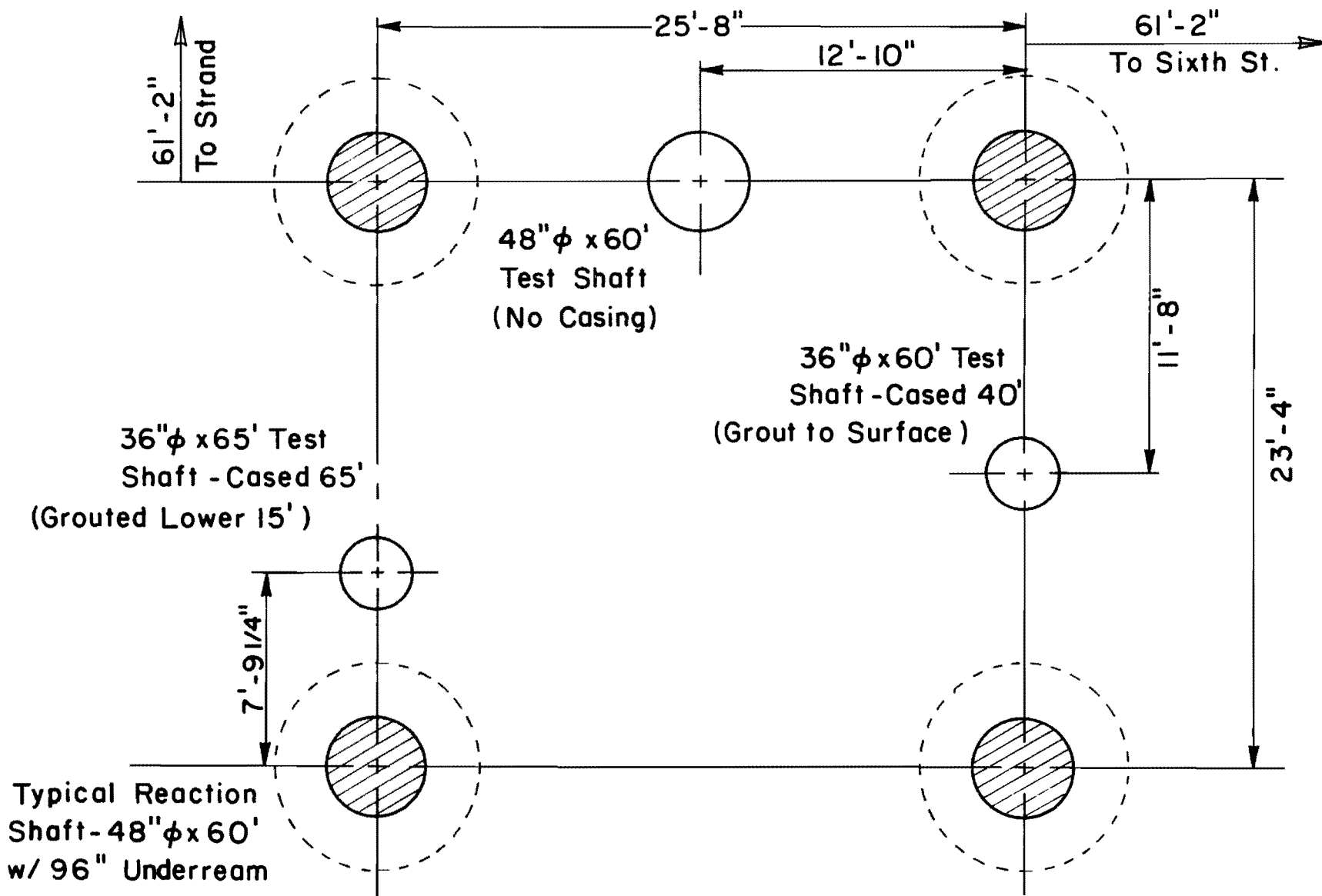


Fig. 5.1 Testing Arrangement, Test Site 1

at 2:20 p.m. A seating pressure of 500 psi was applied to the hydraulic jack. The jack had a capacity of 1250 tons. The pressure on the jack was then increased to 1000 psi, after which it was increased in 200 psi (15 ton) increments to failure, which occurred at 6775 psi. The pressure at failure was equivalent to a load of 495 tons.

The time to load the shaft was approximately one hour and 20 minutes. After attaining the ultimate capacity, the shaft was unloaded in 1000-psi (75-ton) decrements. Unloading began at 3:55 p.m. and took approximately 20 minutes.

The load-settlement curve (all load-settlement curves will be the applied load and the average settlement at the top of the shaft) is shown in Fig. 5.2. As indicated in the figure, the maximum load was 495 tons and the maximum settlement was 1.94 in. Upon unloading, the shaft rebounded and the permanent settlement was 1.70 in.

Test Shaft G-2. Test shaft G-2 was load-tested for the first time on September 4, 1980, 21 days after construction of the shaft. Unless otherwise noted, a 500-ton jack was used for this and subsequent tests. An initial pressure of 750 psi was applied to the hydraulic system. The pressure on the jack was then increased to 1000 psi; the pressure was then increased in 200-psi (5-ton) increments to failure. The pressure at failure was 3400 psi, which is equivalent to a load of 81 tons. After the ultimate capacity of the shaft had been reached, the shaft was unloaded in three decrements of approximately 1000 psi (26 tons) each.

On September 11, 1980 the lower 15 ft of test shaft G-2 was grouted. The grout was allowed to cure for seven days. The second load test on shaft G-2 was performed on September 18, 1980. In this test an initial pressure of

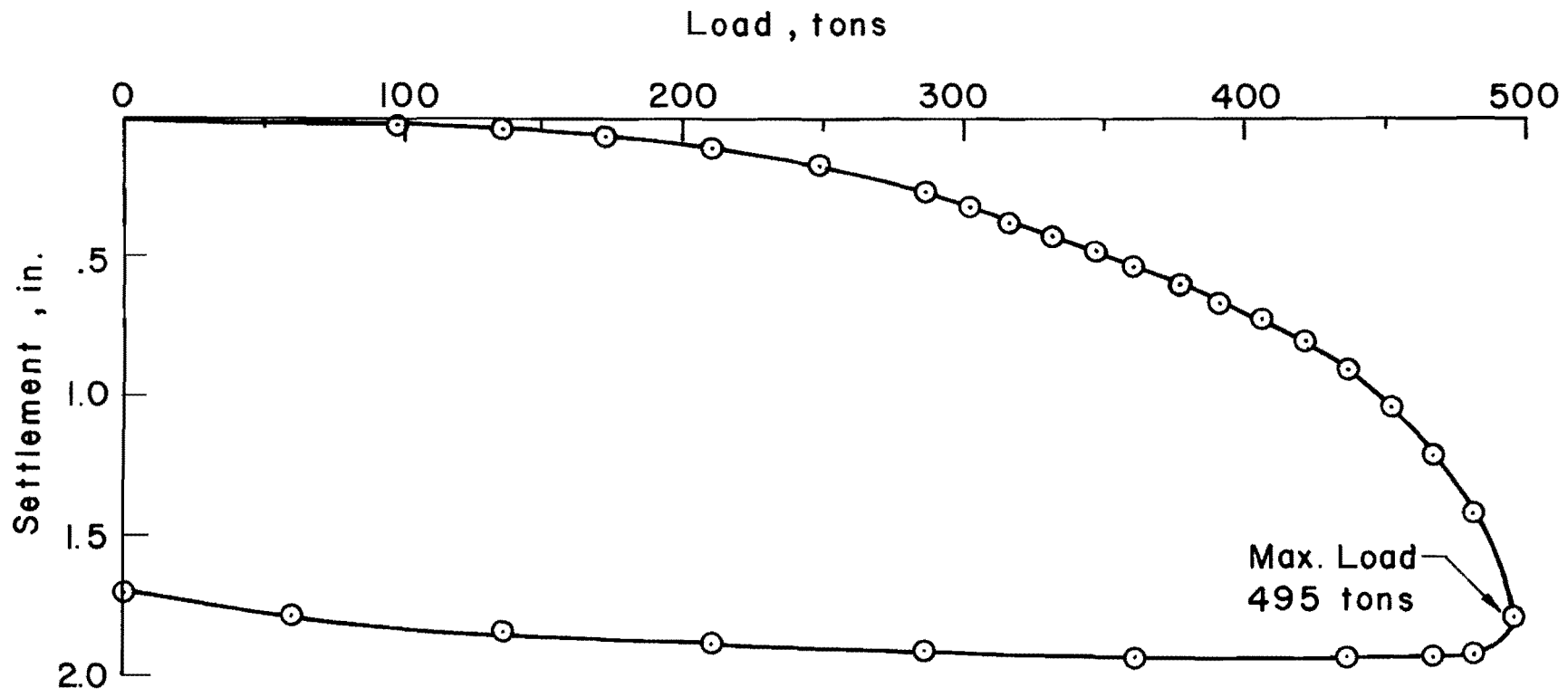


Fig. 5.2 Load Settlement Curve, Test Shaft G-1

500 psi was applied to the loading system. The pressure was then increased to 1000 psi, and then increased in 400-psi (10-ton) increments to failure. The pressure at failure was 14800 psi, which is equivalent to a load of 373 tons. The complete test, loading and unloading, lasted approximately 1 1/2 hours.

The load-settlement curves for both of the tests on test shaft G-2 are shown in Fig. 5.3. As indicated in the figure, the maximum load in test 1 was 81 tons and the maximum settlement was 1.69 in. After unloading in test 1, the shaft rebounded and the permanent settlement was 1.60 in. In test 2, after grouting, the maximum load was 373 tons and the maximum settlement for the test was 1.58 in. After unloading and rebound, there was a permanent settlement of 1.29 in. with reference to the position of the shaft at the beginning of test 2.

Test Shaft G-3. The first load test of test G-3 was performed on September 5, 1980, 20 days after the shaft was poured. An initial pressure of 750 psi was applied to the jacking system. The pressure was then increased to 1200 psi. From 1200 psi to failure the pressure was increased in 400-psi (10-ton) increments. Failure occurred at a pressure of 8400 psi, which is equivalent to a load of 209 tons. After the ultimate capacity of the shaft had been reached, the pressure was released in four decrements of approximately 2000 psi (51 tons). The complete test, loading and unloading, lasted about two hours.

The top 40 ft of test shaft G-3 was then grouted on September 10, 1980. The grout was allowed to cure for seven days. The second load test of shaft G-3 was then performed on September 17, 1980. In this test an initial pressure of 500 psi was applied to the loading system. The pressure was then

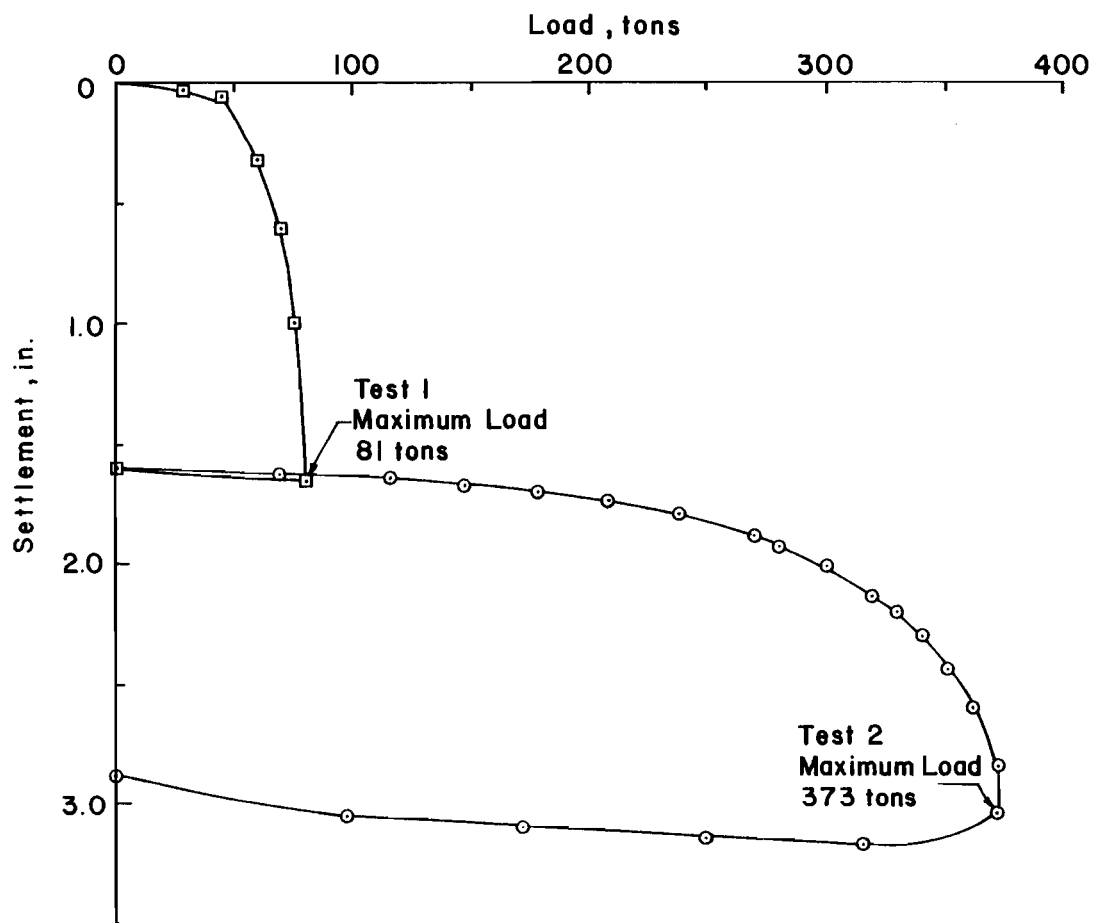


Fig. 5.3 Load Settlement Curves, Test Shaft G-2

increased to 1000 psi, and then the pressure was increased in 400-psi (10-ton) increments until the shaft failed. The pressure at failure was 16,800 psi, which is equivalent to a load of 424 tons. After failure the shaft was unloaded in pressure decrements of approximately 4000-psi (102 tons). The complete test, loading and unloading, lasted about two hours and 45 minutes.

The load-settlement curves of the load tests performed on test shaft G-3 are shown in Fig. 5.4. As indicated in the figure, the maximum load in test 1 was 209 tons and the maximum settlement was 1.23 in. After unloading and rebound, the permanent settlement of the shaft was 1.11 in. In test 2, after grouting, the load at failure was 424 tons and the maximum settlement for the test was 1.88 in. Upon unloading, the shaft rebounded and there was a permanent settlement of 1.71 in. with reference to the position of the shaft at the beginning of test 2.

Test Site 2 - Galveston, Texas

Test Arrangement. The testing arrangement at this site consisted of two reaction shafts and one test shaft. The reaction shafts were both 30 in. in diameter by 80 ft in length, with a small underream (exact size of underream is not known). The test shaft, designated as G-4, was 24 in. in diameter by 80 ft in length. This shaft was instrumented. The arrangement of the two reaction shafts and the test shaft is shown in Fig. 5.5.

Test Results (G-4). Detailed information on this load test, such as the exact date of the test, load increments used, permanent settlement, and duration of test, are not available. It is known that the test was run in June of 1978 and that the shaft plunged at an axial load of 225 tons. Figure 5.6 shows the curve giving settlement of the top of the shaft as a function of axial load.

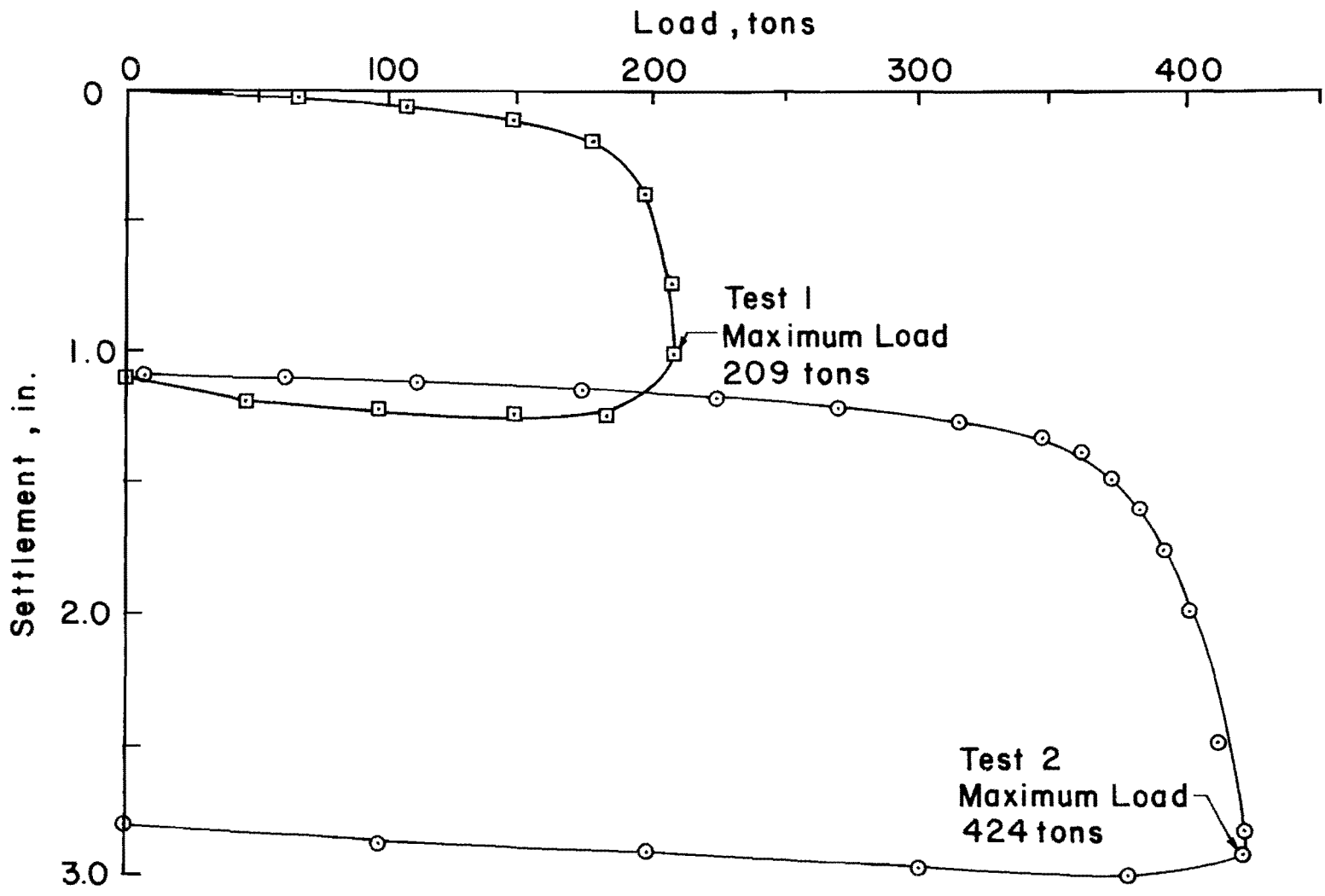


Fig. 5.4 Load Settlement Curves, Test Shaft G-3

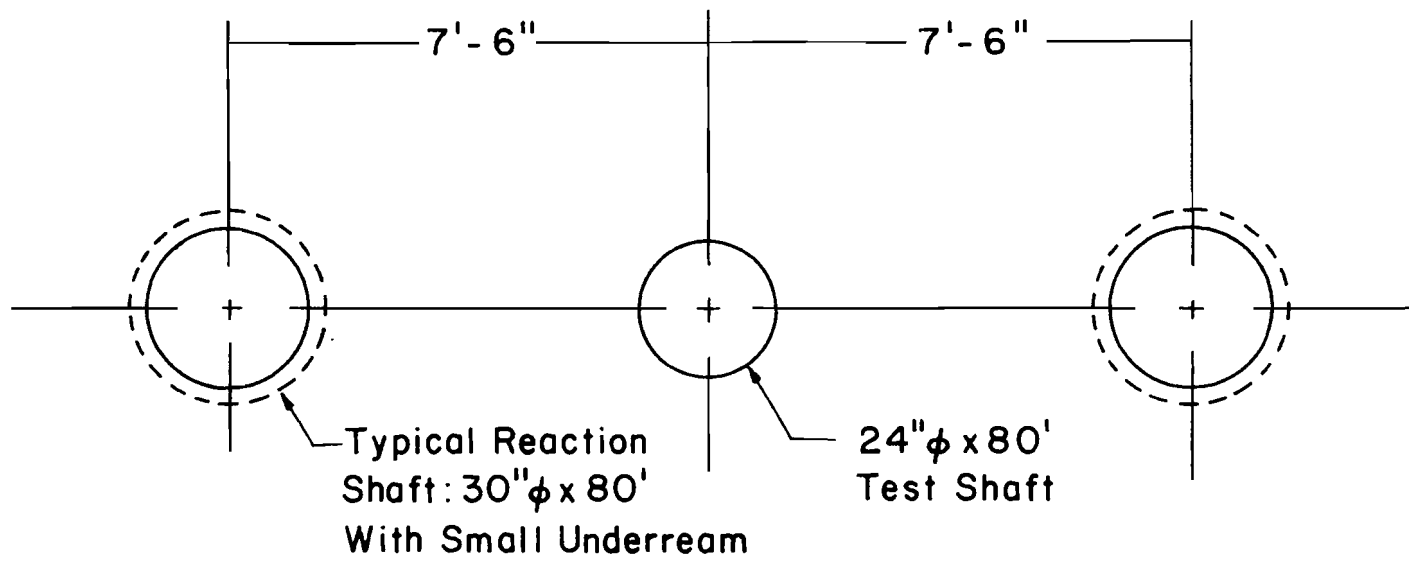


Fig. 5.5 Testing Arrangement, Test Site 2

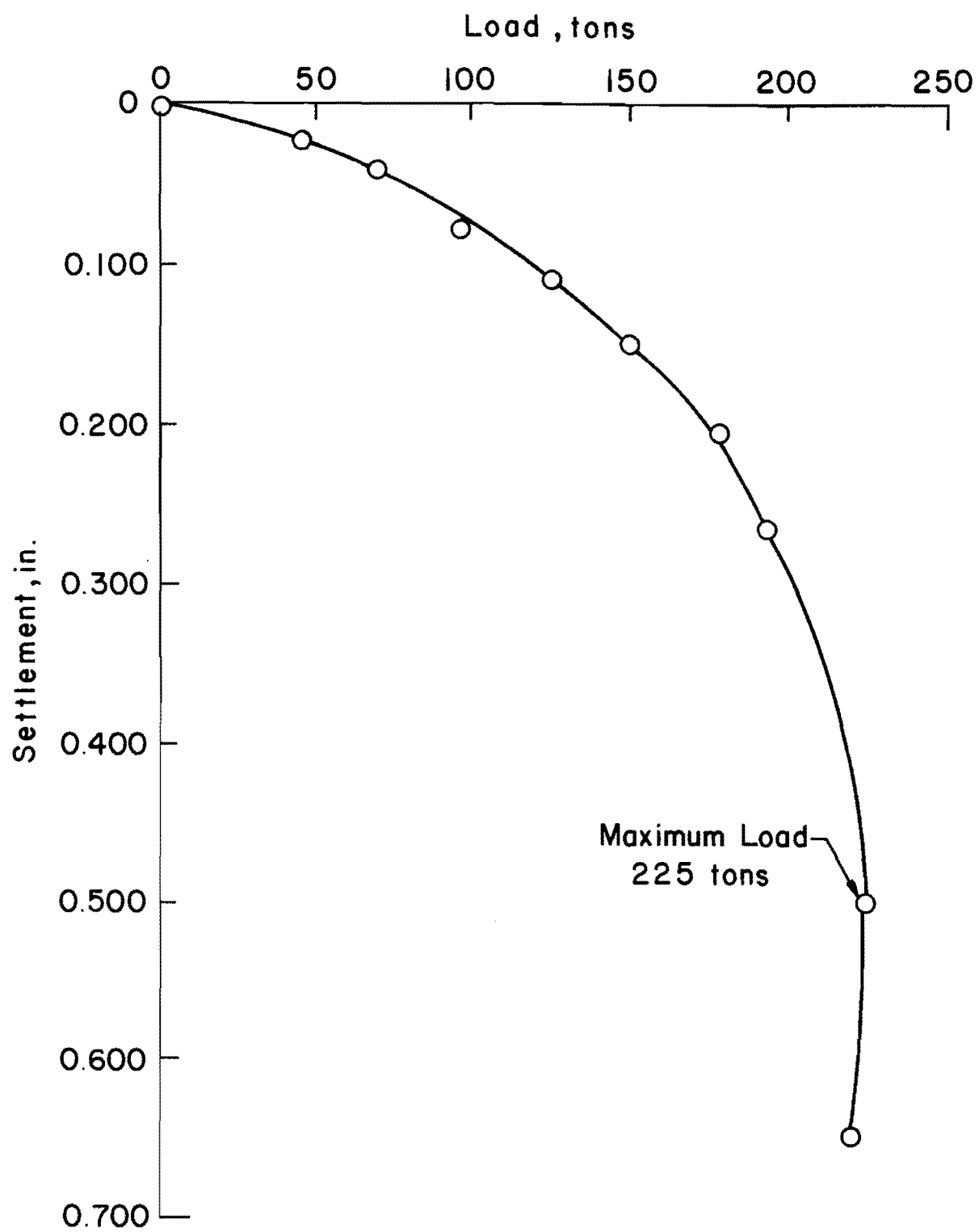


Fig. 5.6 Load Settlement Curve, Test Shaft C-3

Test Site 3 - Eastern Site

Test Arrangement

The testing arrangement at this site consisted of four reaction shafts and two test shafts. All four reaction shafts were 36 in. in diameter by 65 ft in length. The first test shaft, designated as E-1, was 36 in. in diameter by 60 ft in length, with a casing extending the full length of the shaft. The second test shaft, designated E-2, was also 36 in. in diameter by 60 ft in length, but had no casing. The testing arrangement of the Eastern site is shown in Fig. 5.7.

Test Results

Test Shaft E-1. The load test of test shaft E-1 was performed on February 2, 1981, twenty days after construction of the shaft. The test was started at 2:45 p.m. A seating pressure of 500 psi was applied to the hydraulic jack. The hydraulic jack being used had a capacity of 1250 tons. The pressure on the jack was then increased to 1000 psi after which it was increased in 400 psi increments (approximately 30 tons) increments to failure. Failure occurred at a jack pressure of 4800 psi which was equivalent to a load of 345 tons.

The time to load the shaft was approximately 45 minutes. After attaining the ultimate capacity, the shaft was unloaded in 1000 psi (59 ton) decrements. Unloading began at 3:40 p.m. and took approximately 20 minutes.

The load-settlement curve for the top of the shaft is shown in Fig. 5.8. As indicated in the figure, the maximum load was 345 tons and the maximum settlement was 1.06 in. Upon unloading, the shaft rebounded and the permanent settlement was 0.92 in.

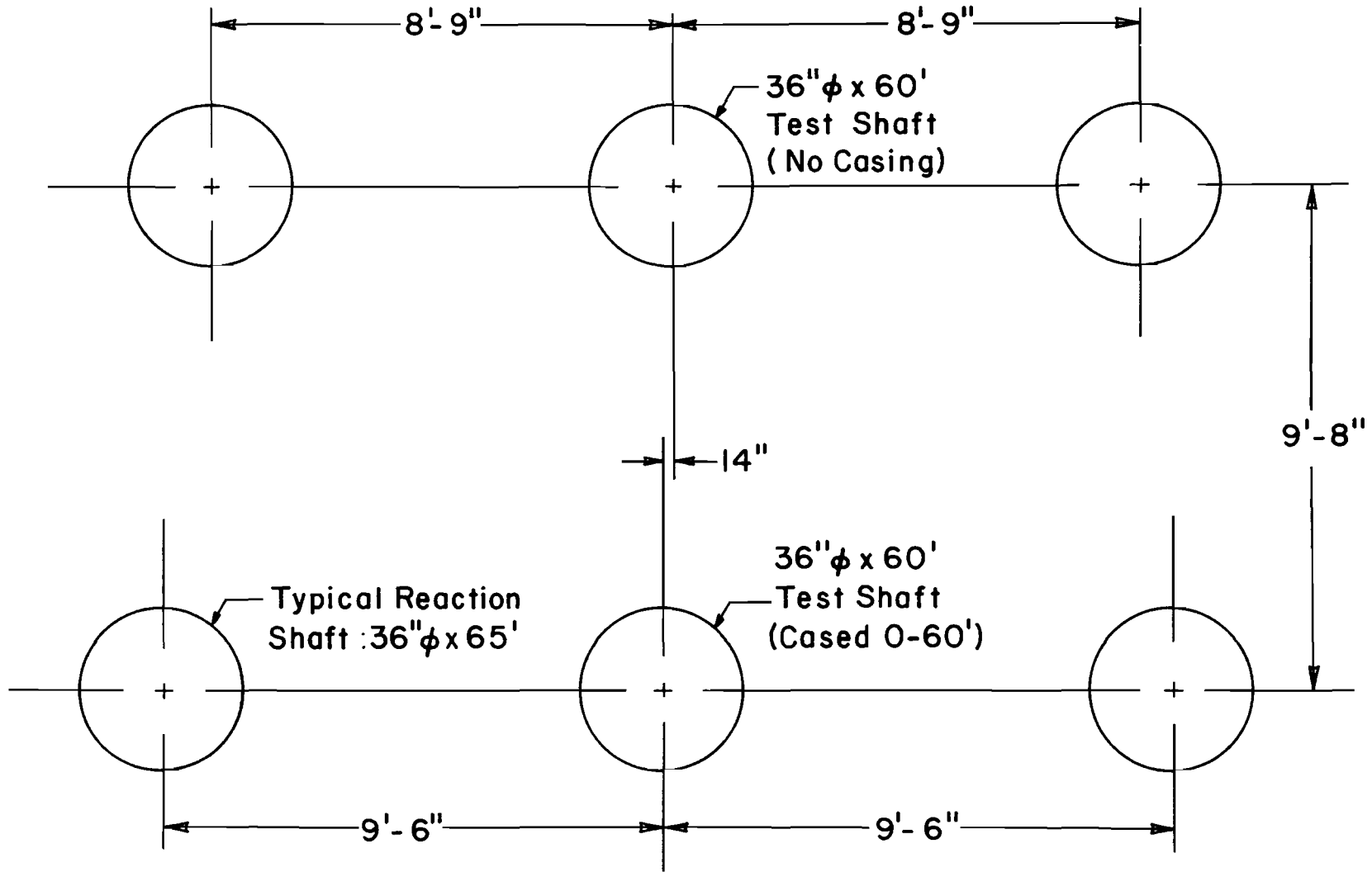


Fig. 5.7 Testing Arrangement, Test Site 4

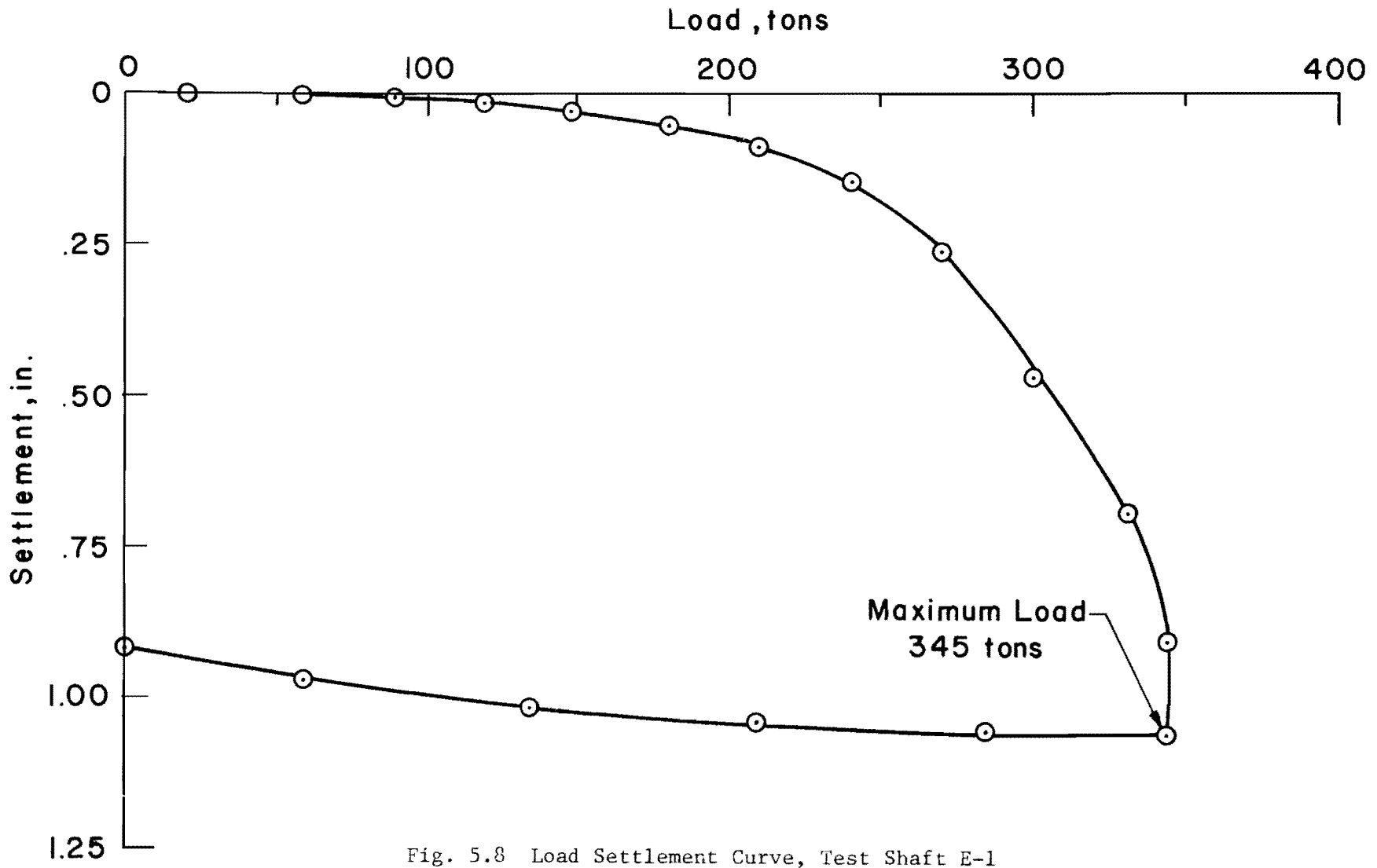


Fig. 5.8 Load Settlement Curve, Test Shaft E-1

Test Shaft E-2. The shaft E-2 was load-tested on February 4, 1981, eight days after construction of the shaft. The test was started at 11:15 a.m. A seating pressure of 500 psi (equivalent to a load of 21 tons) was applied to the hydraulic jack. The hydraulic jack being used had a capacity of 1250 tons. The pressure on the jack was then increased to 1000 psi, after which it was increased in 400-psi increments (approximately 30-ton increments of load) to failure. Failure occurred at a jack pressure of 11,700 psi which was equivalent to a load of 865 tons.

The time to load the shaft was 1 hour and 55 minutes. After attaining the ultimate load, the shaft was unloaded in 3000-psi (210-ton) decrements. Unloading began at 1:15 p.m. and took approximately 15 minutes.

The load-settlement curve for the top of the shaft is shown in Fig. 5.9. As indicated in the figure, the maximum load was 865 tons and the maximum settlement was 1.90 in. Upon unloading, the shaft rebounded and the permanent settlement was 1.56 in.

As mentioned previously, the reaction shafts for the tests at the Eastern site were 36 in. in diameter by 65 ft in length, only 5 ft longer than the test shafts. Because of the reaction shafts being only 5 ft longer than the test shaft and the construction problems mentioned in the previous chapter, the movements of the reaction shafts were monitored. The uplifts of the reaction shafts were measured by a single dial gauge on each shaft. During the load test of shaft E-1, there was no significant movement, but during the load test of shaft E-2, one reaction shaft moved 1.68 in. and the other moved 2.17 in. The load-uplift curves for the reaction shafts used in the load test of shaft E-2 are shown in Fig. 5.10. The load on each reaction shaft is one-half the load on the test shaft. The movements of the reaction shafts

gave additional information on resistance in skin friction. This information will be discussed in a later chapter.

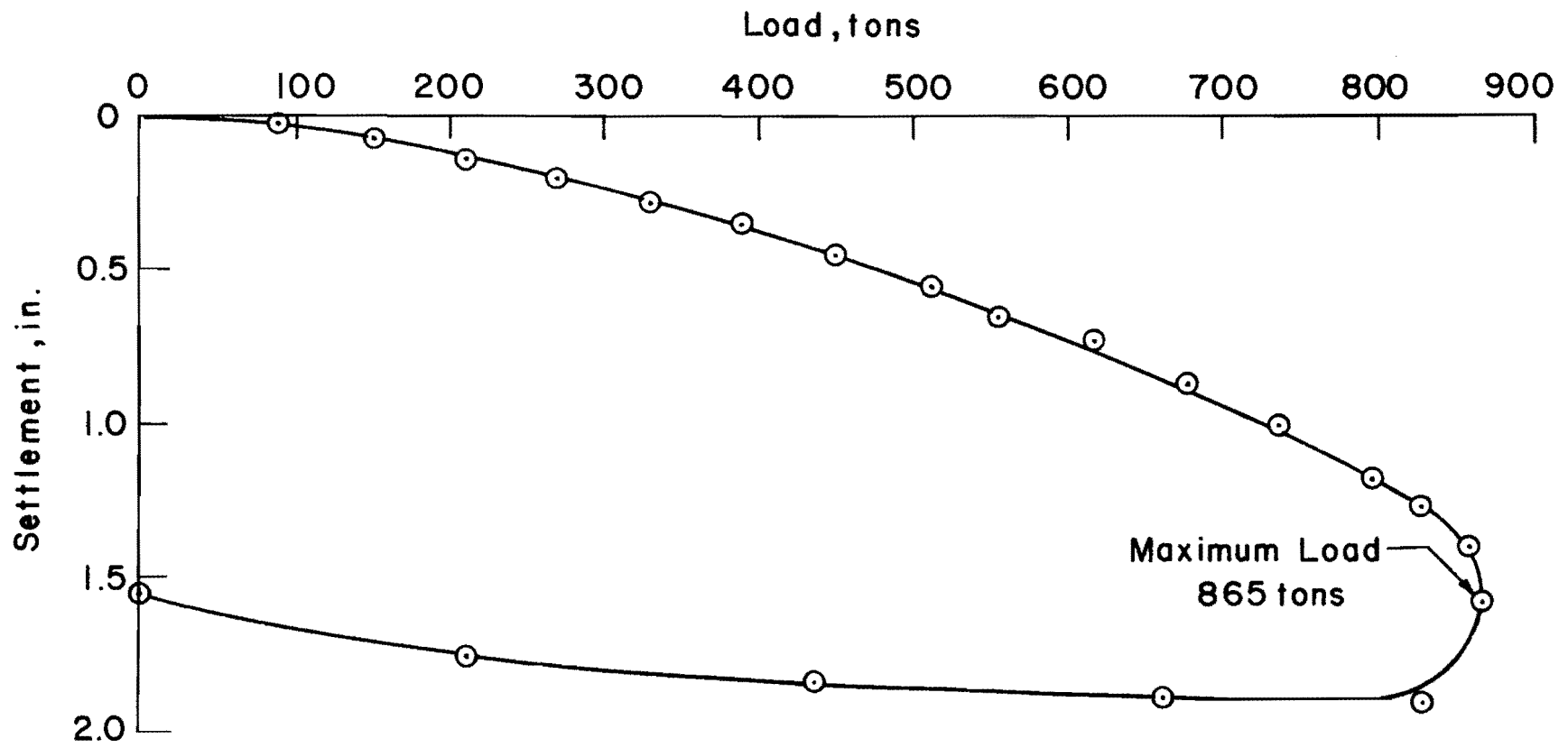


Fig. 5.9 Load Settlement Curve, Test Shaft E-2

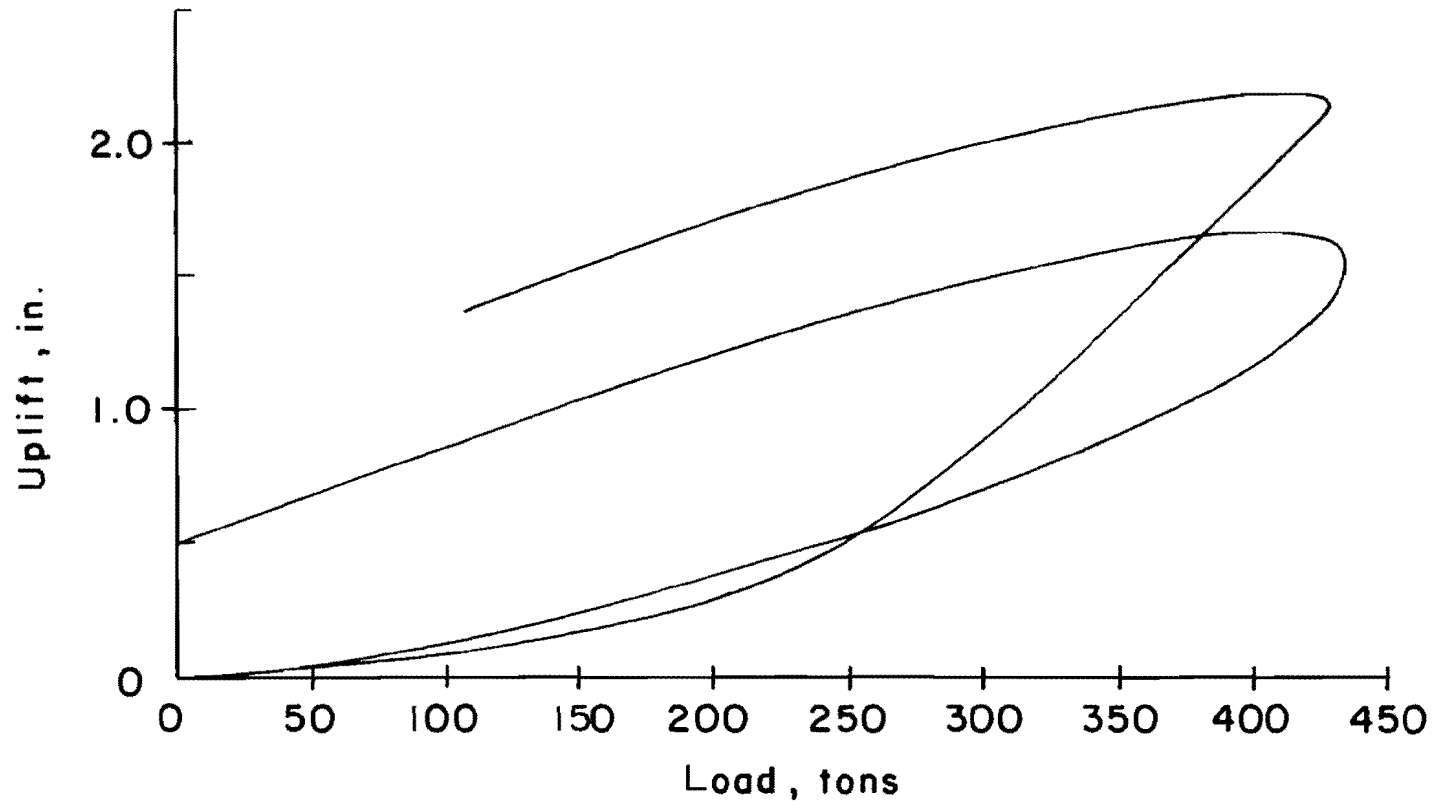


Fig. 5.10 Load Uplift Curves for Reaction Shafts, Test Site E-2

CHAPTER 6. ANALYSIS AND DISCUSSION OF LOAD TESTS

Method of Analysis

Mustran Cell Behavior. The first step in the reduction of the data was to determine if any of the Mustran cells were operating improperly. The changes in Mustran cell readings (change from Mustran cell reading when load was zero) were plotted versus the applied load. For comparison purposes, all the readings of Mustran cells at a particular level were plotted on the same sheet. Best-fit curves were then drawn through the readings from each cell to eliminate any small erratic behavior in the readings. The slopes of these curves are a function of the shaft properties and of the load transfer characteristics of the shaft. These curves were then examined and any Mustran cell exhibiting behavior that was obviously in error was eliminated. Observations concerning these curves are discussed in detail by Touma and Reese (1972). Finally, an average curve was drawn for each level of Mustran cells. These average curves were then used to determine the load at the different levels throughout the shaft.

Calibration of Mustran Cells. The purpose of the top level (calibration level) of Mustran cells was to establish a response curve relating the load in the shaft to the Mustran cell readings. The Mustran cells near the top of the shaft were used for calibration for two reasons:

1. The load at the calibration level is known because there is no load transfer above the level of the calibration cells.

2. The dimensions of the shaft near the ground surface are known accurately.

The calibration curve is then used to convert the readings of Mustran cells at other levels into units of load by assuming that there is a uniformity in the properties of the shaft at each level of Mustran cells.

There are instances when it is known that the properties of the shaft at a particular cell level are not the same as at the calibration level. One such instance is when the diameters are not the same. This occurs on occasions where a casing is used in the construction of part of the shaft. The difference in diameters can be compensated for by adjusting the calibration curve. Adjustment is done by taking the Mustran cell readings from the calibration curve, for different loads, and multiplying them by the ratio of the stiffness of the shaft at the calibration level to the stiffness of the shaft at the level with a smaller diameter. This is shown in the following equation:

$$R_2 = R_1 \frac{EA_1}{EA_2} \quad (6.1)$$

where

R_1 = Mustran cell reading from original calibration curve,

R_2 = adjusted Mustran cell reading for new calibration curve,

EA_1 = stiffness of shaft at calibration level, and

EA_2 = stiffness of shaft at Mustran cell level of lesser diameter.

The adjusted calibration curve is then used for the Mustran cells that are in that part of the shaft with a different diameter.

Also, the shaft properties are not the same at all levels if there is a difference in concrete strength with depth. An example of this is shown in Fig. 6.1. This plot was constructed from unpublished data obtained from the Corps of Engineers. The data are from results of tests of cores from seven different shafts. The plot shows that there is a maximum difference of 2 ksi over a depth of 50 ft. The increase in strength is due to two effects, (1) curing of concrete below the water table and, (2) an increase in strength with depth due to increasing pressure. The possible difference in shaft property with depth is not considered in the analysis described herein because such data as shown in Fig. 6.1 were not available. Furthermore, if cores had been taken from the test shafts with results as shown in Fig. 6.1, corrections would not be very significant.

Load-Distribution Curves. After the calibration curve and individual curves for the Mustran cell readings at the various depths have been plotted, the loads at the different levels within the shaft were determined for each chosen load. Once the load in the shaft was known for each level of Mustran cells, a curve of the load versus depth was plotted. A plot of the load versus depth is known as a "load distribution" curve.

Tip Load. Tip resistance developed at each load was read directly from the load-distribution curves that were calculated for each test. Once the tip load was known, a unit value was calculated by dividing the total load resisted at the tip by the shaft area at the tip, as shown in Eq. 6.2:

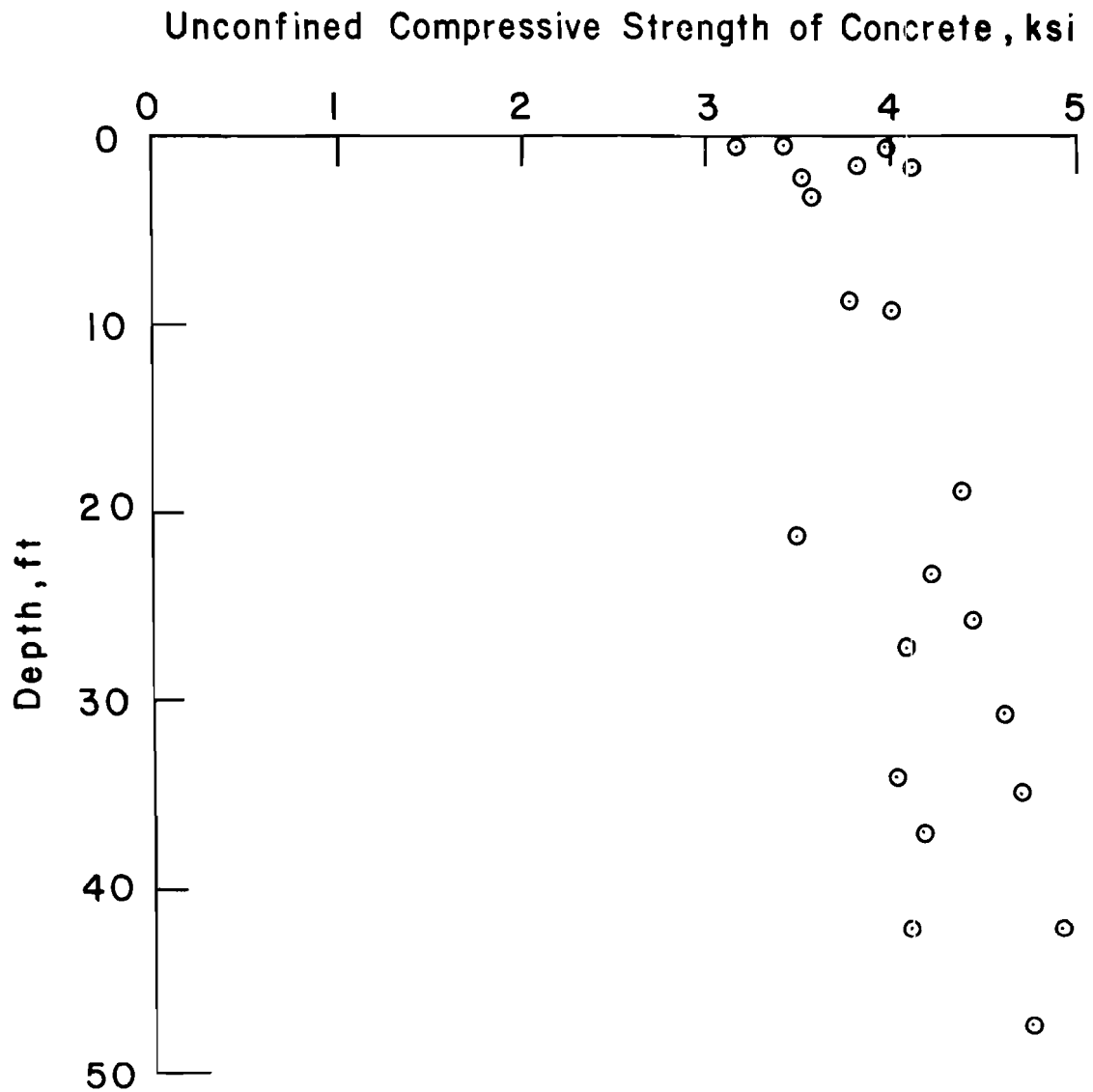


Fig. 6.1 Variation of Concrete Strength as a Function of Depth

$$q = \frac{\text{Total load resisted at tip}}{\text{Shaft area at tip}} \quad (6.2)$$

After the unit value of tip resistance was calculated, a curve showing the unit tip resistance versus tip movement was plotted. The procedure for computing tip movement will be discussed later.

Side Resistance. The total load carried in side resistance (skin friction) was determined by subtracting the load carried at the tip from the applied load. The load transfer is the load per unit area transferred to the supporting material and can be computed at any point from the slope of the load-distribution curve at that point. In this report, values of load transfer were calculated over ten-foot intervals along the length of the shafts, except for test shaft E-2, by use of the following procedure. First, the difference between the total load at two points, ten feet apart, was obtained from the load-distribution curves. Then, the load transfer (t) was obtained by use of Eq. 6.3.

$$t = \frac{\text{Total load carried by skin friction over 10 ft interval}}{\text{Surface area of shaft over 10 ft interval}} \quad (6.3)$$

Once values of load transfer are determined, two sets of curves can be plotted. These are: load transfer versus depth and load transfer versus movement. The latter set of curves is for the ten-foot intervals along the shaft.

Shaft Movement. The shaft movement at any point along the shaft for a selected load can be computed from Equation 6.4:

$$\Delta M_x = \Delta M_{top} - \Delta \delta_x \quad (6.4)$$

where

ΔM_x = movement at point x along the shaft, in.,

ΔM_{top} = movement at top, measured by dial indicators, in.,

and

δ_x = elastic compression of test shaft above point x, in.

The elastic compression of the test shaft above a point (δ_x) was calculated from Equation 6.5:

$$\delta_x = \frac{P L_x}{A_t E_c} \quad (6.5)$$

where

- P_x = average load to point x,
 L_x = distance from top of shaft to point x,
 A_t = transformed cross-sectional area of shaft, and
 E_c = modulus of elasticity of concrete.

The value of $P_x L_x$ was determined by finding the area under the load distribution curve to the point x in question.

The transformed cross-sectional area was calculated using the modulus of elasticity of steel and concrete and the cross-sectional area of the steel and concrete in the test shaft. Equation 6.6 was used to calculate the transformed cross-sectional area of the test shaft used in Eq. 6.5:

$$A_t = A_c + \frac{E_s}{E_c} A_s \quad (6.6)$$

where

- A_t = transformed cross-sectional area,
 A_c = cross-sectional area of concrete in test shaft,
 A_s = cross-sectional area of steel in test shaft,
 E_s = modulus of elasticity of steel, and
 E_c = modulus of elasticity of concrete.

The modulus of elasticity of concrete was calculated from the unconfined compressive strength of concrete cylinders tested on the day of the load test. Equation 6.7 was used to calculate the modulus of elasticity of concrete (E_c) that was used in Equations 6.5 and 6.6:

$$E_c = 57,500 \sqrt{f'_c} \quad (6.7)$$

where

$$f'_c = \text{unconfined compressive strength of concrete.}$$

Analysis of Load Tests

The results of the analyses that were performed for each instrumented load test are presented in the following pages. The results are presented in graphical form with only a brief discussion. A more complete discussion and comparison will be presented in a later section.

The results are presented separately for each of the instrumented tests in the following order: the load-distribution curves, load transfer versus shaft movement curves, and the unit end-bearing curves.

Test Shaft G-1. The load-distribution curves are plotted in Fig. 6.2. The curves indicate that little load is being transferred to the soil between the ground surface and 20 ft. At the maximum applied load of 495 tons approximately 56 tons is being carried by the tip.

The curves of load-transfer versus shaft movement are shown in Fig. 6.3. The curves indicate that the maximum load transfer occurs between 30 and 40 ft.

The curve of unit end-bearing versus tip movement is shown in Fig. 6.4. This curve indicates that the maximum bearing capacity of 4.4 tsf was achieved.

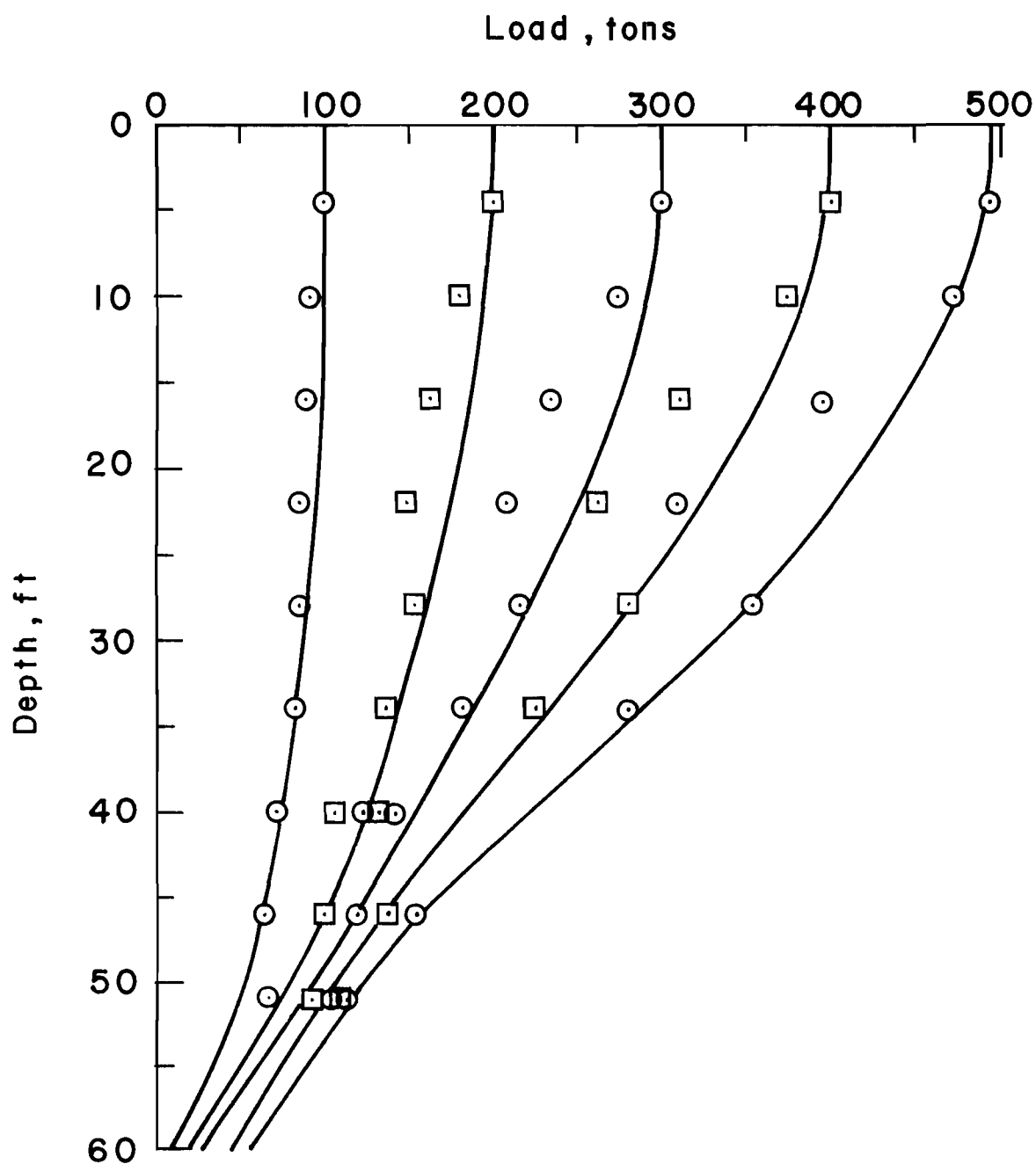


Fig. 6.2 Load Distribution Curves, Test Shaft G-1

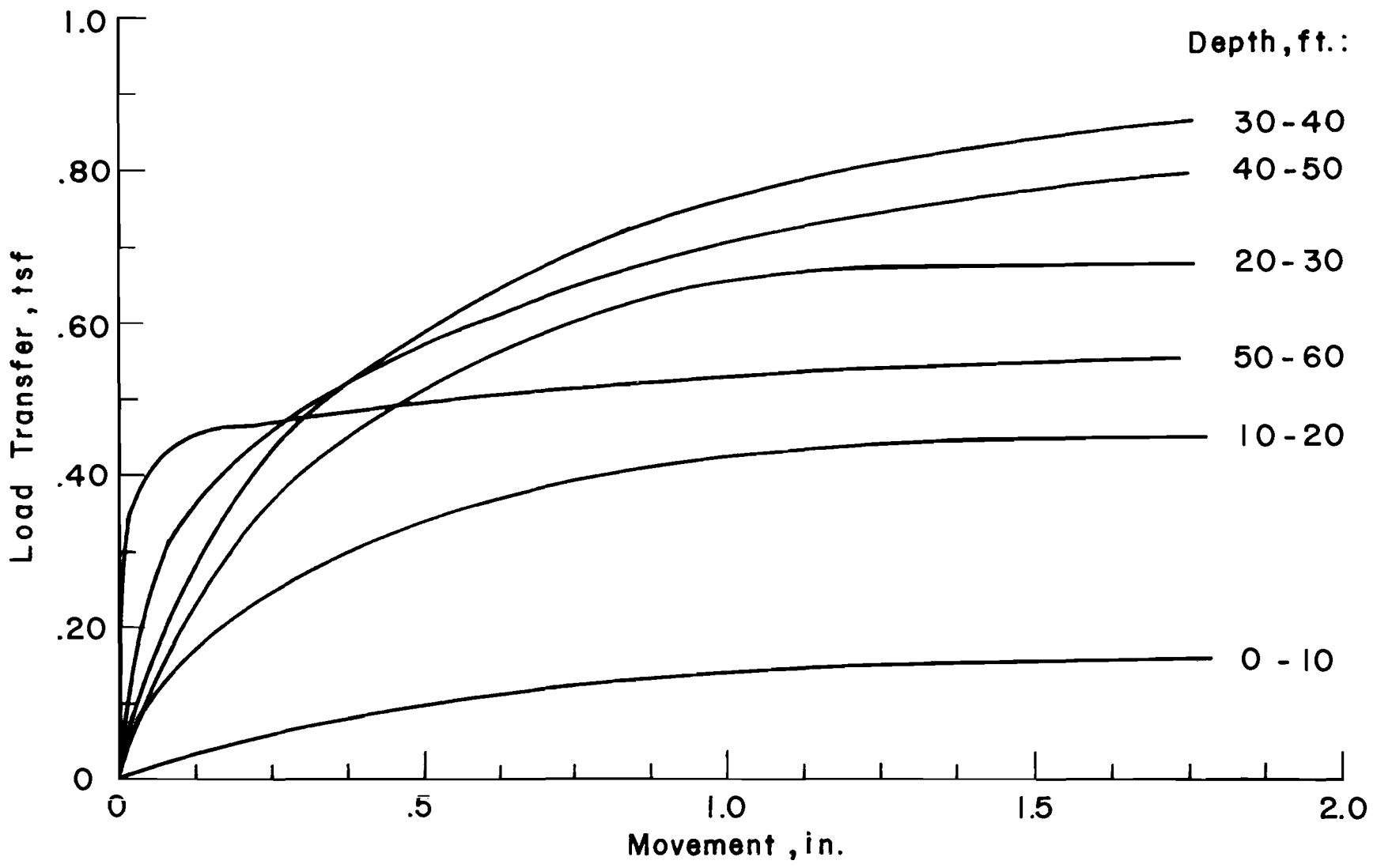


Fig. 6.3 Load Transfer in Skin Friction vs Movement, Test Shaft G-1

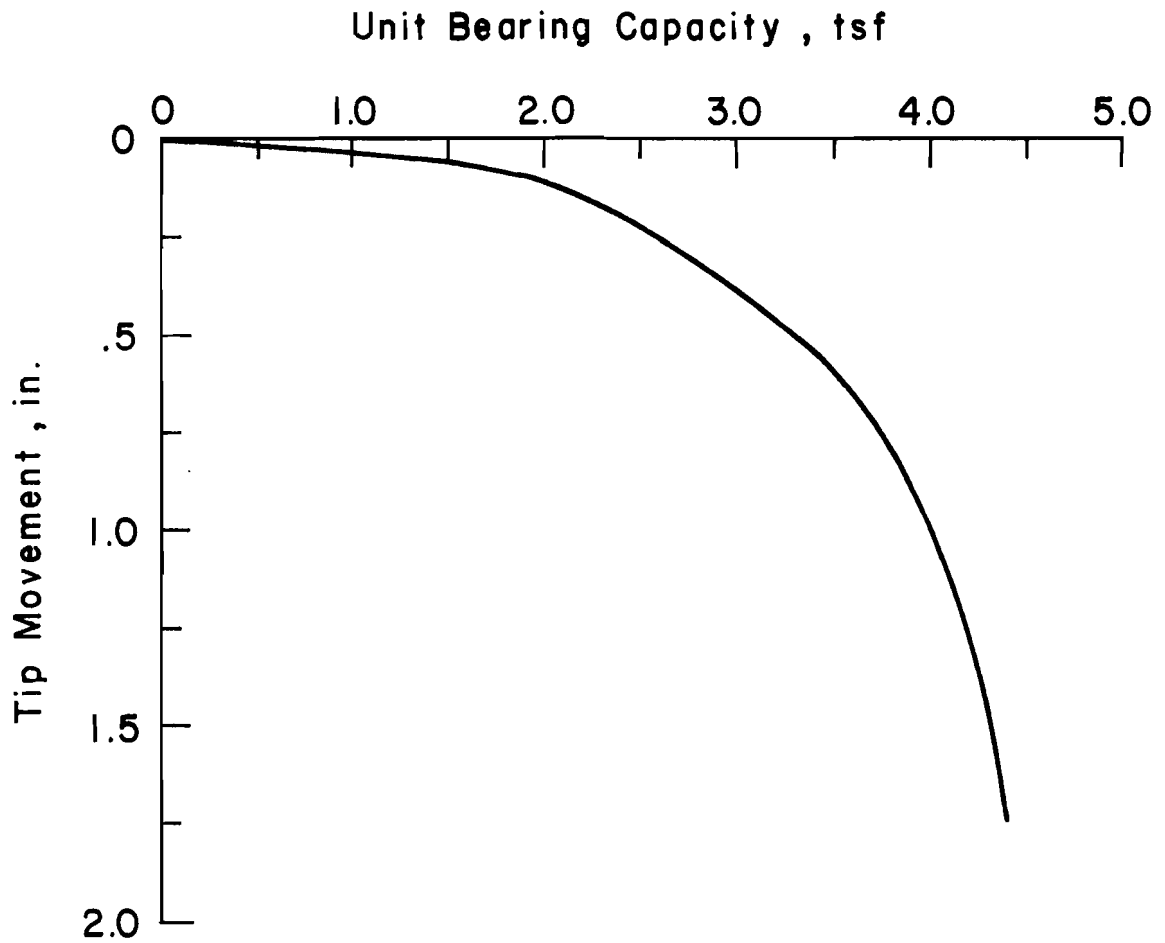


Fig. 6.4 Unit End Bearing Versus Tip Movement, Test Shaft G-1

Test Shaft G-3, Test 1. The load-distribution curves for this test are shown in Fig. 6.5. The curves indicate that very little load was carried in the top 40 ft. of the shaft, which was cased. At the maximum applied load of 209 tons approximately 28 tons was being carried by the tip.

Load-transfer versus shaft-movement curves are shown in Fig. 6.6. The curves indicate that maximum load transfer has been developed at all depths.

The plot of unit end-bearing versus tip movement is shown in Fig. 6.7. The curve shows that the ultimate bearing capacity probably was achieved, at the value of 3.9 tsf.

Test Shaft G-3, Test 2. Load-distribution curves for the second load test on test shaft G-3 are shown in Fig. 6.8. The curves indicate that the load transfer is fairly uniform from 40 to 60 ft and that grouting of the top 40 ft. has definitely increased the load transfer in that region. At the maximum applied load of 424 tons approximately 27 tons was carried by the tip.

Load-transfer versus shaft-movement curves are shown in Fig. 6.9. The curves also indicate that the load-transfer values are fairly constant from 40 to 60 ft. The curves also indicate that maximum values of load transfer were reached at all depths.

A plot showing the unit bearing capacity versus tip movement is shown in Fig. 6.10. The curve indicates that an ultimate value probably was reached and that it is 3.8 tsf.

Test Shaft G-4. The load distribution curves for this shaft are shown in Fig. 6.11. The curves indicate that a negligible amount of load is carried

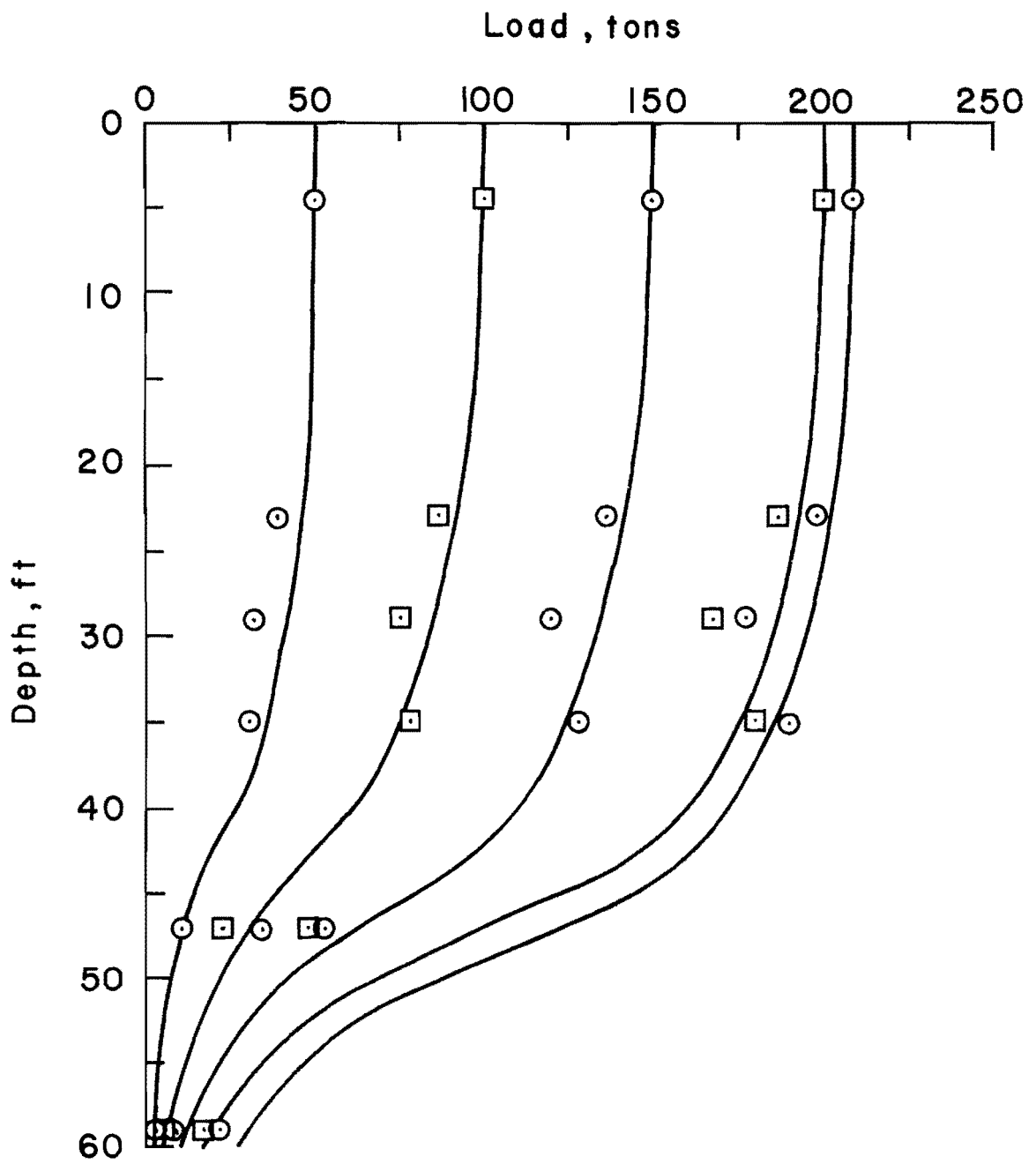


Fig. 6.5 Load Distribution Curves, Test Shaft G-3, Test 1

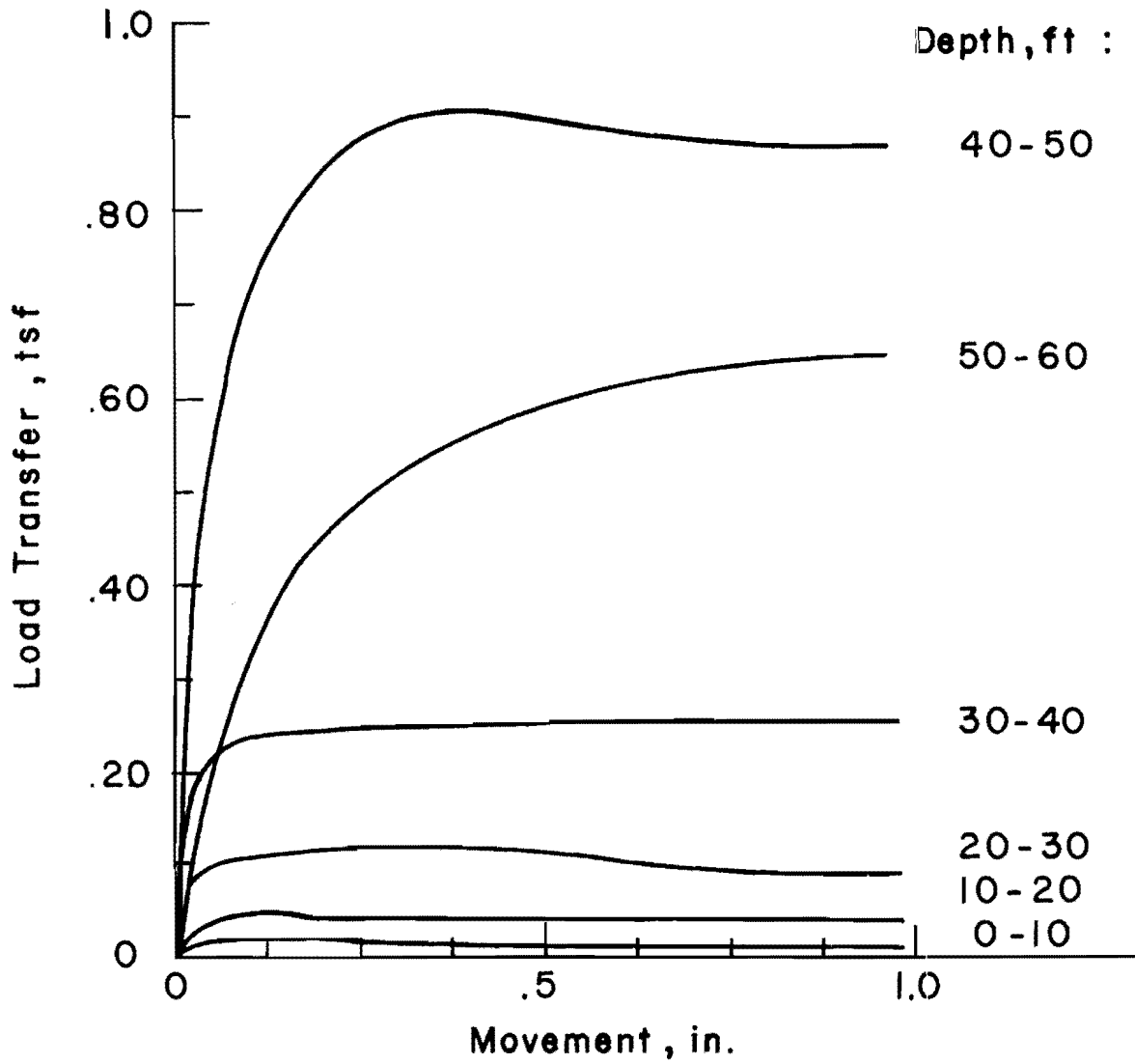


Fig. 6.6 Load Transfer in Skin Friction versus Movement, Test Shaft G-3, Test 1

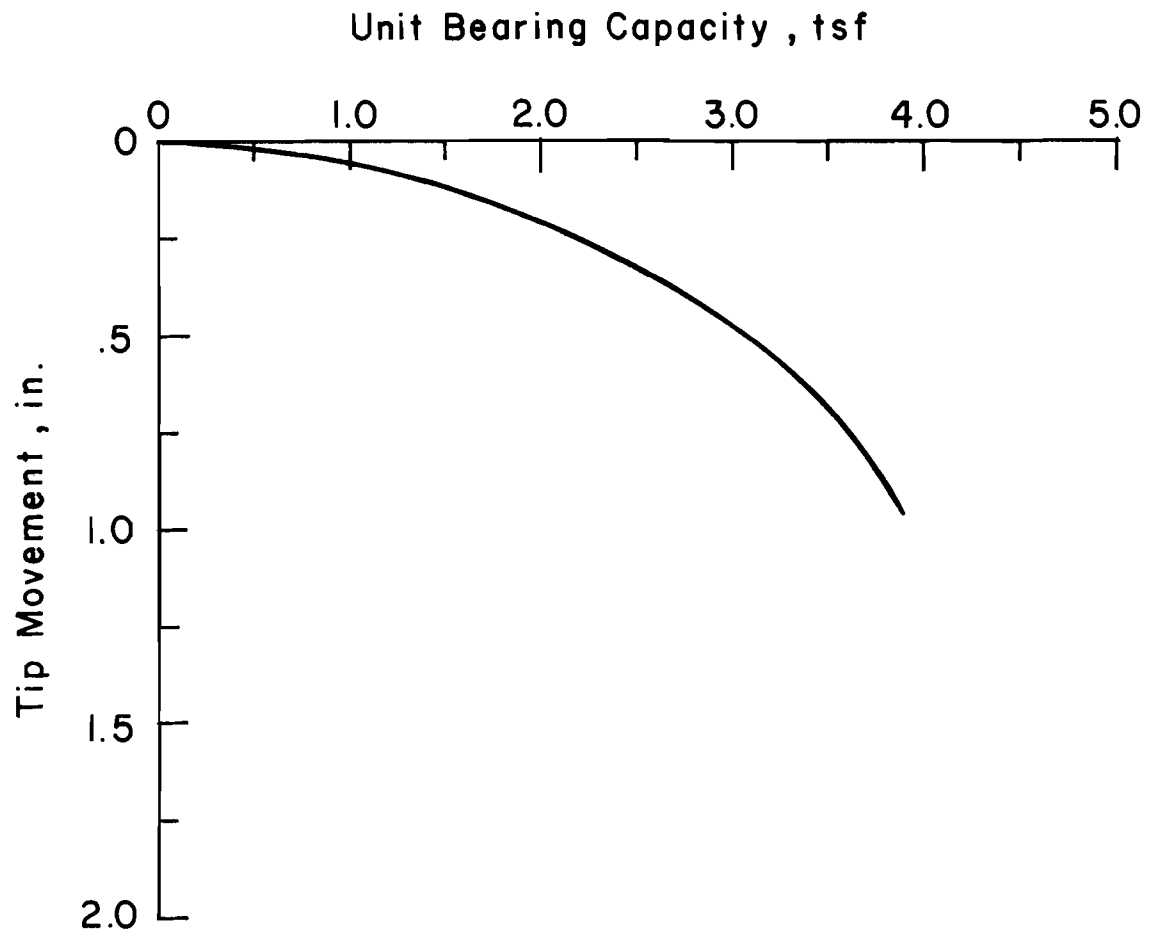


Fig. 6.7 Unit End Bearing versus Tip Movement, Test Shaft G-3, Test 1

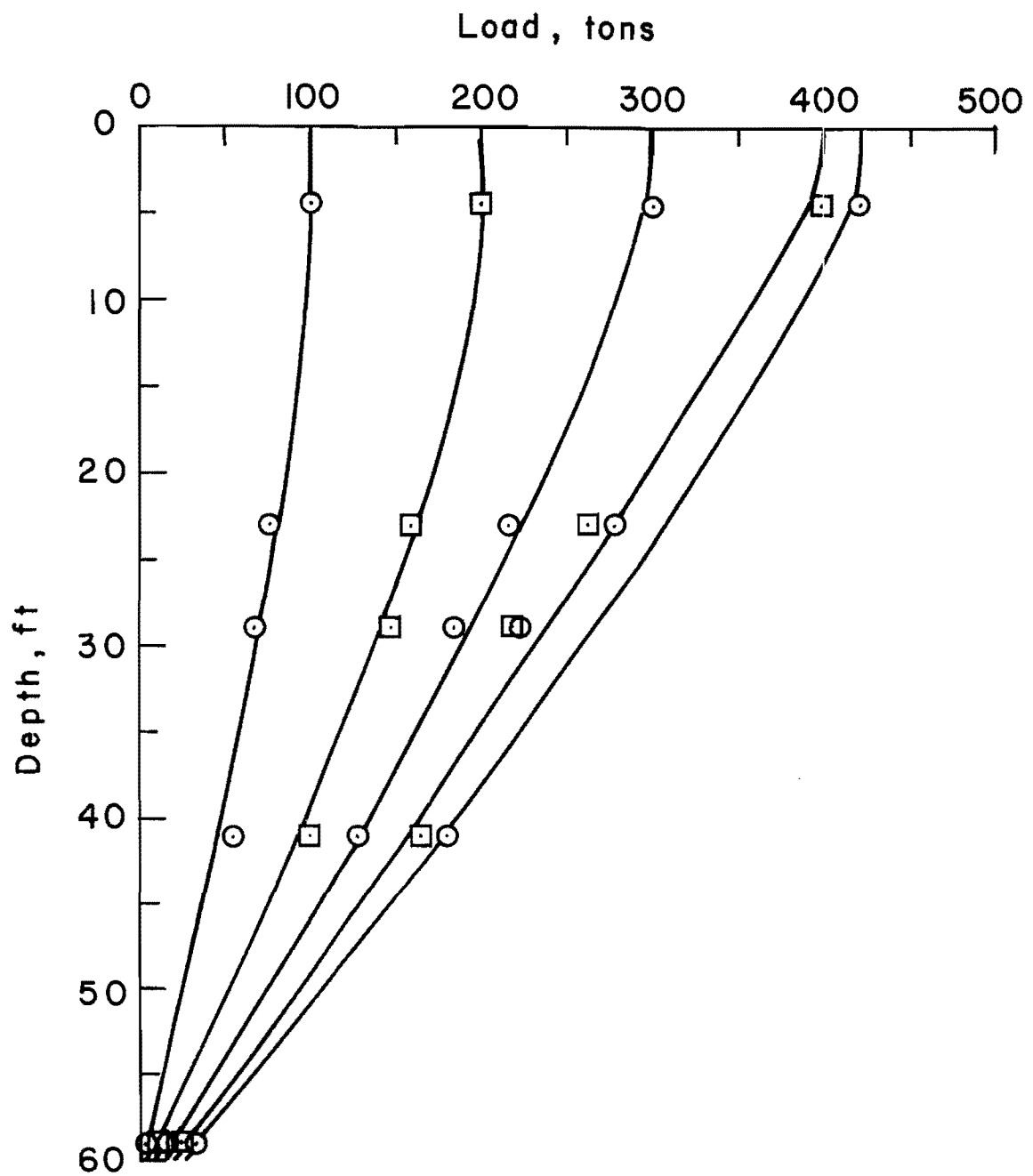


Fig. 6.8 Load Distribution Curves, Test Shaft G-3, Test 2

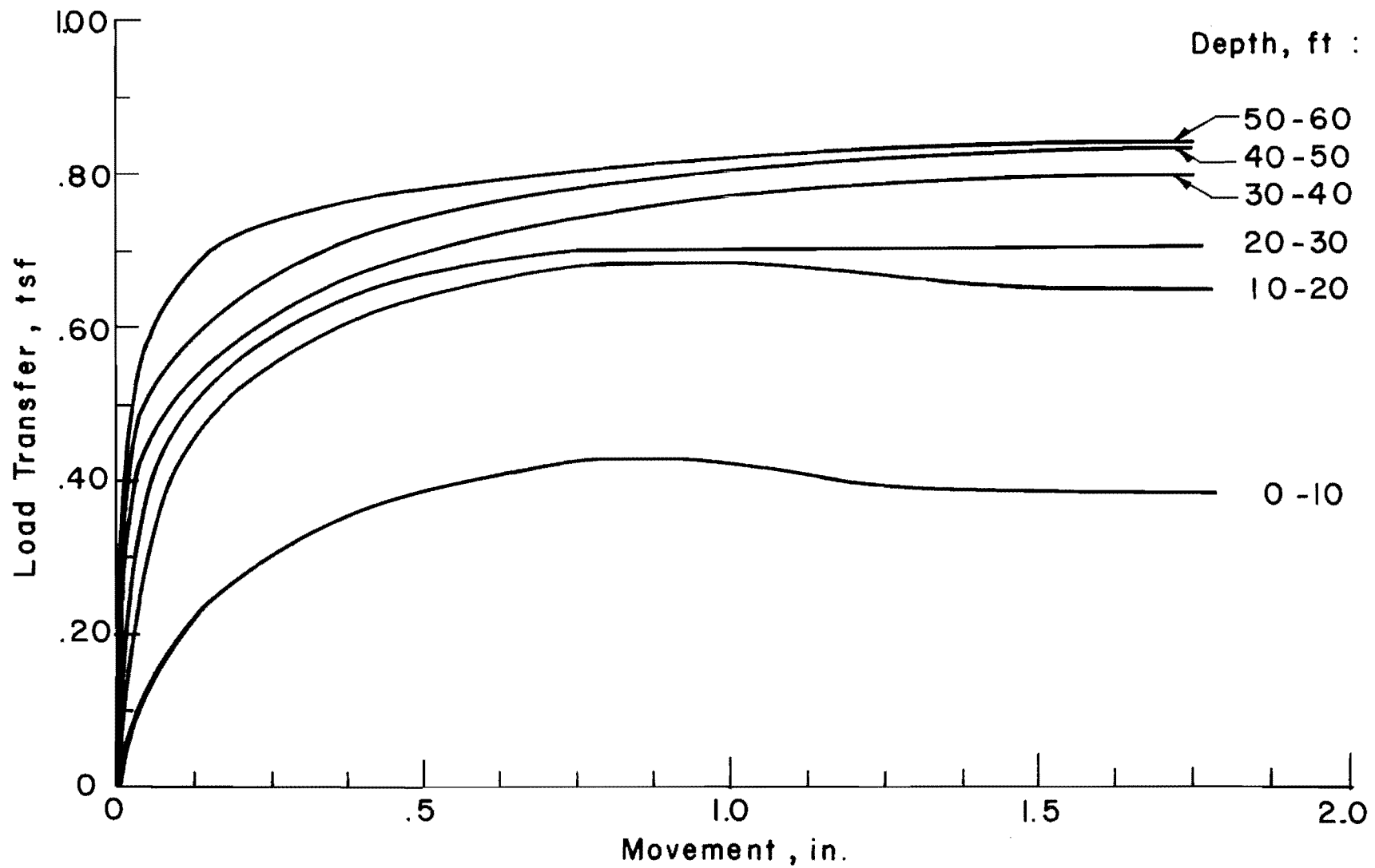


Fig. 6.9 Load Transfer in Skin Friction versus Movement, Test Shaft G-3, Test 2

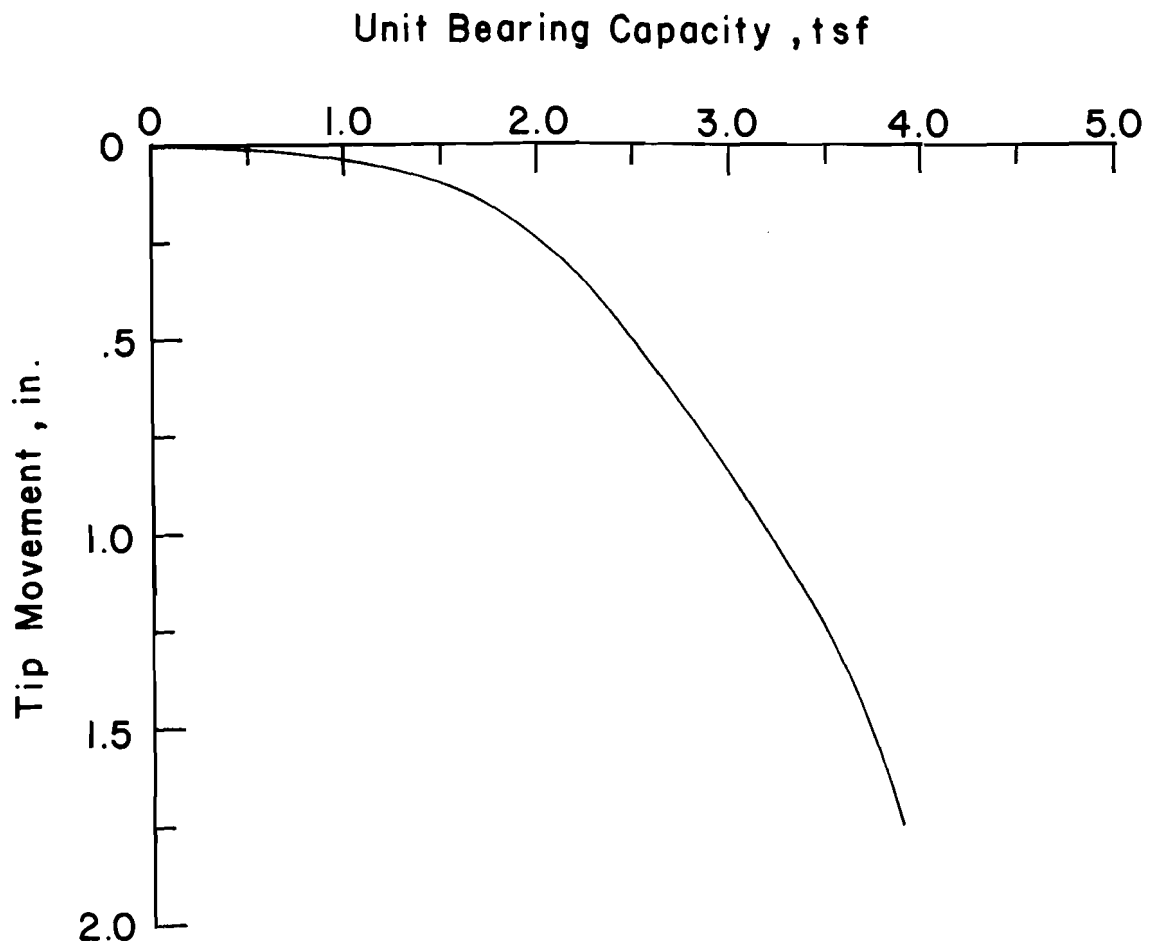


Fig. 6.10 Unit End Bearing versus Tip Movement, Test Shaft C-3, Test 2

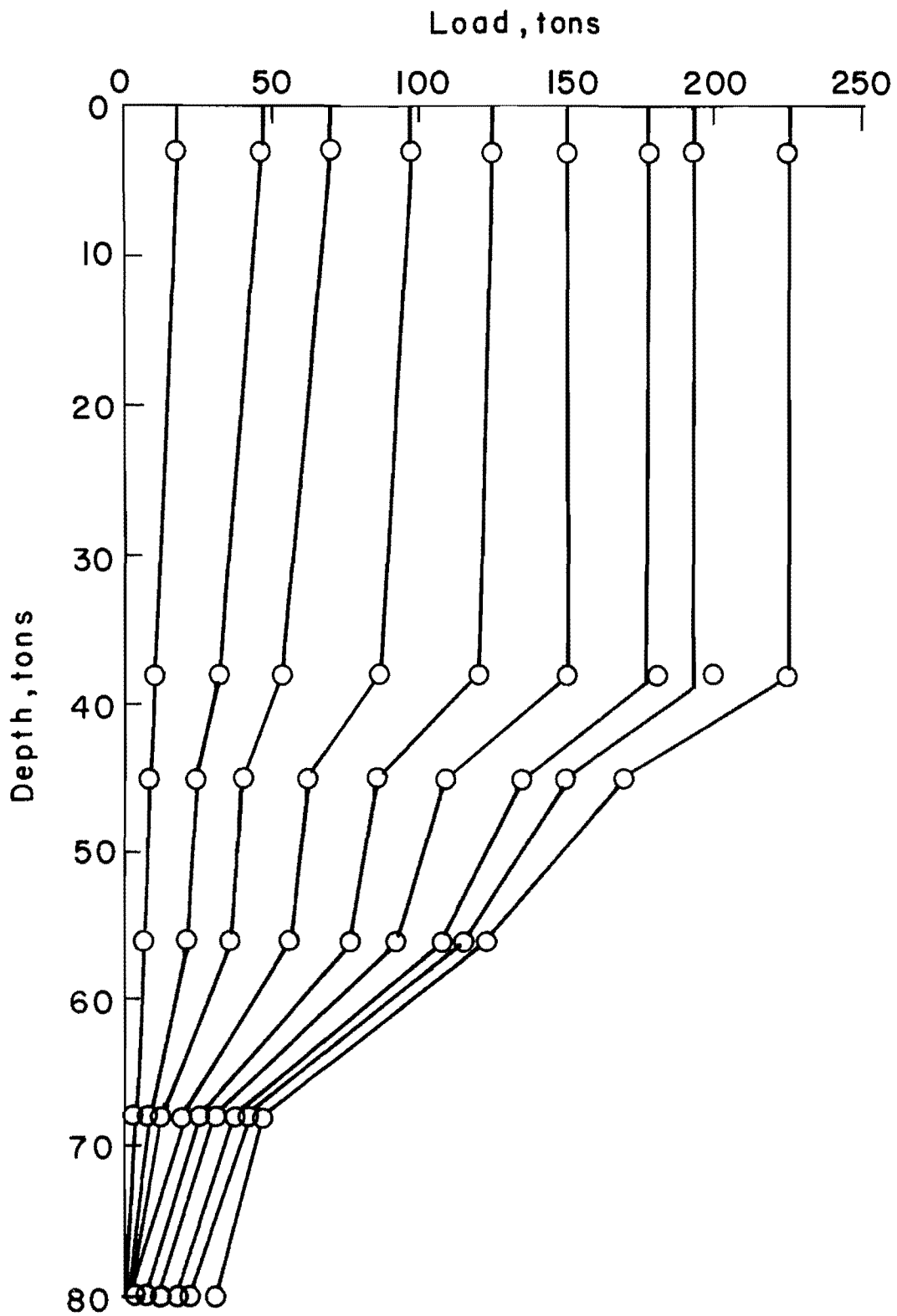


Fig. 6.11 Load Distribution Curves, Test Shaft G-4

in the top 40 ft of the shaft. At the maximum applied load of 225 tons approximately 32 tons were being carried by the tip.

Load-transfer versus shaft-movement curves are shown in Fig. 6.12. The curves indicate that maximum values of load transfer were reached at all depths. The curves show that the maximum load transfer occurred between 40 and 50 ft.

The plot of unit end bearing versus tip movement is shown in Fig. 6.13. The curve shows that the ultimate bearing capacity was reached, at the value of 10.2 tsf.

Test Shaft E-1. Load distribution curves for this shaft are shown in Fig. 6.14. The curves indicate that the load transfer in the top 10 ft. (0-10 ft.) and the bottom 10 ft. (50-60 ft.) is very small. The load-distribution curves also show that at the maximum applied load of 345 tons approximately 99 tons were being carried by the tip.

The plots of load transfer versus shaft movement are shown in Fig. 6.15. The load-transfer curves show that the maximum load transfer occurs between 20 and 30 ft. The curves also indicate that maximum load transfer has been developed at all depths.

Unit end-bearing versus tip movement is shown in Fig. 6.16. The curve indicates that the ultimate bearing capacity was achieved at the value of 14.0 tsf.

Test Shaft E-2. Load-distribution curves for this shaft are shown in Fig. 6.17. The curves indicate that very little load is being transferred in the top 20 ft. of the shaft. The load-distribution curves also show that the maximum applied load of 865 tons approximately 420 tons were carried by the tip.

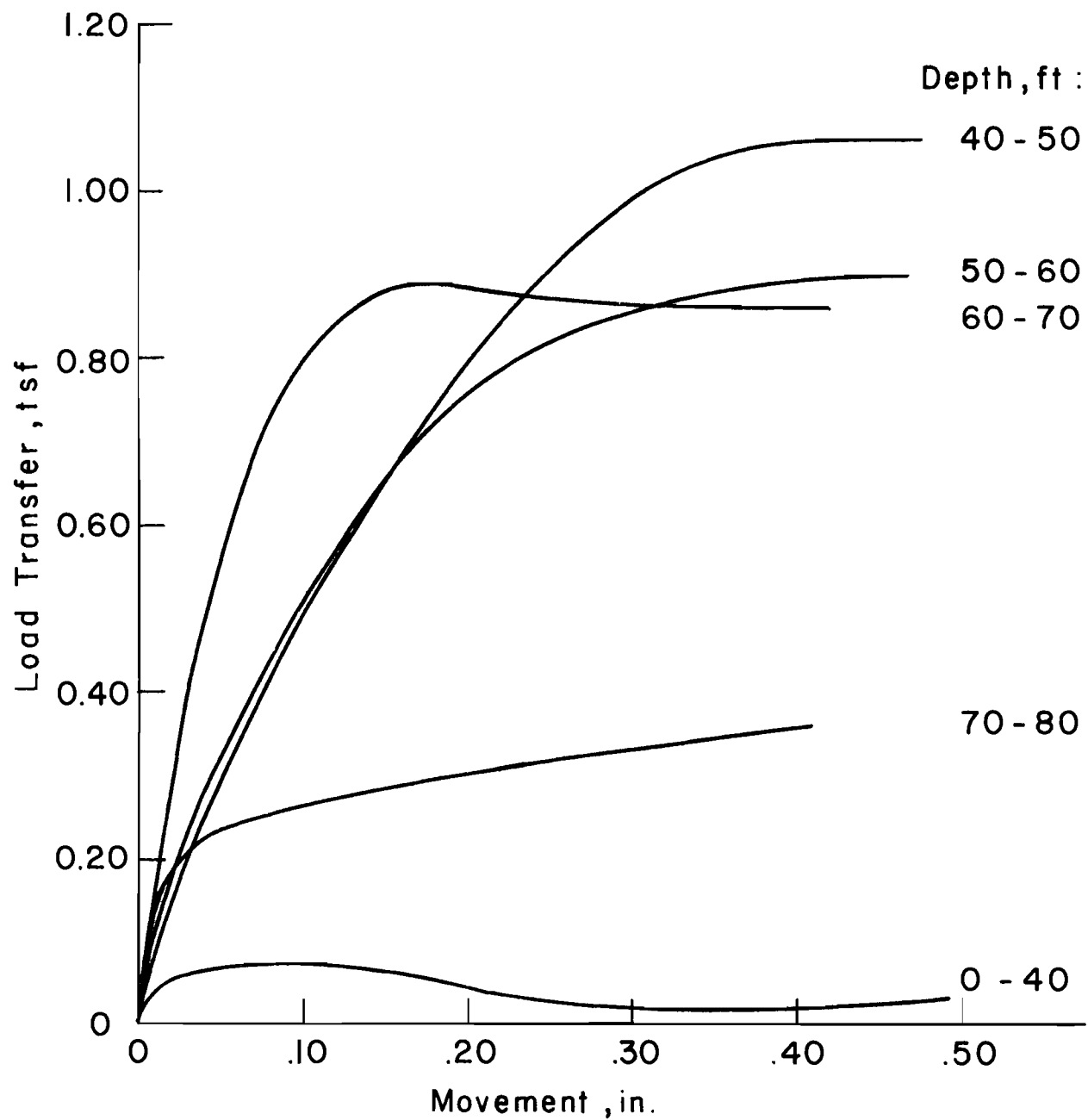


Fig. 6.12 Load Transfer in Skin Friction versus Movement, Test Shaft G-4

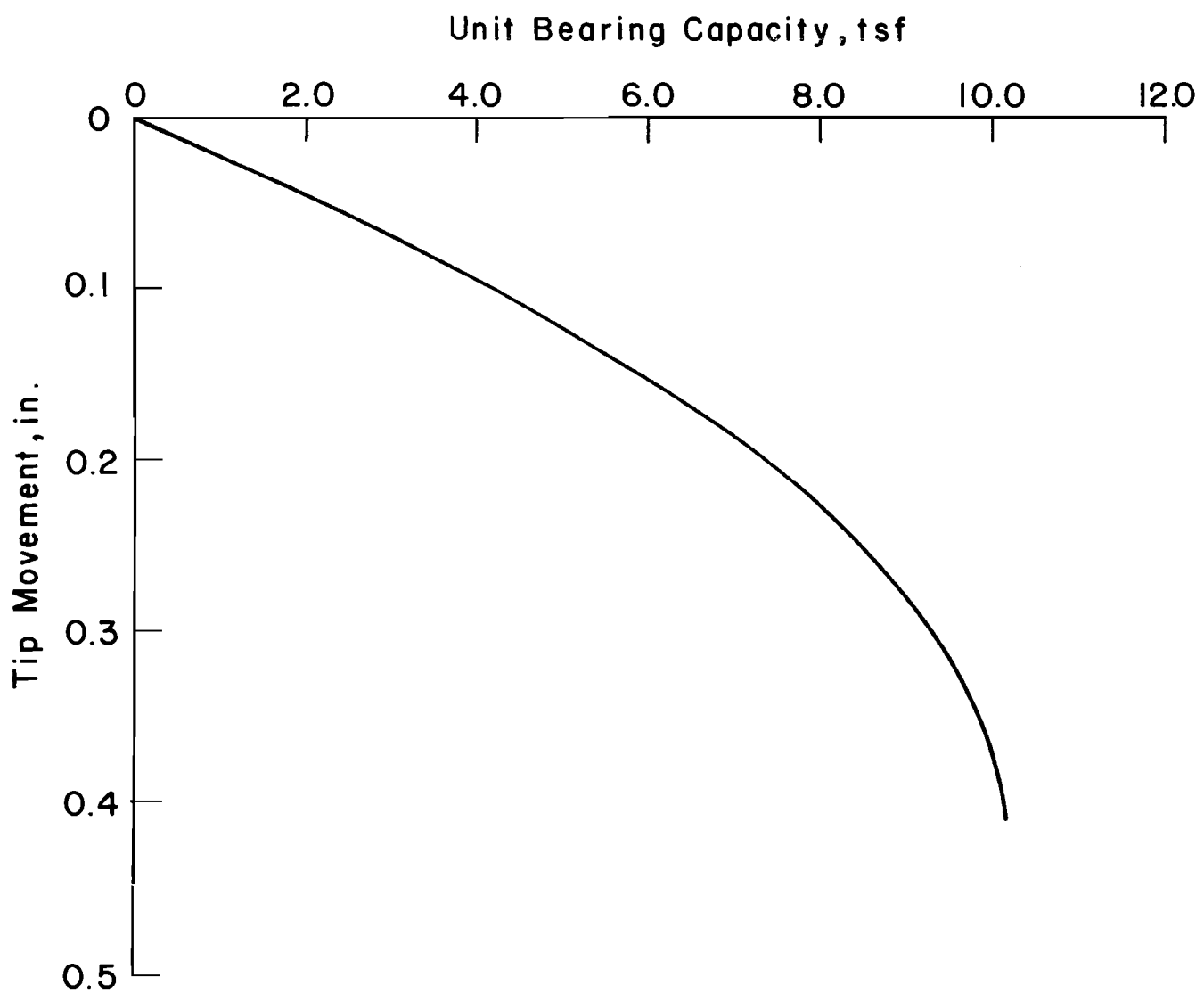


Fig. 6.13 Unit End Bearing versus Tip Movement, Test Shaft G-4

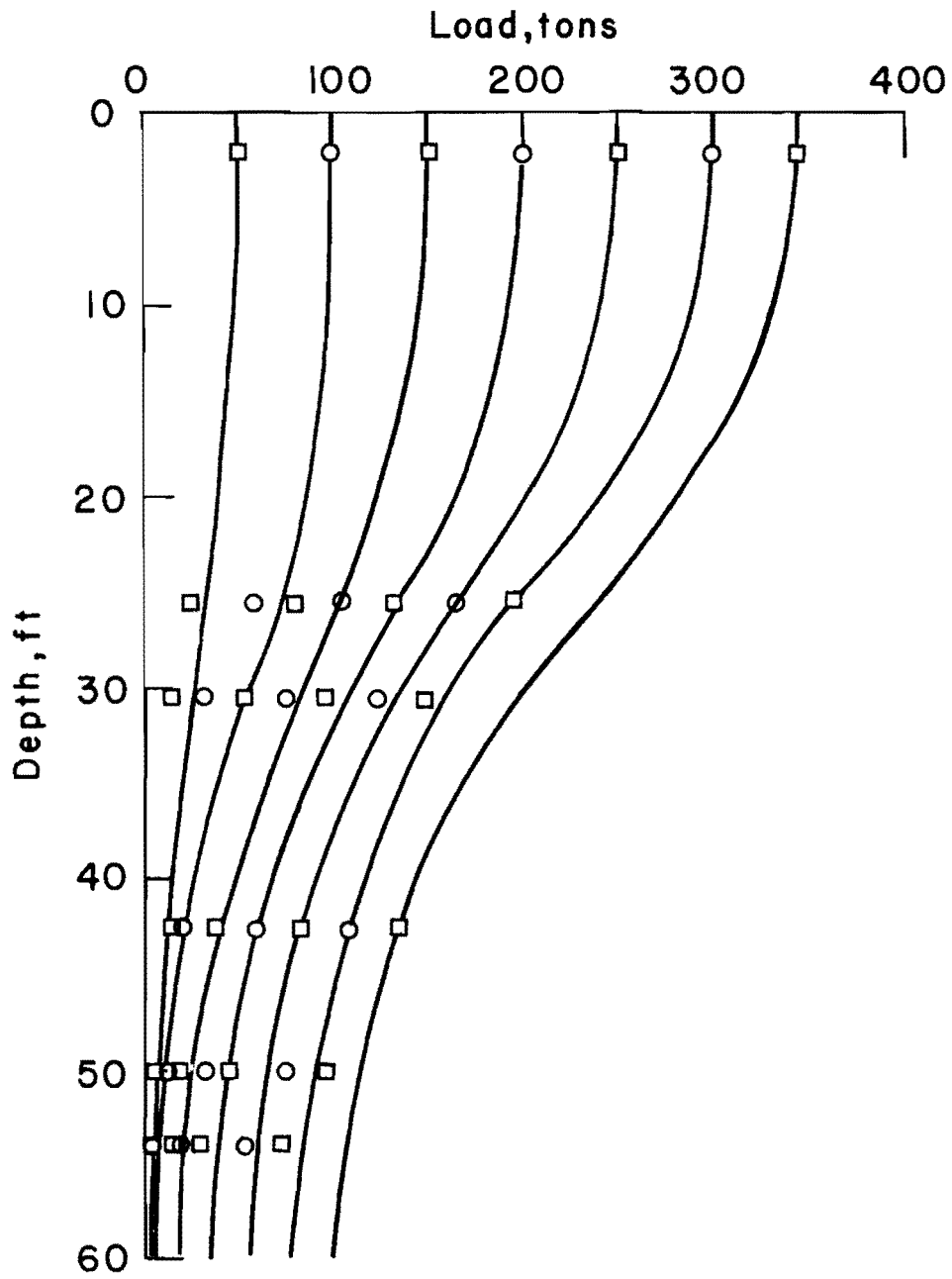


Fig. 6.14 Load Distribution Curves, Test Shaft E-1

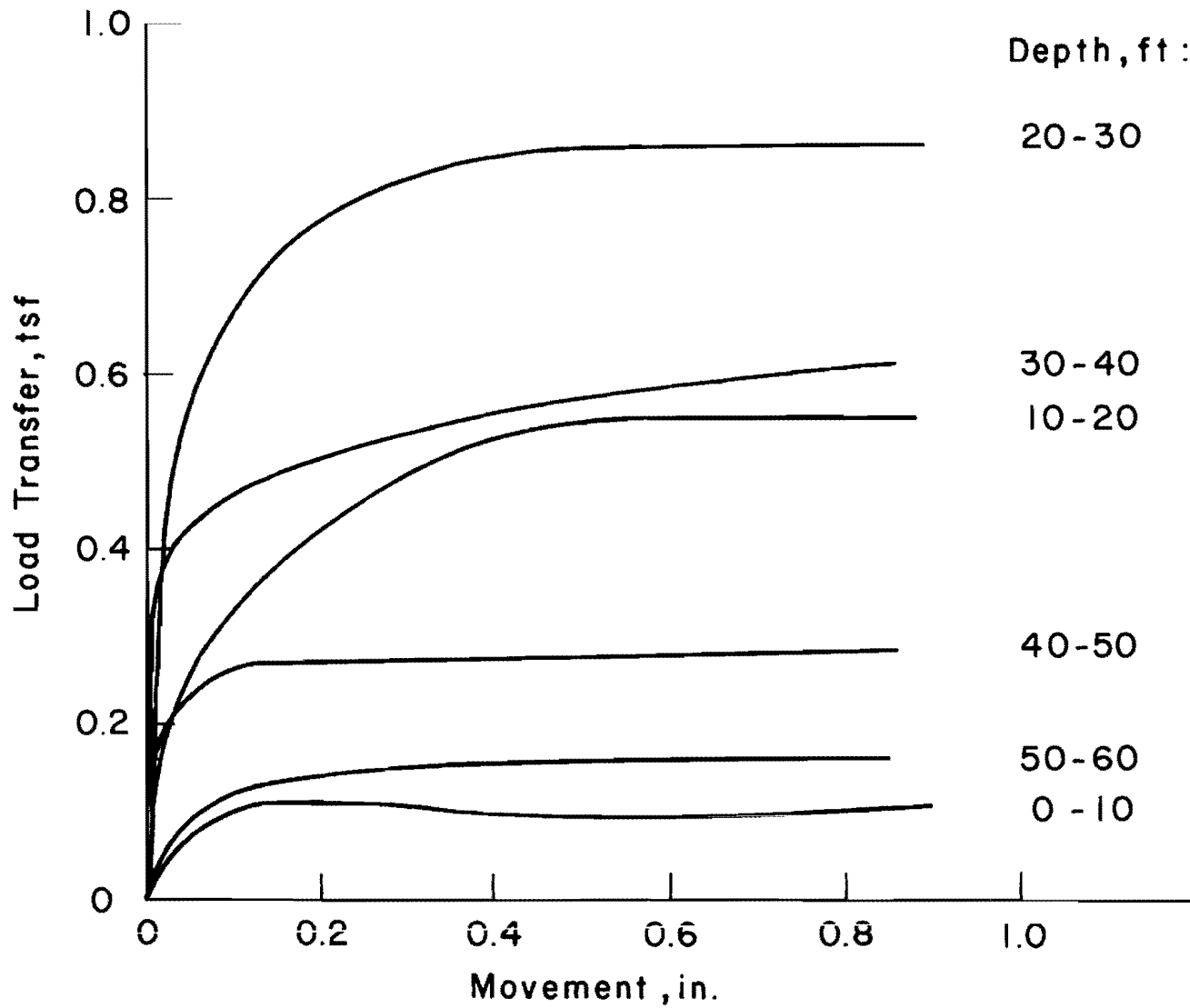


Fig. 6.15 Load Transfer in Skin Friction versus Movement, Test Shaft E-1

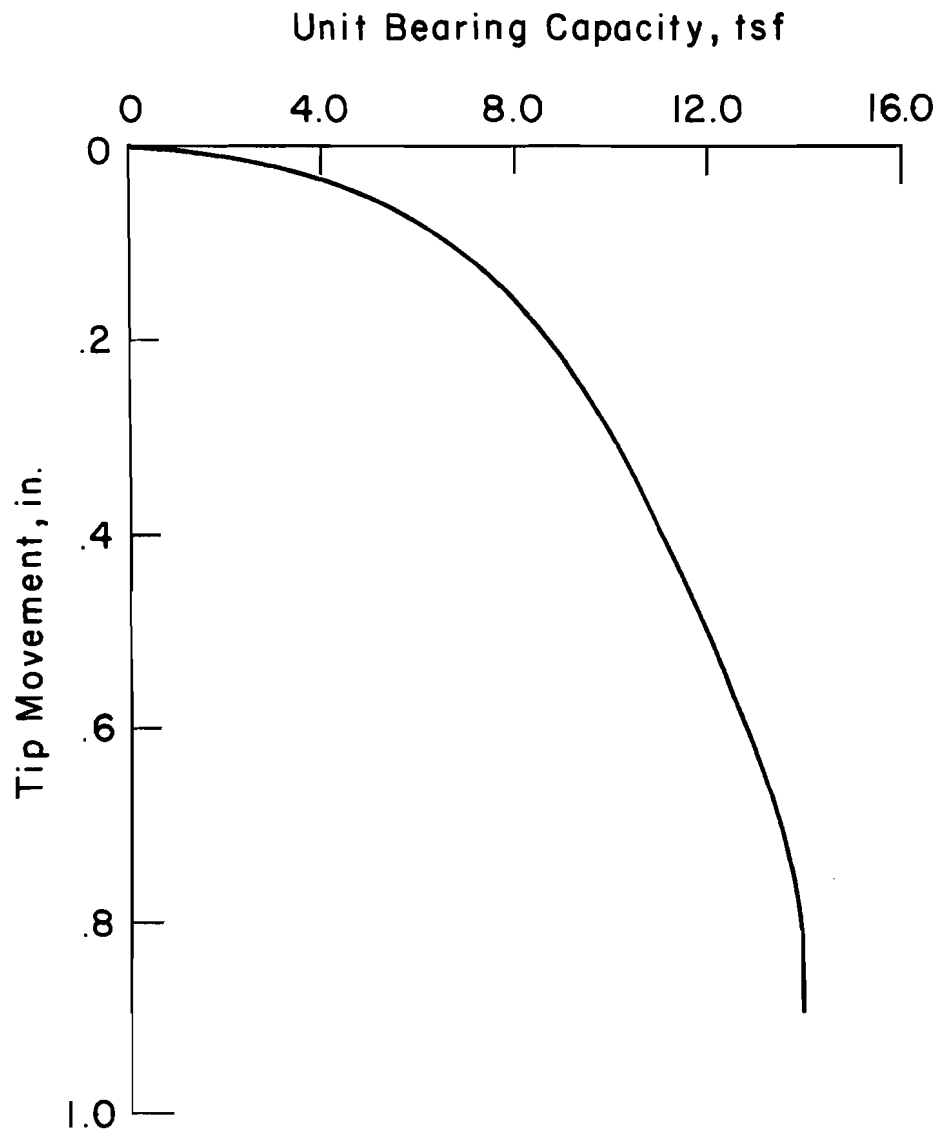


Fig. 6.16 Unit End Bearing versus Tip Movement, Test Shaft E-1

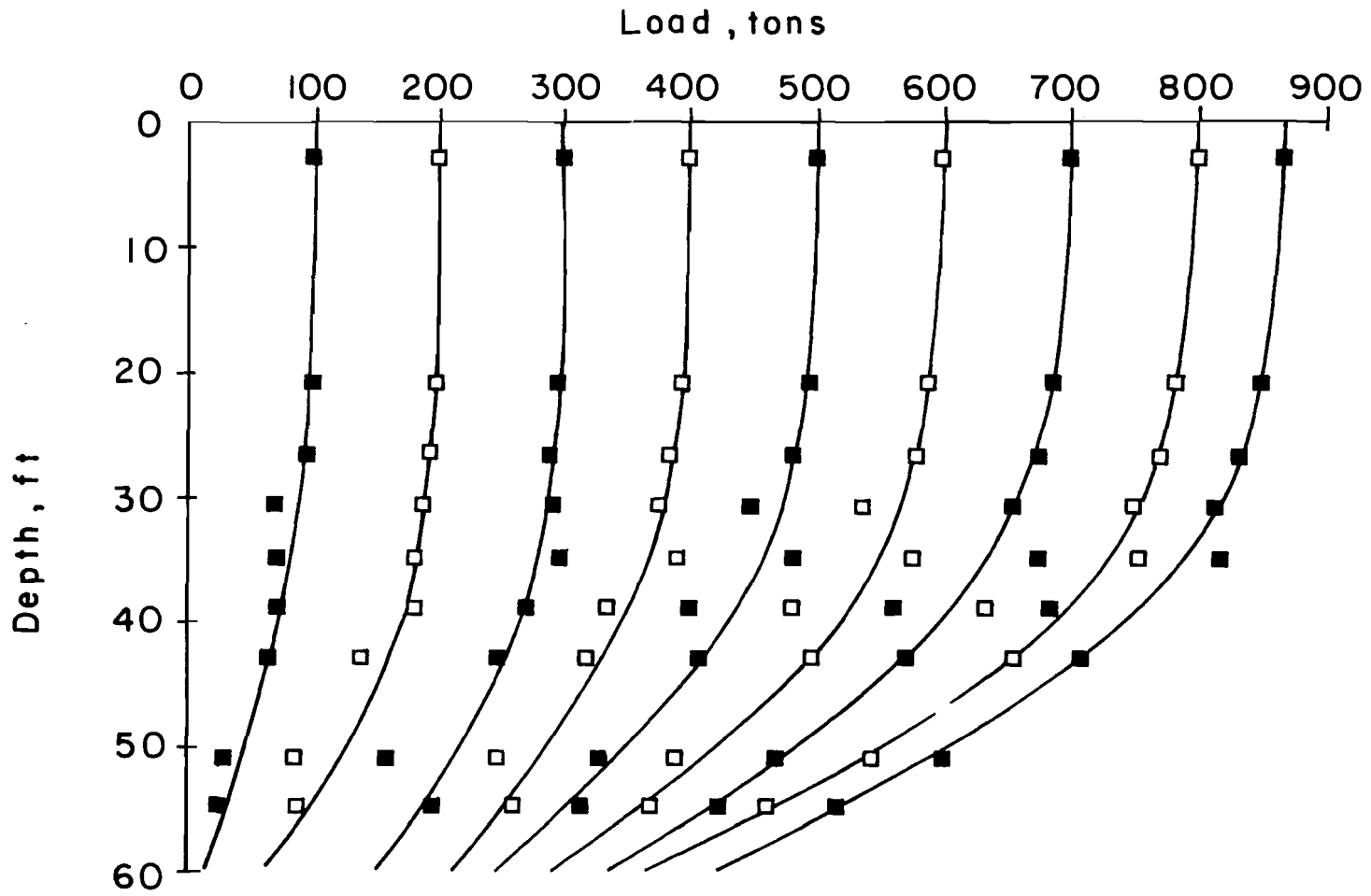


Fig. 6.17 Load Distribution Curves, Test Shaft E-2

Load transfer versus shaft-movement curves are shown in Fig. 6.18. The curves in Fig. 6.18 indicate that maximum load transfer was developed at all depths with the maximum load transfer occurring between 51 and 60 ft.

Unit end bearing versus tip movement is shown in Fig. 6.19. The curve shows that substantially all of the end bearing had been developed and that the maximum value was 59.5 tsf.

Discussion of Load Tests

Discussions of the results from testing shafts G-1, G-3, G-4, E-1, and E-2 will be presented first because these shafts were instrumented. The discussions concern tip resistance in clay, tip resistance in sand, side resistance in clay, side resistance in sand, and the influence of construction procedures. The discussion of the load test of shaft G-2 will be given in the section on construction procedures.

The principal thrust of the research reported in this report was to investigate the effect of leaving the casing in place when the construction plan called for removing the casing. Prior to discussing the results of the research study related to that topic, it is desirable to discuss the specifics of load transfer from drilled shafts to the supporting soil, as noted above. Results pertaining to the effects of leaving casing in place and of the grouting of the casing will be discussed in the section on the influence of construction procedures.

Tip Resistance in Clay. There were three instrumented test shafts that had their tips in clay. These were test shafts G-1, G-3, and G-4. As men-

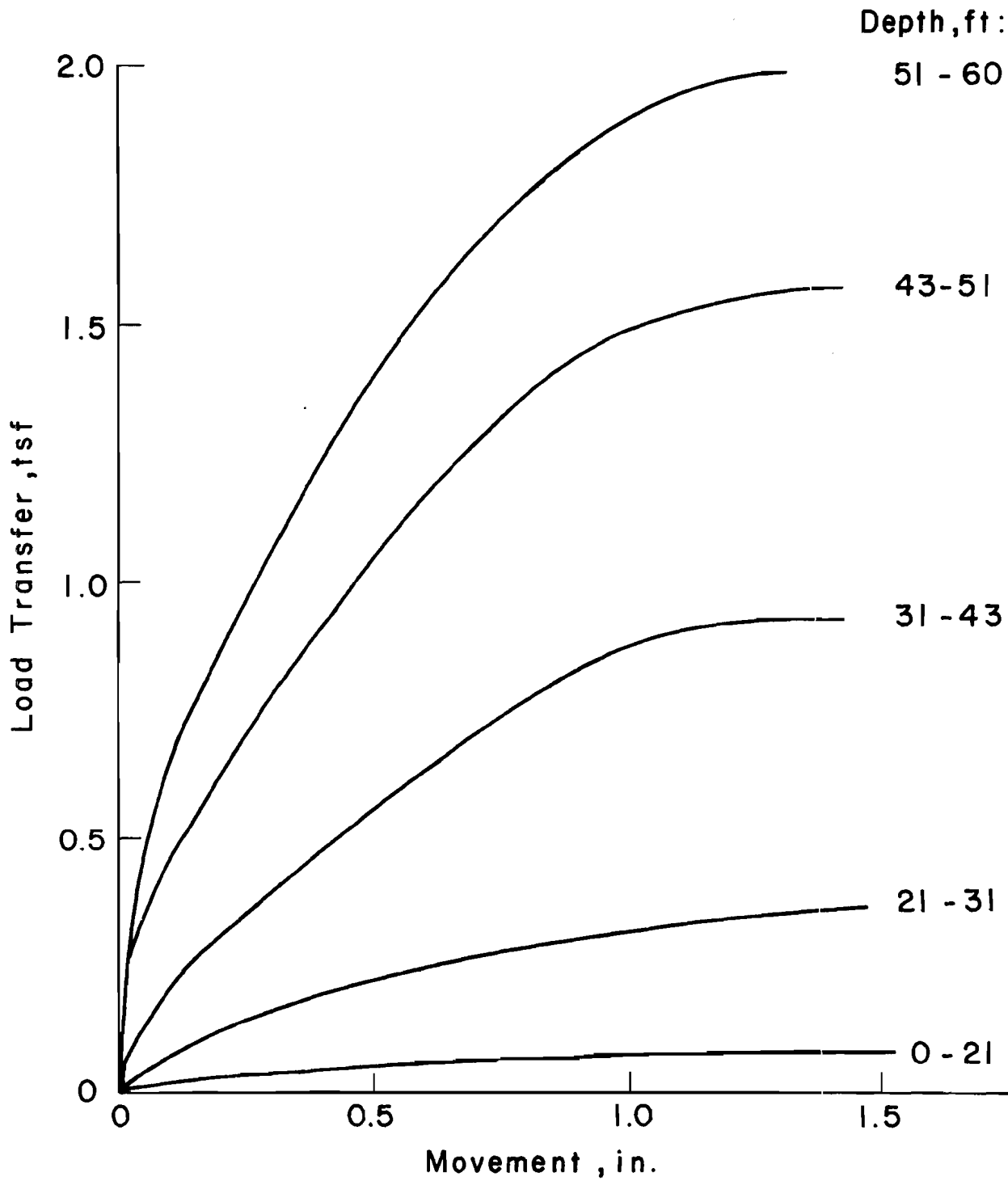


Fig. 6.18 Load Transfer in Skin Friction versus Movement, Test Shaft E-2

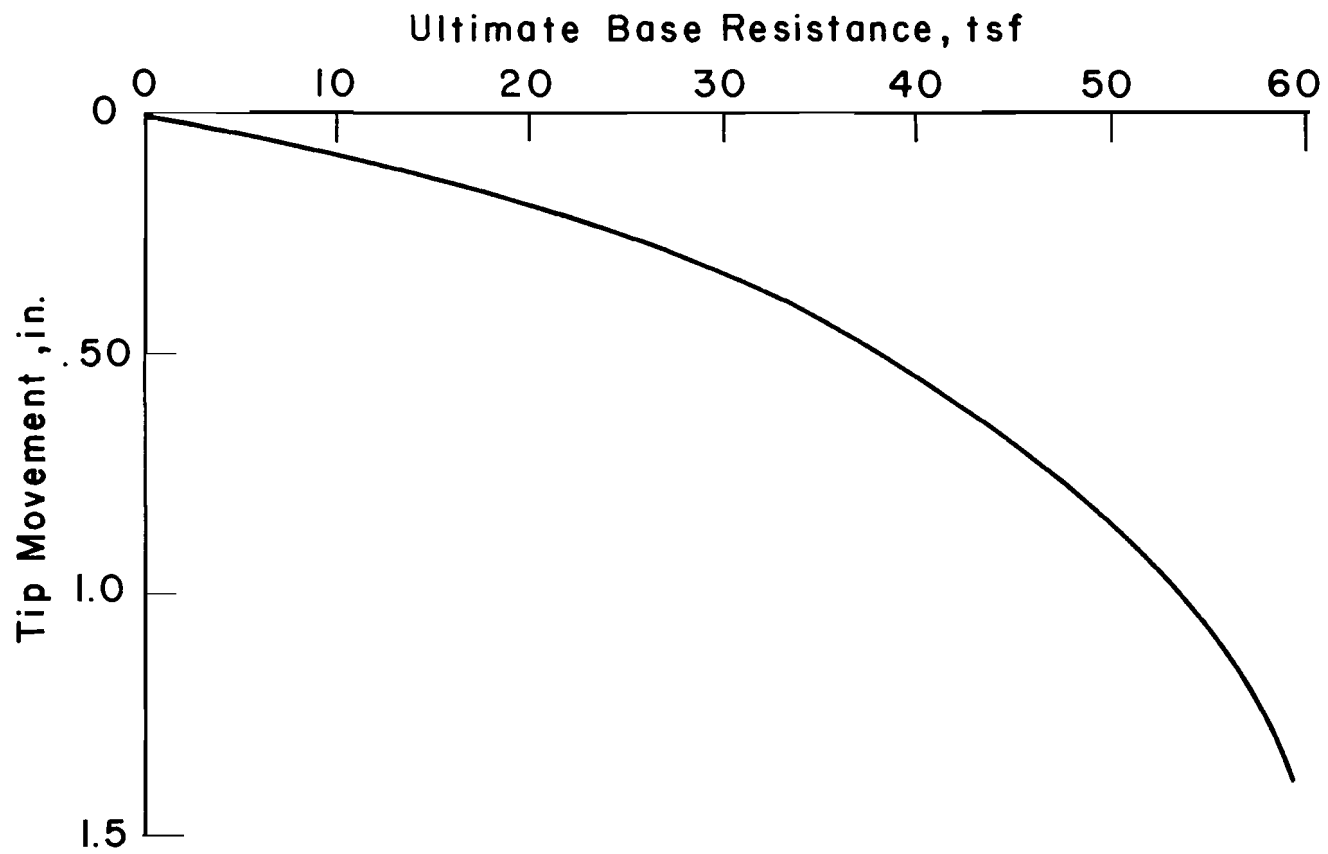


Fig. 6.19 Unit End Bearing versus Tip Movement, Test Shaft E-2

tioned earlier, the ultimate unit bearing capacities for the shafts were 4.4 tsf for shaft G-1, 3.9 and 3.8 tsf for the two tests of shaft G-3, and 10.2 tsf for shaft G-4.

A plot of the unit end bearing versus tip movement for Site 1 is shown in Fig. 6.20. Test shafts G-1 and G-3 were used to develop this plot because the tips for both shafts were at a depth of 60 ft. The results from the three test loadings are plotted, along with an average curve.

Theoretical bearing capacity values were calculated using Equation 6.8.

$$q_b = N_c s_u \quad (6.8)$$

where

N_c = bearing capacity factor (assumed to have a value of 9.0),

q_b = unit base resistance, and

s_u = undrained shear strength.

It is of interest to note that the use of Eq. 6.8 yielded a value of 3.6 tsf for test site 1 and a value of 8.6 tsf for test site 2.

The downward movement necessary to develop full end bearing ranged from about 3 to 5% of the diameter of the base at test site 1 and was 2% of the diameter of the base at test site 2.

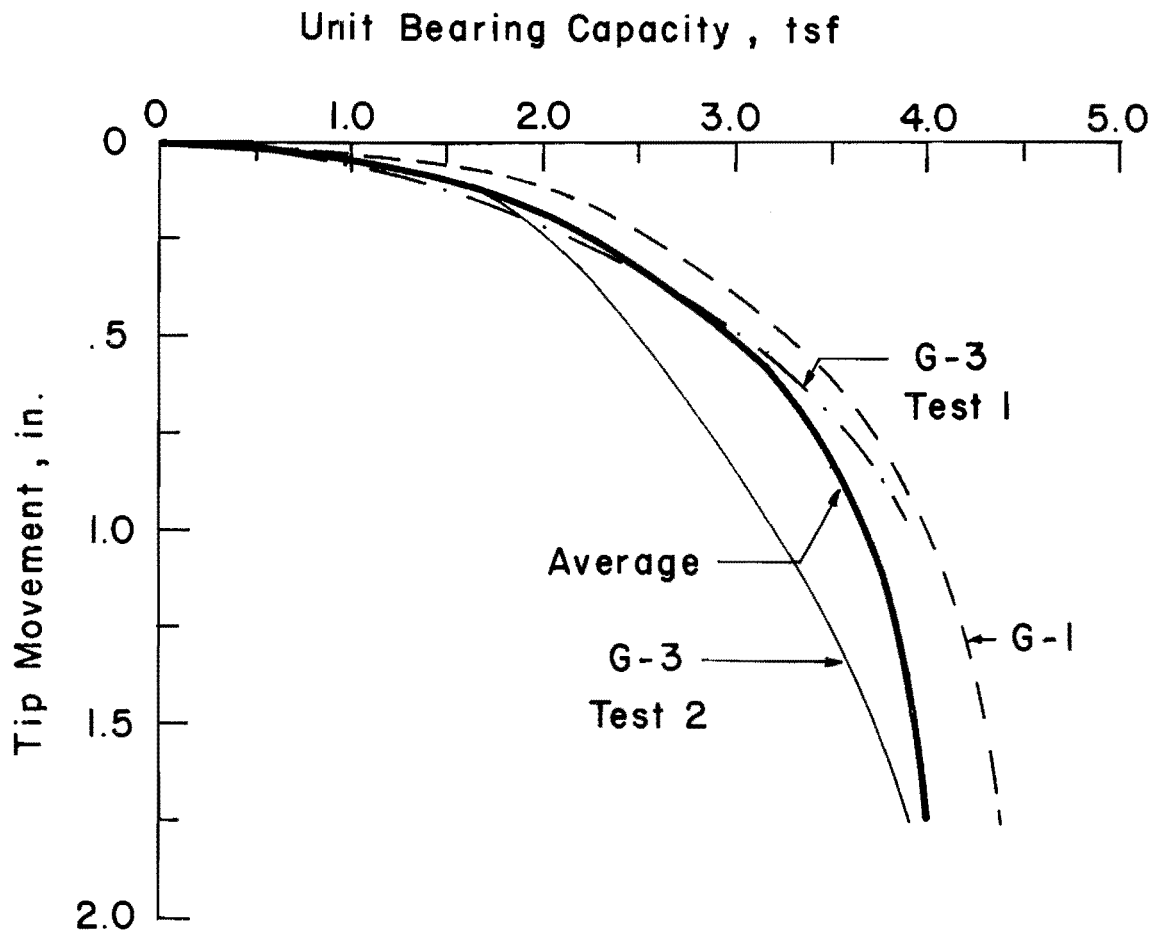


Fig. 6.20 Unit End Bearing versus Tip Movement for Clay

Tip Resistance in Sand. Only two test shafts had their tips in sand. These were test shafts E-1 and E-2. As mentioned in an earlier section, the ultimate unit bearing capacity for shafts E-1 and E-2 were 14.0 tsf and 59.5 tsf respectively. Considering that the shafts were both at the same depth, 60 ft, and were approximately 10 ft apart, the difference in the ultimate unit bearing capacities would seem quite large. A possible explanation of the difference would be that test shaft E-2 is resting on the layer of limestone that was mentioned in Chapter 4. The limestone was excavated in the construction of test shaft E-1, whereas there was none excavated in the construction of test shaft E-2. By making the above explanation for the differences in bearing capacity, it is assumed that the ultimate bearing capacity of test shaft E-1 would be what would normally be expected for the sand at the test site.

Table 6.1 presents a tabulation of some computed values of unit bearing capacity along with a reference and a brief description of the method of computation. It should be noted that methods of computed bearing capacity of the tips of driven piles are included in Table 6.1. Such methods are included because, in the construction of both test shafts, a steel casing was driven with a vibratory hammer to a depth of 60 ft, therefore, there should be some correspondence between the behavior of the tips of the test shafts and the tips of driven piles.

TABLE 6.1 TABULATION OF THEORETICAL VALUES
OF BEARING CAPACITY IN SAND

(Depth = 60 ft., Diameter = 3 ft., $\phi = 30^\circ$)

Reference	Brief Description of Method	Calculated Unit Bearing Capacity, tsf
Quiros and Reese (1977)	$q_u = q_b/K$; for 1.0 inch of movement	9
Reese and Wright (1977)	Design graph; at settle- ment of 0.05B	13
API (1980)	$q_u = P_o N_q$; for driven and/or bored piles	8
Coyle and Castello (1981)	Design graph, for driven piles	38
Meyerhof (1976)	$q_u = 1.2N$; for bored piles	19
Meyerhof (1976)	$q_u = 4N$, for driven piles	64

where

q_u = unit bearing capacity,

q_b = base capacity at 5 percent tip movement,

K = reduction factor,

B = diameter of base,

P_o = effective overburden pressure,

N_q = bearing capacity factor, and

N = average standard penetration blow count.

Side Resistance in Sand. Only test shafts G-1 and E-2 will be discussed in this section on side resistance in sand. The other tests will be discussed in a later section of this chapter dealing with the influence of construction methods.

Test shaft G-1 was constructed at test site 1 in Galveston. Approximately the top 40 ft of the shaft was in sand. The shaft failed at an axial load of 495 tons with 270 tons carried in skin friction by the sand. Referring to Fig. 6.3, it can be seen that the maximum load transfer in skin friction occurred at a downward movement of approximately 3.6% of the shaft diameter. The amount of skin friction that was measured was higher than what was expected, based on past tests. It is believed that the large amount of load transferred developed was due to the high slump (9-1/2 to 10 in) of the concrete. Having a high slump concrete enabled the concrete to displace the slurry in the excavation more efficiently and to flow outward easily and produce a better soil-concrete contact when the casing was removed.

Table 6.2 shows a comparison of theoretical values of skin friction for test site 1, as computed from different criteria. Shown in Fig. 6.21 is a plot of the ultimate load transfer versus depth for each of the measured values. Values of load transfer were calculated for 5 ft intervals and straight lines were used to approximate the values between the computed points. As can be seen in Table 6.2, the method of O'Neill and Reese (1978)

TABLE 6.2 TABULATION OF THEORETICAL VALUES FOR
SKIN FRICTION OF DRILLED SHAFTS IN SAND

(Test Site 1, 48-in. shaft, 40 ft in sand)

Reference	Brief Description of Criteria	Theoretical Ultimate Skin Friction, tons.	Notation On Graph
Meyerhof (1976)	$f_s = Kp \tan \phi$ K taken from graph	141	1
Meyerhof (1976)	$f_s = N/100$	110	2
Reese and Wright (1977)	$f_s = Kp \tan \phi$ K = 0.7	163	3
Reese and Wright (1977)	$f_s = \frac{N}{34}$ for $N \leq 53$ $f_s = \frac{N-53}{450} + 1.6$ for $53 < N < 100$	317	4
Reese and Quiros (1977)	$f_s = .026 N$	330	5
Reese and Touma (1972)	$f_s = \alpha p \tan \phi$ α is a function of depth	149	6
O'Neill and Reese (1978)	$f_s = \beta p$ β is a function of l/d	381	7
O'Neill and Reese (1978)	$f_s = \beta_c P_c$ $\beta_c = \tan(\phi - 5)$ for $\frac{l}{d} < 12$	259	8
Unpublished	$f_s = K_c p_c \tan \phi$ Kc = 1.0	314	9

(continued)

TABLE 6.2. (Continued)

where

- f_s = ultimate skin friction in tsf,
- K = lateral earth pressure coefficient,
- p = effective overburden pressure of soil, tsf,
- ϕ = effective angle of friction,
- N = average standard penetration test blow count,
- α = lateral pressure coefficient,
- β = factor relating load transfer to in-situ vertical soil pressure,
- β_c = factor relating load transfer to in-situ vertical concrete pressure,
- P_c = effective overburden pressure of concrete, tsf, and
- K_c = lateral concrete pressure coefficient.

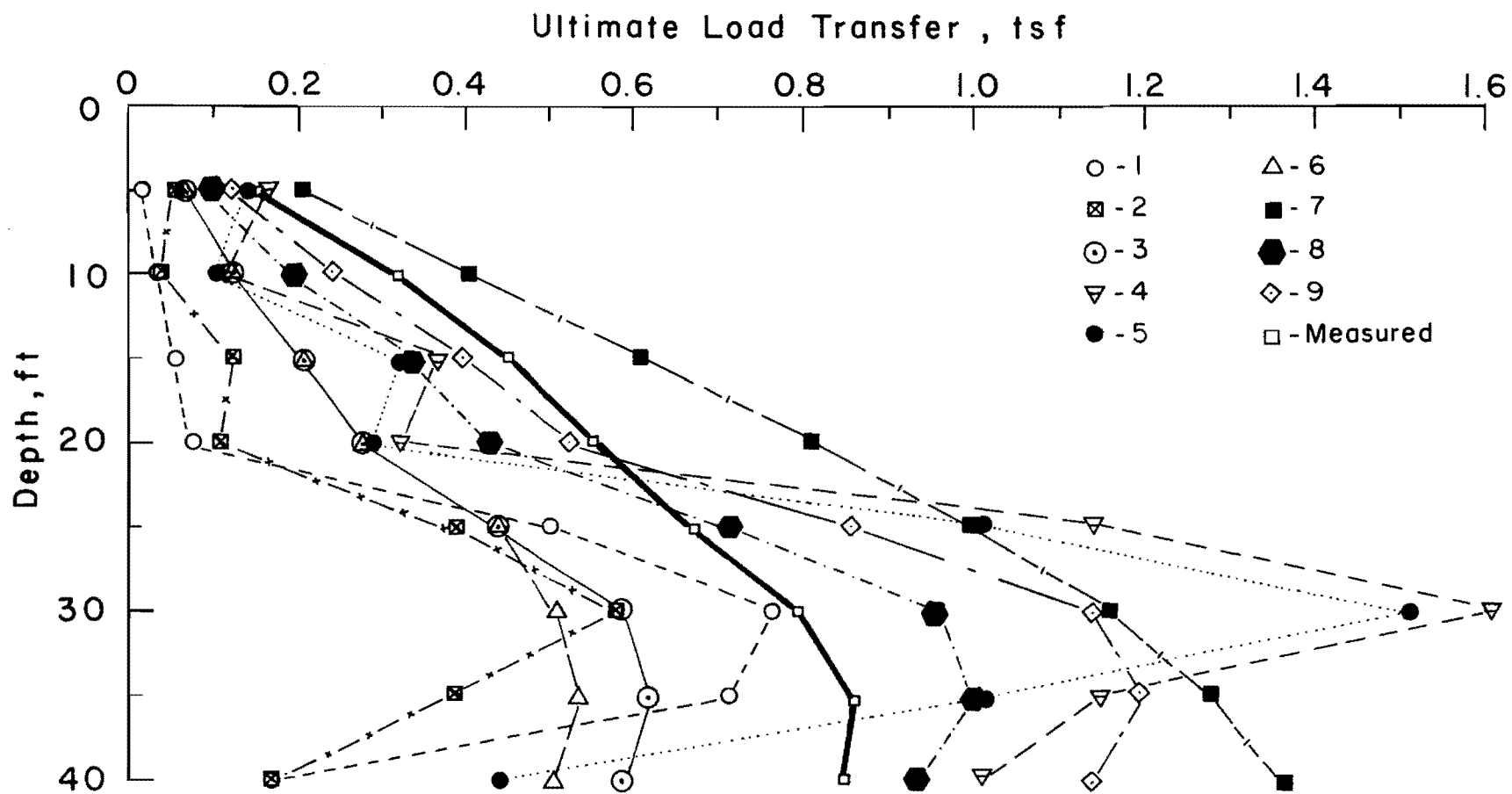


Fig. 6.21 Theoretical and Measured Unit Skin Friction in Sand, Test Site 1

yields an ultimate skin friction load of 259 tons, which is very close to the measured value of 270 tons. Other methods that also predict values that are fairly close are Reese and Wright (1977), 317 tons and the unpublished criteria, 214 tons. It should be noted that two of the three methods that gave reasonable values, O'Neill and Reese (1978) and the unpublished criteria, assume that the load transfer is to be interpreted as being controlled by the lateral fluid pressure from the concrete.

Test shaft E-2 was constructed at test site 3. The shaft was completely embedded in sand. Shaft E-2 failed at an axial load of 865 tons with 445 tons carried in skin friction. Referring to Fig. 6.18, it can be seen that the maximum load transfer in skin friction occurred at a downward movement of approximately 4.0% of the shaft diameter. Again, the amount of skin friction that was measured was higher than what was expected, based on past tests. As mentioned before, it is believed that the large amount of skin friction developed was due to the high slump concrete.

Table 6.3 shows a comparison of theoretical values of skin friction for test site 3 as computed from different criteria. Shown in Fig. 6.22 is a plot of the ultimate load transfer versus depth for each of the methods in Table 6.3 and for the measured value. As can be seen in Table 6.3, the unpublished criteria computes an ultimate skin friction load of 429 tons, which is comparable to the measured value of 445 tons. Again it is of interest to note that the theoretical method that best predicted the ultimate load in skin friction was one that assumed the load transfer was controlled by the lateral fluid pressure of the concrete.

TABLE 6.3 TABULATION OF THEORETICAL VALUES FOR
SKIN FRICTION OF DRILLED SHAFTS IN SAND

(Test Site 3, 36" x 60 ft)

Reference	Brief Description of Criteria	Theoretical Ultimate Skin Friction, tons.	Notation on Graph
Meyerhof (1976)	$f_s = K \rho \tan \phi$ K taken from graph	64	1
Meyerhof (1976)	$f_s = N/100$	64	2
Reese and Wright (1977)	$f_s = K \rho \tan \phi$ K = 0.7	228	3
Reese and Wright (1977)	$f_s = \frac{N}{34}$ for $N < 53$ $f_s = \frac{N-53}{450} + 1.6$ for $53 < N < 100$	187	4
Reese and Quiros (1977)	$f_s = 0.026N$	165	5
Reese and Touma (1972)	$f_s = \alpha \rho \tan \phi$ α is a function of depth	183	6
O'Neill and Reese (1978)	$f_s = \beta p$ β is function of l/d	524	7
O'Neill and Reese (1978)	$f_s = \beta_c p_c$ $\beta_c = \tan(\phi - 5)$ for $l/d < 12$ $\tan(\phi - 17)$ for $12 < \frac{l}{d} < 23$	241	8
Unpublished	$f_s = K_c p_c \tan \phi$	438	9

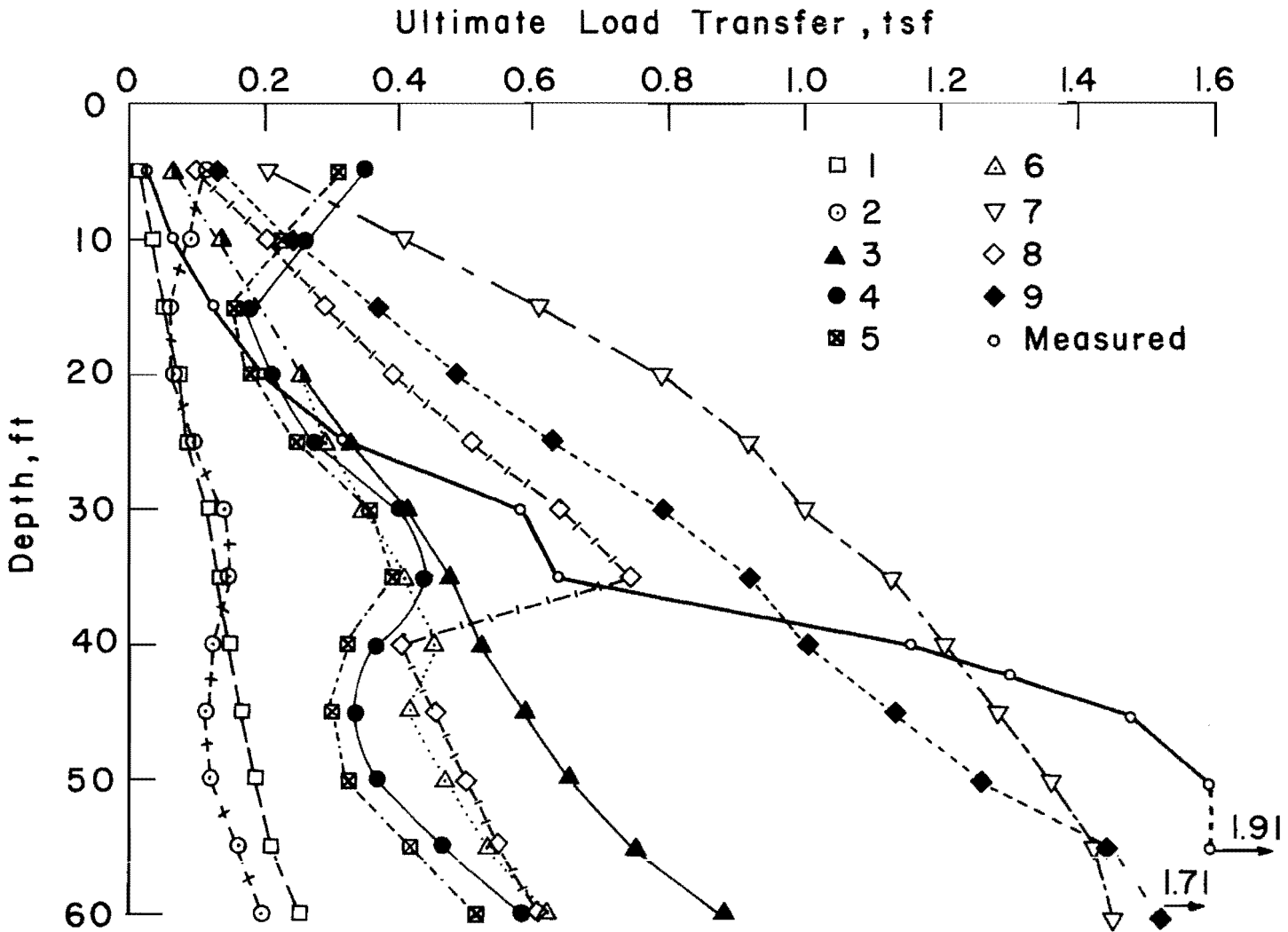


Fig. 6.22 Theoretical and Measured Unit Skin Friction in Sand

In general there are two methods that are used to calculate theoretical values of load transfer in sand, the first method determines load transfer by using equations of the form

$$f_s = Kp \tan \phi \quad (6.9)$$

where K = lateral pressure coefficient for earth (K_c for concrete),
 p = overburden pressure for earth (p_c for concrete), and
 ϕ = angle of friction of soil.

In this method values of p are computed, ϕ is estimated or determined by correlation with N -Values, and values of K are usually specified in the particular method.

The other method used to calculate load transfer is one that computes the load transfer from results of the Standard Penetration Test (SPT).

This method is of the form

$$f_s = x N \quad (6.10)$$

where

$$f_s = x N$$

x = correlation factor, and

N = blow count from SPT.

In Tables 6.4 and 6.5 are comparisons of theoretical and measured values of K and x for test site 1 and test site 3, respectively. The measured values of K and x were calculated using the values of load transfer that were determined from results of the load tests. As may be seen in the tables, several methods for design of drilled shafts were investigated.

Referring to Figs. 6.21 and 6.22 and to Tables 6.2 and 6.3, it is

TABLE 6.4 COMPARISON OF MEASURED AND THEORETICAL
VALUES OF K AND α FOR TEST SITE 1

Depth, Ft	Measured K_c	Unpublished K_c	Measured K	Meyerhof (1976) K	Reese & Wright (1977) K	Reese & Touma (1972) α	Measured α	Meyerhof (1976) α	Reese & Wright (1977) α	Reese & Quiros (1977) α
5	1.28	1.0	1.72	0.2	0.7	0.7	.028	.01	.029	.026
10	1.30	1.0	1.75	0.2	0.7	0.7	.079	.01	.029	.026
15	1.15	1.0	1.55	0.2	0.7	0.7	.036	.01	.029	.026
20	1.06	1.0	1.43	0.2	0.7	0.7	.051	.01	.029	.026
25	.79	1.0	1.06	0.8	0.7	0.7	.017	.01	.029	.026
30	.70	1.0	.94	0.9	0.7	0.6	.014	.01	.028	.026
35	.72	1.0	.973	0.8	0.7	0.6	.022	.01	.029	.026
40	.75	1.0	1.01	0.2	0.7	0.6	.050	.01	.029	.026

TABLE 6.5 COMPARISON OF MEASURED AND THEORETICAL
VALUES OF K AND x FOR TEST SITE 3

Depth, Ft	Measured K_c	Unpublished K_c	Measured K	Meyerhof (1976) K	Reese & Wright (1977) K	Reese & Touma (1972) α	Measured x	Meyerhof (1976) x	Reese & Wright (1977) x	Reese & Quiros (1977) x
5	.24	1.0	.32	0.2	0.7	0.7	.002	.01	.029	.026
10	.26	1.0	.35	0.2	0.7	0.7	.007	.01	.029	.026
15	.34	1.0	.46	0.2	0.7	0.7	.021	.01	.029	.026
20	.39	1.0	.53	0.2	0.7	0.7	.027	.01	.029	.026
25	.50	1.0	.68	0.2	0.7	0.7	.034	.01	.029	.026
30	.74	1.0	1.00	0.2	0.7	0.6	.042	.01	.029	.026
35	.70	1.0	.94	0.2	0.7	0.6	.043	.01	.029	.026
40	1.15	1.0	1.54	0.2	0.7	0.6	.093	.01	.029	.026
45	1.30	1.0	1.76	0.2	0.7	0.5	.129	.01	.029	.026
50	1.27	1.0	1.50	0.2	0.7	0.5	.128	.01	.029	.026
55	1.32	1.0	1.78	0.2	0.7	0.5	.119	.01	.029	.026

obvious that theories that use SPT values to determine skin friction in sand do not work well for test sites 1 and 3. Theories that use lateral earth pressure K all seem to give lower values of skin friction than what was measured, indicating that possibly the value that is used for K should be increased.

The unpublished theoretical method that uses the lateral pressure of fluid concrete K_c seems to be the best method for calculating values of skin friction at test sites 1 and 3. This method calculated a higher value of total skin friction at site 1 by 44 tons and a lower value of total skin friction at site 3 by 7 tons.

Side Resistance in Clay. There were only two instrumented test shafts, constructed without casings, that had any portion of the shaft in clay. These were test shafts G-1 constructed at test site 1, and G-4 constructed at test site 2. Test shaft G-1 was embedded in clay from 40 to 60 ft, and test shaft G-4 was embedded in clay from 40 to 80 ft.

Test shaft G-1 failed at an axial load of 495 tons of which 169 tons was skin friction in the clay. Referring to Fig. 6.3, it can be seen that the maximum load transfer in skin friction occurred at a downward movement of approximately 3.6% of the shaft diameter. Test shaft G-4 failed at an axial load of 225 tons of which 175 tons was skin friction in the clay. Referring to Fig. 6.12 it can be seen that the maximum load transfer in skin friction occurred at a downward movement ranging from 0.7 to 1.9% of the shaft diameter.

Theoretical values of unit skin friction in clay are calculated using 6.11 from Reese and Quiros (1977):

$$f_s = \alpha s_u \quad (6.11)$$

where

f_s = unit skin friction, tsf,

α = correlation factor, and

s_u = undrained shear strength, tsf.

Quiros and Reese recommend that a value of 0.6 be used for α .

A plot is shown in Fig. 6.23 of the maximum load transfer versus depth for the portions of test shafts G-1 and G-4 that are in clay. Also shown in this plot is a theoretical curve of load transfer that was calculated using Equation 6.11. Values of shear strength from unconfined compression tests and unconsolidated-undrained triaxial tests from both sites were combined and were used in determining values of s_u at the depths where data points are shown in Fig. 6.23. It was assumed that the properties of the soil at both sites were identical, because the two sites are only 700 feet apart. The profiles of soil properties confirm the above assumption. Load-transfer values were calculated only at depths indicated by data points.

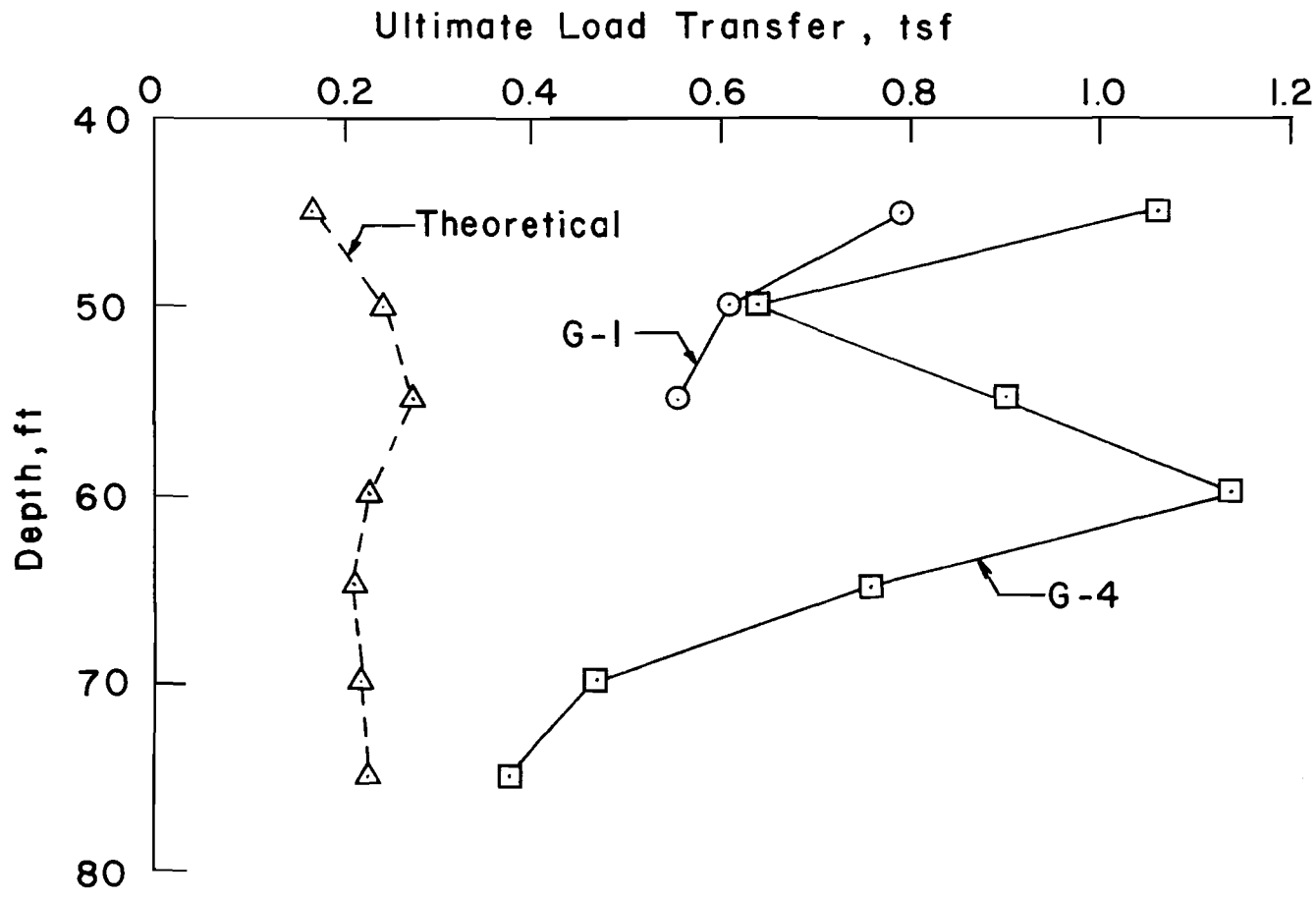


Fig. 6.23 Theoretical and Measured Unit Skin Friction in Clay, Test Sites 1 and 2

Referring to Fig. 6.23, it can be seen that the theoretical method of computing load transfer did not work very well. The plot of load transfer versus depth for test shaft G-4 seems quite erratic, but the scatter is due principally to the way the load-distribution curves were drawn, with straight lines instead of a smooth curve.

Table 6.6 shows a comparison of measured and theoretical values of α for test shafts G-1 and G-4. The measured value of α was determined in the following manner:

1. The measured side resistance at the desired depth was obtained from the load distribution curves.
2. The average shear strength at the desired depth was obtained by averaging shear strength values from unconfined compression tests and unconsolidated-undrained triaxial tests from 5 ft above and below the desired depth.
3. The value of α was computed by Eq. 6.11.

As was expected the measured values of α were much greater than the theoretical value of 0.6. It is of interest to note that other investigations have reported α values generally ranging from 0.25 to 0.7; however, in some cases values greater than 1.0 have been reported. The "actual" value of α should not exceed 1.0 because this means that the load transfer is equal to the in-situ shear strength of the soil, which should be the maximum load transfer possible. However, values of α greater than 1.0 can be calculated from load tests if conventional laboratory tests underestimate the in-situ strength of the soil, which is entirely possible.

TABLE 6.6 COMPARISON OF MEASURED AND
THEORETICAL VALUES OF α

Depth, Ft.	Undrained shear strength, tsf	Theoretical α	Shaft G-1 Measured α	Shaft G-4 Measured α
45	0.275	0.6	2.89	2.85
50	0.406	0.6	1.50	1.58
55	0.456	0.6	1.22	1.97
60	0.375	0.6	-	3.04
65	0.344	0.6	-	2.21
70	0.369	0.6	-	1.27
75	0.425	0.6	-	0.89

Influence of Construction Methods

In the load tests that are discussed in this report there are three influences of construction that can be discussed. These are: (1) the influence of a steel casing on the load-carrying capacity when the casing is put in an over-drilled hole; (2) the influence of a driven steel casing on the load capacity; (3) the influence of the concrete's flow qualities.

The influence of a steel casing on the load capacity when the casing was put in an over-drilled hole was investigated at test site 1. As mentioned before, there were three test shafts at this site, G-1, G-2, and G-3, with shafts G-2 and G-3 having casings extending part of or for the full length of the shaft. As expected, when shafts G-2 and G-3 were first tested, they failed at relatively low axial loads. When the second load tests were done on shafts G-2 and G-3, after grouting, the axial loads at failure increased significantly.

Since test shafts G-1 and G-3 were both instrumented, a comparison of measured values of the ultimate load transfer can be made. This comparison was made in Fig. 6.24 where a plot is given of the maximum load transfer versus depth. The results from the three test loadings are plotted. This plot shows that the grouting was effective in increasing the load transfer in the grouted region 0 to 40 ft of test shaft G-3.

Due to the large quantity of grout that was used, 8 cu yd, another computation of the load transfer was made assuming that there was a uniform increase in diameter over the grouted zone. A new diameter of 3.98 ft was

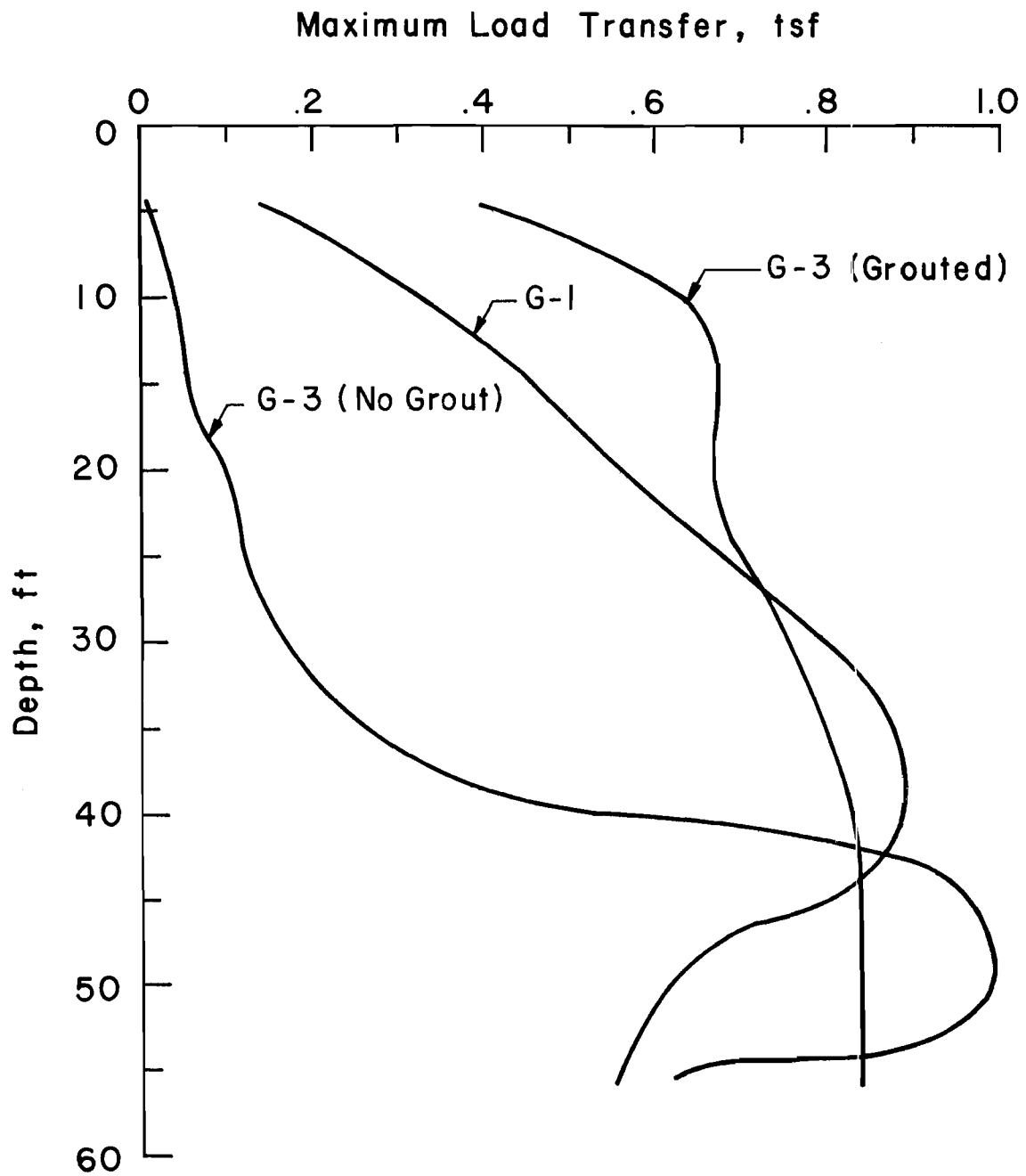


Fig. 6.24 Load Transfer in Skin Friction versus Depth, Test Shafts G-1 and G-3

calculated for the top 40 ft of the shaft. Maximum values of load transfer determined using a diameter of 3.98 ft are 25% less than the maximum values determined using a 3.00-ft diameter.

Test shaft G-2 was not an instrumented shaft so only the load-settlement curves are available. The unit end bearing was estimated as 4 tsf, yielding a load on the tip of 28 tons.

In the first load test of test shaft 2 the maximum applied load was 89 tons. Thus, it is estimated that 61 tons were carried in skin friction. Assuming that there is no load transfer in the top 10 ft, an average load-transfer value of 0.12 tsf can be computed. The value of 0.12 tsf seems reasonable in comparison with the maximum load-transfer curve in Fig. 6.24 for the top 40 ft of the 36-in.-diameter shaft without grout.

In the second load test of test shaft 2, after grouting the lower 15 ft the maximum applied load was 373 tons. Subtracting the computed end bearing of 28 tons leaves 345 tons carried in skin friction. Using the previous load-transfer value of 0.12 tsf for the top 50 ft of the shaft, where no grouting was done, yields a total load of 45 tons. This leaves 300 tons of load carried in skin friction in the grouted area, which gives a load-transfer value of 2.1 tsf.

This value of 2.1 tsf seems quite large, even after grouting. Considering the large amount of grout used, 6 cu yd, it is possible that grouting caused a larger effective diameter. Assuming that there was a uniform increase in diameter over the grouted zone, a new diameter was calculated for the lower 15 ft of the shaft. Using this diameter of 4.77 ft, a new value

for the load carried in end bearing was determined to be 71 tons. Subtracting the end bearing and the 45 tons carried in skin friction in the top 50 ft, leaves 257 tons of load carried by the grouted area. A load-transfer value for the lower 15 ft of 1.1 tsf was then computed. The value of 1.1 tsf seems much more reasonable in comparison to values shown in Fig. 6.24.

The influence of a driven steel casing on the load capacity was investigated at test site 3. As mentioned before, there were two instrumented test shafts at this site, E-1 and E-2. Test shaft E-1 had a casing extending the complete length of the shaft. Test shaft E-2 had no casing. The results of the analyses of readings from the Mustran cells showed that test shaft E-1 carried a total load of 246 tons in skin friction while test shaft E-2 carried 445 tons in skin friction. A comparison of the maximum load transfer values for the two shafts was done and is shown in Fig. 6.25. This plot shows that in the upper portion that the load transfer is higher for test shaft E-1, but overall the load transfer is greater for shaft E-2.

Test shaft E-1 was then analyzed as a driven pile. Table 6.7 shows a comparison of theoretical values of skin friction, for driven piles, using different methods. Shown in Fig. 6.26 is a plot of the ultimate load transfer versus depth for each of the methods in Table 6.7 and for the measured values. As can be seen in Table 6.7 and Fig. 6.26, the method suggested by Meyerhof (1976) gives the best results.

The fact is well known that the flow characteristics of concrete (slump) have an important bearing on the quality of drilled shafts. There have been a number of instances where drilled shafts have been excavated and found to be structurally unsound because concrete has failed to flow through rebar cages

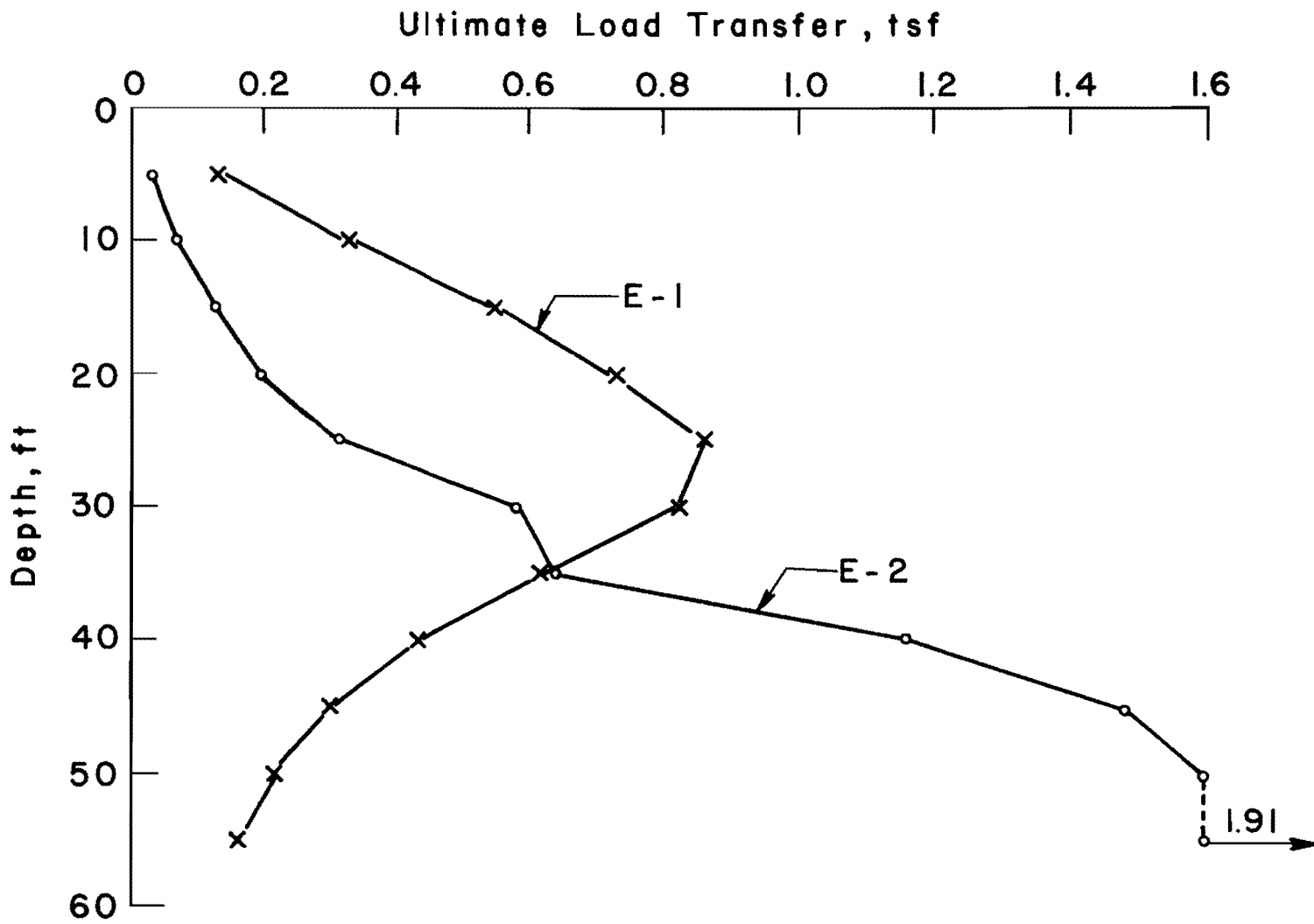


Fig. 6.25 Load Transfer in Skin Friction versus Depth for Test Shafts E-1 and E-2

TABLE 6.7 TABULATION OF THEORETICAL VALUES FOR
SKIN FRICTION OF DRIVEN PILES IN SAND

(Test Site 3, 48-in shaft by 60 ft long)

Reference	Brief Description of Criteria	Theoretical Ultimate Skin Friction, tons	Notation on Graph
Meyerhof (1976)	$f_s = N/50$	128	1
Meyerhof (1976)	$f_s = Kp \tan \phi$ K taken from graph	260	2
Coyle & Castello (1981)	Taken from design graph	71	3

where

f_s = ultimate unit skin friction,

K = coefficient of lateral earth pressure,

p = effective overburden pressure, and

ϕ = effective angle of friction.

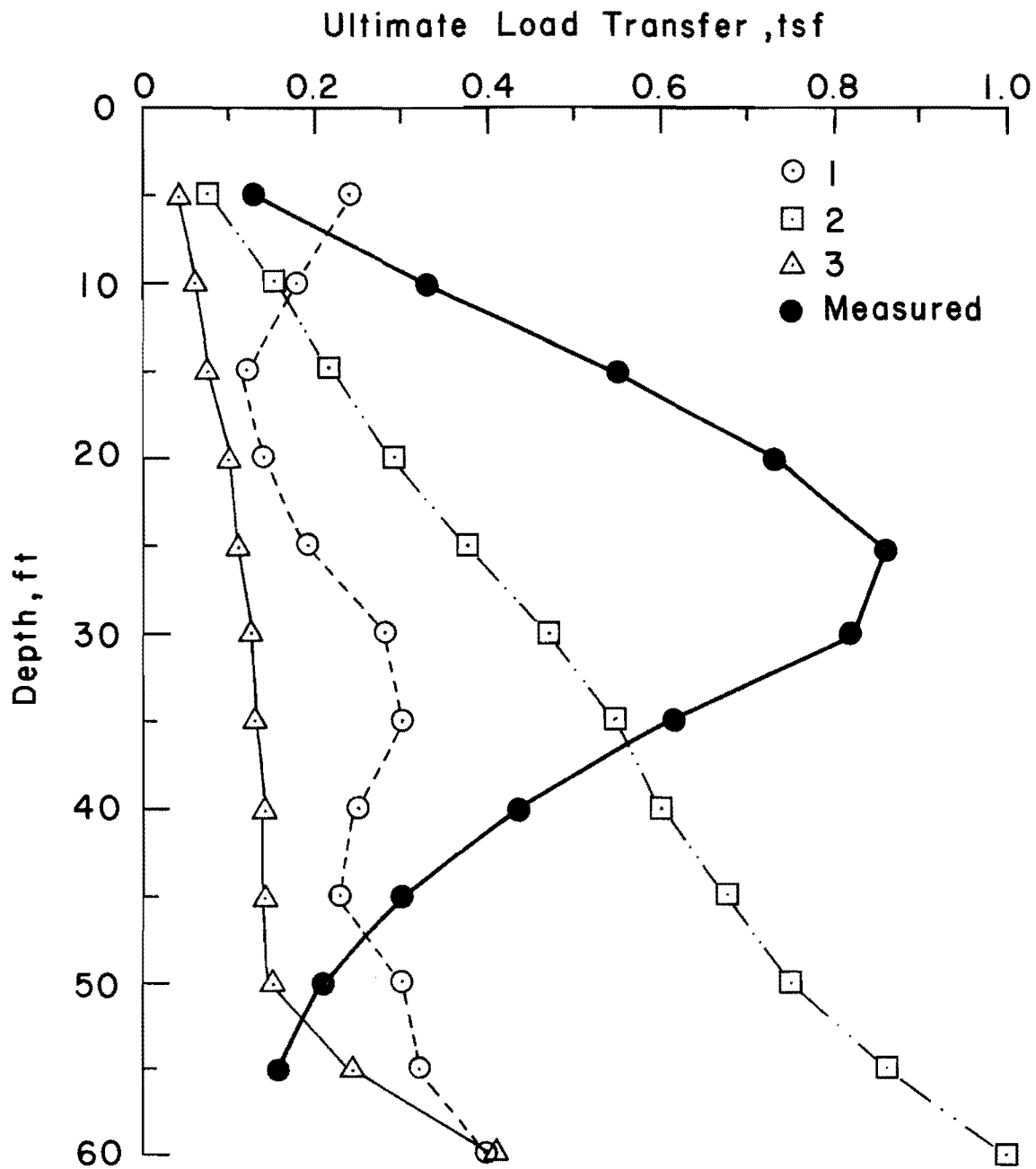


Fig. 6.26 Theoretical and Measured Load Transfer, Test Shaft E-1

or has failed to displace slurry completely in the excavation.

There are little data, however, on the degree to which the slump of concrete affects load transfer in skin friction. As mentioned in Chapter 4, when test shaft G-4 was constructed the concrete had a low slump when it arrived on the job site, water was then added to increase the slump, but by the time the pour was complete the slump was again low. Data from the Mustran cells revealed virtually no load transfer in the 40-ft thick surface stratum of sand. The load test of test shaft G-4 was only a short distance from test shaft G-1 making a comparison possible. The comparison of the maximum load transfer versus depth for test shafts G-1 and G-4 is shown in Fig. 6.27. The difference in load transfer in skin friction in the sand is striking.

Had the unit load transfer in the G-4 shaft in the sand been equal to the value obtained from the G-1 shaft, a load of 157 tons would have been carried in the sand by shaft G-4. The experience suggests the desirability of using a concrete that acts almost like a liquid and the possibility of basing computations of axial load in sand on stresses in the fresh concrete rather than on overburden stresses in the soil.

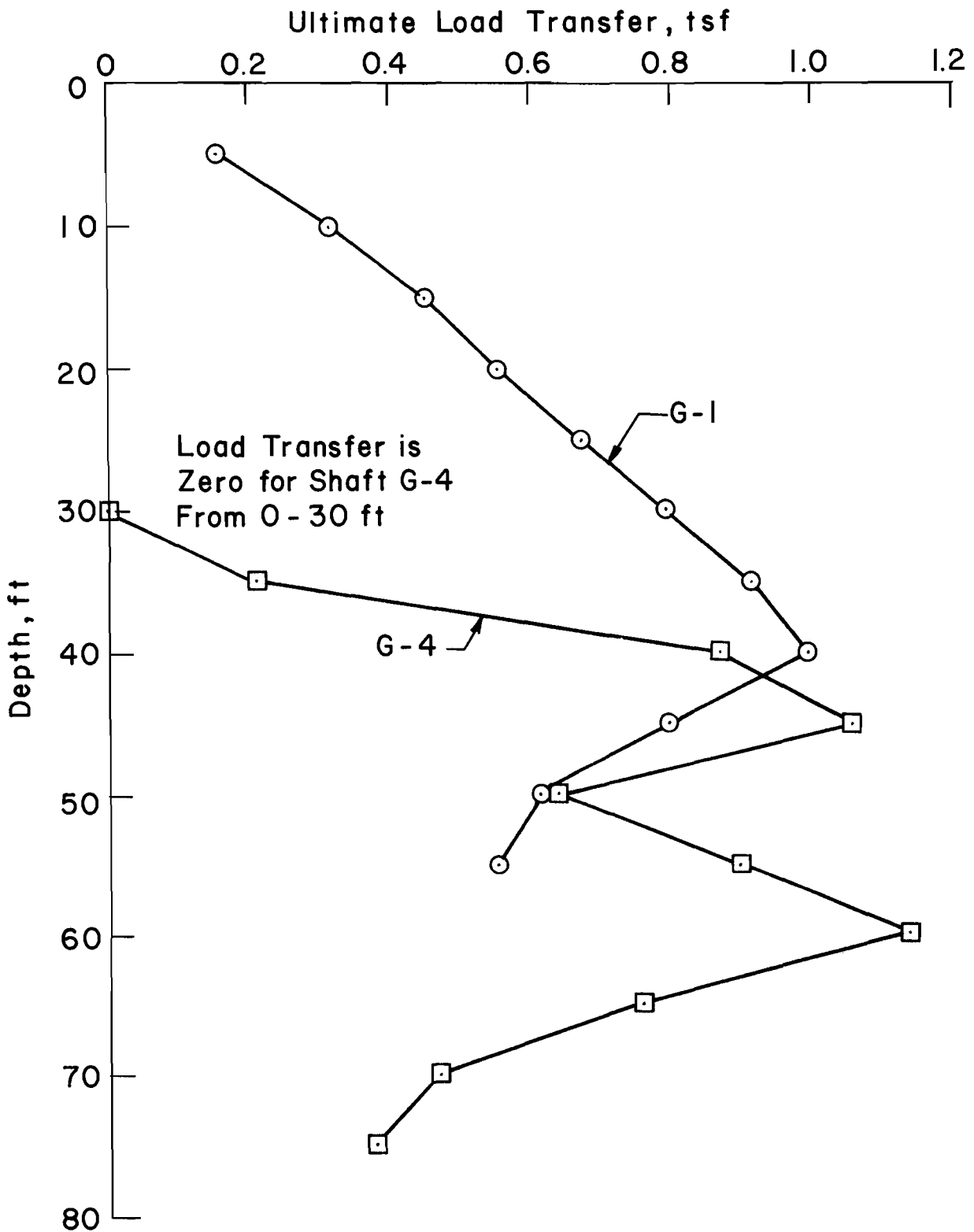


Fig. 6.27 Load Transfer versus Depth, Test Shafts G-1 and G-4

CHAPTER 7. SUGGESTIONS CONCERNING CONSTRUCTION METHODS

Due to the results of the investigation of the influence of construction procedures, the following suggestions are made concerning construction methods. First, it has been shown that when a casing has to be left in place, the load capacity of the shaft is greatly reduced. This was true whether the casing was driven or placed in an over-drilled hole. Therefore, some type of remedial measure must be taken.

A remedial measure that can be taken is grouting around the shaft if the casing was placed in an over-drilled hole. This was done at test site 1 and proved to be quite successful. It should be noted that these were the only tests of this sort that have been performed; therefore, grouting cannot be considered a proven method of increasing the load capacity. If grouting is the remedial measure that is chosen, then some technique should be used to prove the load capacity of the shaft. A method has been developed and used in Europe for some time that can be effective. It is called the TNO method, after the firm in the Netherlands that did the development.

Robert Arias (1977) reported that the Institute TNO for Building Materials and Building Structures, a Netherland organization for applied scientific research, has developed a method of dynamic pile testing. The TNO organization claims the test will provide information regarding load-carrying capacity, skin friction, and static deformation.

A schematic of the testing arrangement is shown in Fig. 7.1. The top of a shaft is prepared with a layer of epoxy to which a steel plate is fastened. In addition to being held by epoxy, the plate is held by bolts that are fastened into the concrete. An electronic load cell is bolted to the steel plate. The shaft or pile is stressed by a blow from a small drop hammer (approximately 880 lbs.). An electronic theodolite keeps track of the movements at the top of the shaft to obtain a time-displacement curve. The data recorded are analyzed by use of a proprietary computer program and the results from the computations allow a load-settlement curve to be plotted. TNO claims that the force-displacement curve obtained can be analyzed to obtain the load carried in skin friction.

Actually, the TNO method is just a variation of the wave-equation method of analysis of pile foundations. That method has had extensive development in the United States, principally by researchers at Texas A & M University and at Case Institute. The wave-equation method can readily be extended to drilled shafts.

Other remedial measures that can be taken are to add one or more drilled shafts, next to the drilled shaft with the casing, to compensate for the reduced capacity of the original shaft. This type of remedial measure would probably be done if the steel casing were driven because there would then be no annular space to grout.

Another suggestion related to the research that was performed has to do with the flow characteristics of concrete. From the tests that were performed, there seems to be evidence to indicate that increasing the liquidity of fresh

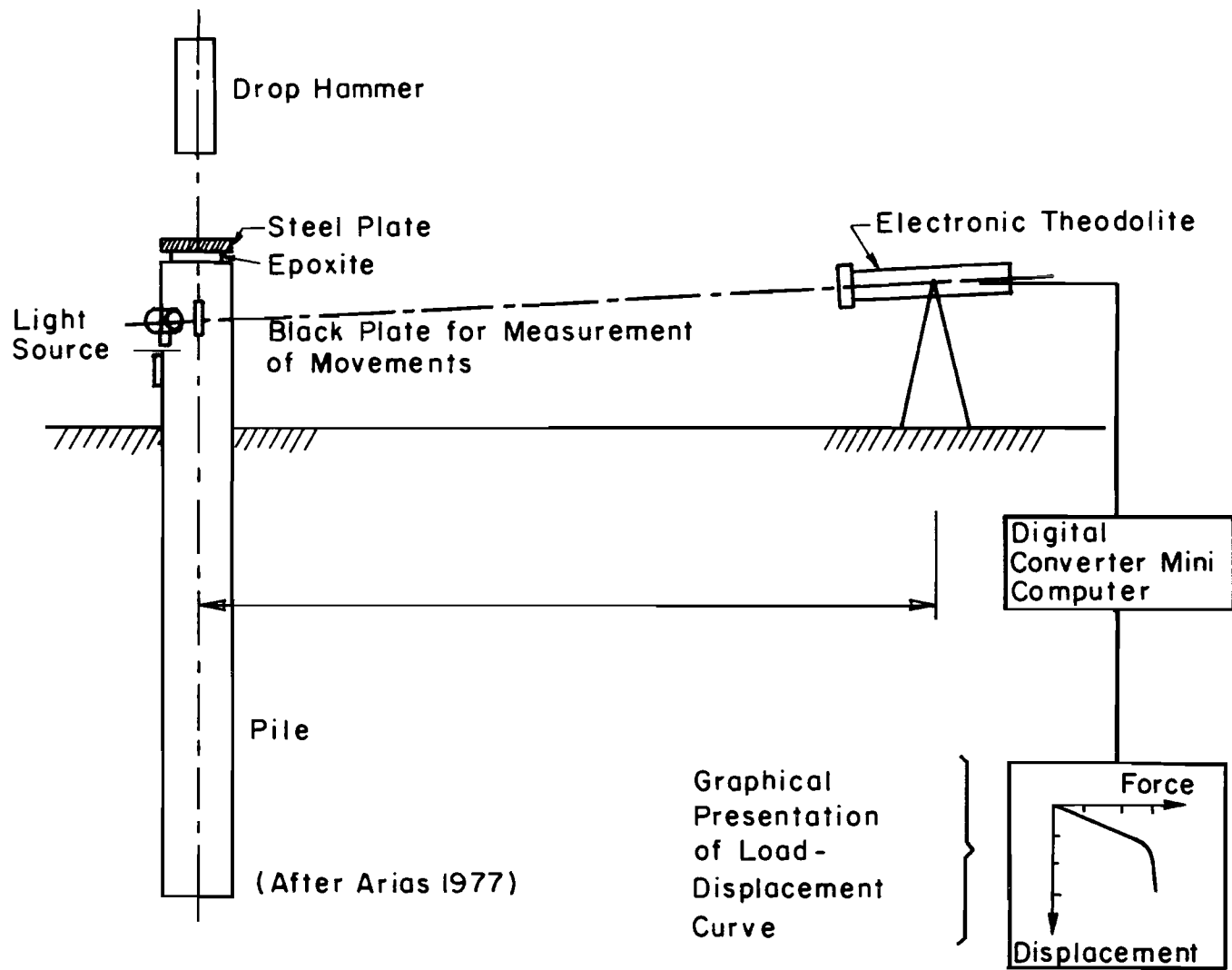


Fig. 7.1 Schematic of TNO Testing Arrangement

concrete (increasing the slump) increases the load transfer in skin friction. With additives that can be put in concrete, slumps of 9 to 10 inches will yield concrete of appropriate strength and apparently will yield larger values of load transfer in skin friction. Additional research is needed to confirm this tentative conclusion.

The studies that were performed indicate that the leaving of casing in place should be avoided if at all possible. Appendix D presents a discussion of some cases where it would be difficult to retrieve a casing.

CHAPTER 8. CONCLUSIONS AND RECOMMENDATIONS

This study has been concerned with the influence of construction procedures on the load carrying capacity of drilled shafts. In the study drilled shafts with casings left in place were compared to drilled shafts with no casings. Also, a drilled shaft constructed with concrete of bad flow characteristics was compared to one constructed with concrete of good flow characteristics. Six full-scale test shafts were constructed by the casing method, five of which were instrumented with Mustran cells. In the analysis of these tests, the results were not only compared to each other, as mentioned above, but were also compared with recommended design procedures. In the following sections the main conclusions and recommendations concerning the construction, design, and instrumentation of drilled shafts will be summarized.

Conclusions

1. Leaving casing in place when the excavation has been over-drilled dramatically reduced the capacity of a drilled shaft.
2. The grouting of the annular space between the casing and the excavation caused a significant increase in capacity for these tests.
3. Leaving the casing in place when the casing has been driven in sand dramatically reduced the capacity of a drilled shaft.
4. There is evidence to indicate that increasing the liquidity of fresh concrete (increasing its slump) increases the load transfer in skin friction.

5. The load transfer in skin friction was a nonlinear function of the downward movement of a drilled shaft.

6. The maximum load transfer in skin friction occurred at a small downward movement of a drilled shaft.

7. The maximum load transfer in skin friction for sand increased with depth with almost a linear function.

8. The maximum end bearing in clay agreed well with bearing capacity theory and required more downward movement than did the maximum skin friction.

9. The present design procedures for drilled shafts in sand tend to underestimate the load carried in skin friction.

10. Design procedures that use standard penetration blow counts greatly underestimated loads carried in skin friction.

11. The unpublished design equation ($f_s = K_c p_c \tan\theta$) was the best overall method of predicting the measured loads in skin friction for sand.

12. A value of $\alpha = 0.6$ has been recommended for design of drilled shafts in clay. A value for α of more than 1.0 was obtained from the limited data from the load tests reported herein.

13. The Mustran-cell instrumentation system provided an adequate method of the measurement of axial loads in a drilled shaft.

Recommendations

1. When a casing has to be left in place, some type of remedial measure should be taken to insure the integrity of the foundation.

2. Grouting of the annular space is recommended as a remedial measure when the casing is left in an over-drilled hole.

3. Any type of remedial measure that is taken should be verified by use of some type of load test.

4. When fluid concrete (slump 9 to 10 in.) is used in constructing drilled shafts in sand, the following design equation can be used to predict the side resistance:

where $f_s = K_c p_c \tan \phi$

f_s = ultimate unit skin friction,

K_c = lateral pressure of concrete,

p_c = effective overburden pressure of concrete, and

ϕ = effective angle of internal friction of soil.

5. Internal instrumentation for the measurement of the distribution of axial load with depth should be employed in any future test shafts. Experience has shown that extreme care must be used in the installation and operation of any of the available systems (see Appendix C) in order to obtain results of the best quality.

APPENDIX A

BORING LOGS

Test Site 1
Galveston, Texas

LOG OF BORING

PROJECT: Physical Plant Building & Pharmacology Addition
Galveston, Texas

BORING NO. CB-1

CLIENT: The University of Texas System
Austin, Texas

FILE NO. 80-39

DATE 3-7-80

Page 2

SOIL SYMBOL	FIELD DATA		LABORATORY DATA						DRY AUGERED	TO	FEET				
	DEPTH (feet)	SAMPLES	Penetration Resistance (N) or TSF	Moisture Content %	Dry Density, PCF	Compressive Strength TSF	Failure Strain - %	ATTERBERG LIMITS			WASH BORED	TO	FEET		
								Liquid	Plastic	Plasticity Index	FREE WATER ENCOUNTERED			YES	NO
											AT	FT. DEPTH.	WATER AT	FT. AFTER	
							LL	PL	PI	DESCRIPTION OF STRATUM					
	45	0.5	34	79	0.46	6				Soft gray CLAY (CH) w/shell, sand pockets & layers					
	50	0.4	33	91	0.87 (15)	10				Firm gray SILTY FINE SAND (SM) w/shell & soft clay layers					
	55	1.0	41	75	0.88	6				Medium gray CLAY (CH) w/shell - stiff & red w/sand pockets @ 58'					
	60	2.0	32	89	0.63	4				- very stiff, tan & light gray @ 63'					
	65	4.0	23												
	70	3.25	25	98	0.71	4				Medium tan & light gray VERY SILTY CLAY (CL)					
	75	2.20	28							Firm tan & light gray CLAYEY SILT (ML) w/clay layers					
	80	2.25	32	91	0.82	8				Medium tan & light gray SILTY CLAY (CL) w/clay layers					

* SLICKENSIDED FAILURE
() CONFINING PRESSURE, PSI
G.S. GRAIN SIZE

Penetration Resistance Bottom @ 80 ft.
(N) - STANDARD PENETRATION RESISTANCE (SPT)
TSF - POCKET PENETROMETER OR TORVANE
ESTIMATED UNCONFINED COMPRESSIVE
STRENGTH, TONS PER SQ. FOOT

LOG OF BORING

PROJECT: Physical Plant Building & Pharmacology Addition Galveston, Texas		BORING NO. CB-2									
CLIENT: The University of Texas System Austin, Texas		FILE NO. 80-39									
		DATE 3-7-80									
SOIL SYMBOL	FIELD DATA		LABORATORY DATA					DRY AUGERED 0 TO 10 FEET WASH BORED 10 TO 60 FEET			
	DEPTH (feet)	SAMPLES	Penetration Resistance (N) or TSF	Moisture Content %	Dry Density, PCF	Compressive Strength TSF	Failure Strain %	ATTERBERG LIMITS			FREE WATER ENCOUNTERED YES NO AT 5.0 FT. DEPTH. WATER AT FT. AFTER
								Liquid	Plastic	Plasticity Index	
DESCRIPTION OF STRATUM											
			N=12 (-200= 6.2%)							Firm tan & gray SILTY FINE SAND (SM) w/shell "FILL"	
	5		N=1							- loose 4-6'	
			N=9							- organic matter & soft clay layers @ 6.5'	
	10									- loose below 8'	
			N=1								
	15										
			N=3							- much shell @ 18'	
	20										
			0.4	52	65	0.14	3	97	35	62	Very soft gray CLAY (CH) w/shell & sand layers
	25										
			N=44							Dense gray SILTY FINE SAND (SM)	
	30										
			N=34 (-200= 10.8%)								
	35										
			0.5	37	85	0.35	4				Soft gray CLAY (CH) w/sand layers
	40										
			* SLICKENSIDED FAILURE () CONFINING PRESSURE, PSI G.S. GRAIN SIZE		(N) - STANDARD PENETRATION RESISTANCE (SPT) TSF - POCKET PENETROMETER OR TORVANE ESTIMATED UNCONFINED COMPRESSIVE STRENGTH, TONS PER SQ. FOOT		PENETRATION RESISTANCE				

LOG OF BORING

PROJECT: Physical Plant Building & Pharmacology Addition
Galveston, Texas

BORING NO. CB-2
FILE NO. 80-39
DATE 3-7-80

CLIENT: The University of Texas System
Austin, Texas

Page 2

SOIL SYMBOL	FIELD DATA		LABORATORY DATA						DRY AUGERED	TO	FEET		
	DEPTH (feet)	SAMPLES	Penetration Resistance (N) or TSF	Moisture Content %	Dry Density, PCF	Compressive Strength TSF	Failure Strain - %	ATTERBERG LIMITS			WASH BORED	TO	FEET
								Liquid	Plastic	Plasticity Index	FREE WATER ENCOUNTERED	YES	NO
	LL	PL	PI	AT	FT. DEPTH.	WATER AT	FT. AFTER	DESCRIPTION OF STRATUM					
	45		0.5	39				59	23	36			Soft gray CLAY (CH) w/sand layers - shell & sand pockets @ 43'
	50		0.5	31	88	0.21	7						- stiff @ 53'
	55		1.25	42	77	1.02	4						- red & light gray @ 58'
	60		3.0	36				71	24	47			Bottom @ 60 ft.

* SLICKSIDED FAILURE
() CONFINING PRESSURE, PSI
G.S. GRAIN SIZE

PENETRATION RESISTANCE
(N) - STANDARD PENETRATION RESISTANCE (SPT)
TSF - POCKET PENETROMETER OR TORVANE
ESTIMATED UNCONFINED COMPRESSIVE
STRENGTH, TONS PER SQ. FOOT

T. and Highway Department
Form 513
Rev. 4-63

Sheet _____ of _____

DRILLING LOG

County Galveston Structure UT Galveston Med. Bldg District No. _____
 Highway No. U.T. System Hole No. 1 (SDHPT) Date 9/17/80
 Cor. No. _____ Station Center of Bldg. Grd. Elev. _____
 Loc. from Centerline Rt. _____ Lt. _____ Grd. Water Elev. _____

ELEV. (FT.)	LOG	THD PEN. TEST NO. OF BLOWS		DESCRIPTION OF MATERIAL	METHOD OF CORING
		1st 6"	2nd 6"		
0				SAND (top soil) (SM)	0
		7	6		D. Bbl.
		*0	0	SAND, fine, gray, wet (SM)	
		6	4		
10		3	12	SILT, gray, soft, moist (ML)	10
		11	19	SAND, silty, gray (SM)	
		17	18	SAND, gray & shell fragments (SM)	20
		3	3		
		50/4 1/2	50/2 1/2	SAND, silty, gray (SM)	
		50/5 1/4	50/4 1/4	SAND, gray, dense (SM)	
30		50/3 1/2	50/3 1/2		30
		19	12		
		5	16	SAND, silty, gray - some clay (SM - CH)	40
		2	2		
		3	4		
		1	2		
50		2	2	CLAY, silty, gray, soft(muck) (CH)	50
		3	3		
		4	5		
60		7	8		60
				CLAY, tan & gray (CH)	
		12	12		
		12	13	SAND, silty, brown (SM)	70

*REMARKS: *Penetrated from 6' to 10' under weight of drill stem and hammer.
 D. Bbl. used with circulated water.

Driller William Willman Logger William Willman Title Engr. Tech. III

Indicate each foot by shading for core recovery, leaving blank for no core recovery, and crossing (X) for undisturbed laboratory samples taken.
 NOTE: Refer to Foundation Exploration and Design Manual for directions in filling out this form. For distribution, forward one copy to the Bridge Division (D-5) and one copy to the Materials and Tests Division (D-9) if samples are submitted and make a note of same on D-5 copy.

State Highway Department
Form 513
Rev. 4-63

Sheet _____ of _____

DRILLING LOG

County _____ Structure _____ District No. _____
 Highway No. _____ Hole No. _____ Date _____
 Control _____ Station _____ Grd. Elev. _____
 1 _____ Loc. from Centerline Rt. _____ Lt. _____ Grd. Water Elev. _____

ELEV. (FT.)	LOG	PEN. TEST NO OF BLOWS		DESCRIPTION OF MATERIAL	METHOD OF CORING	*
		1st 6"	2nd 6"			
70	[Shaded]	12	13	SAND, silty, brown (SM)	0	
	[Shaded]	8	7		10	
80					20	
					30	
20					40	
					50	
30					60	
					70	
40						
50						
60						
70						

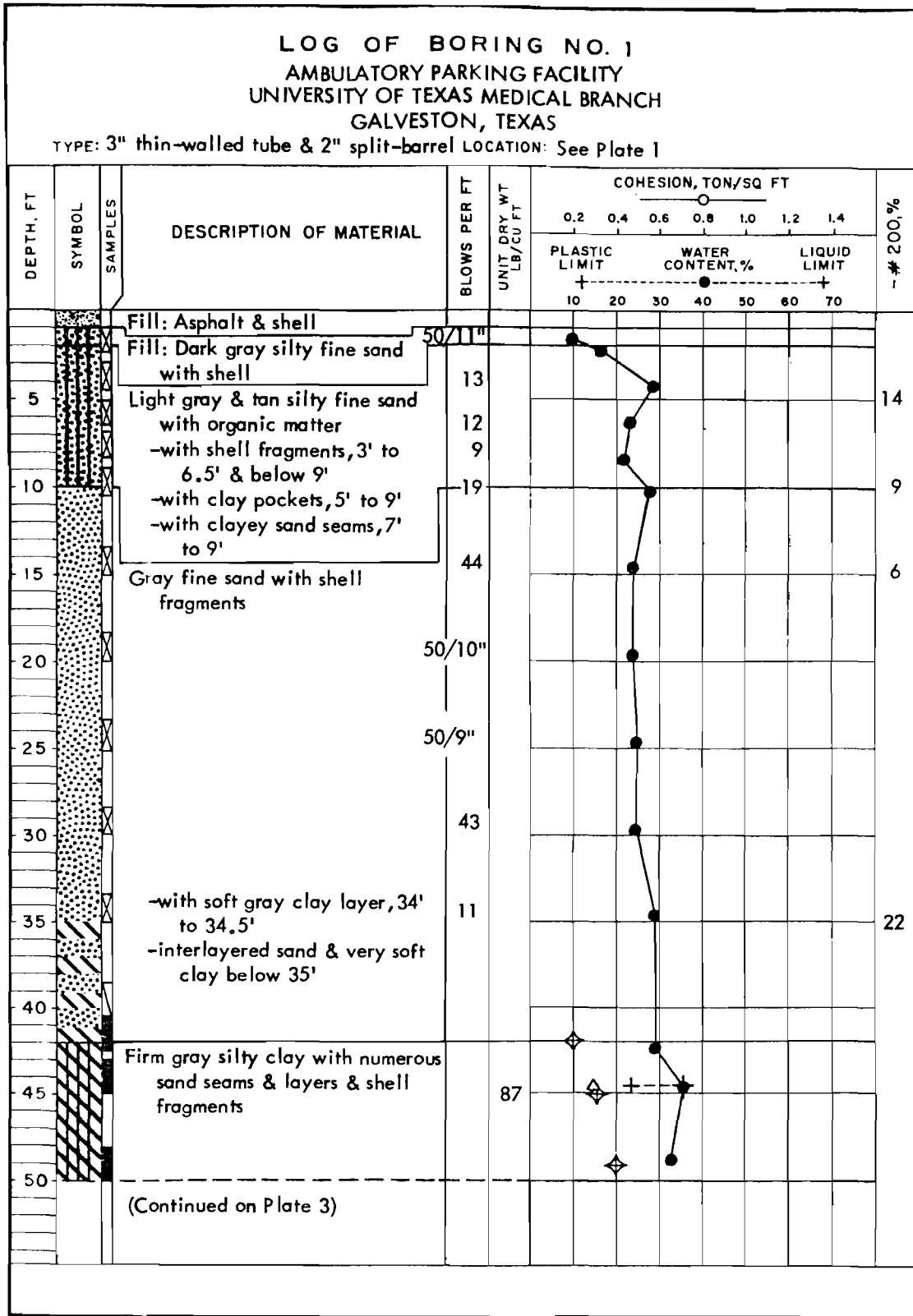
*REMARKS:

Driller _____ Logger _____ Title _____

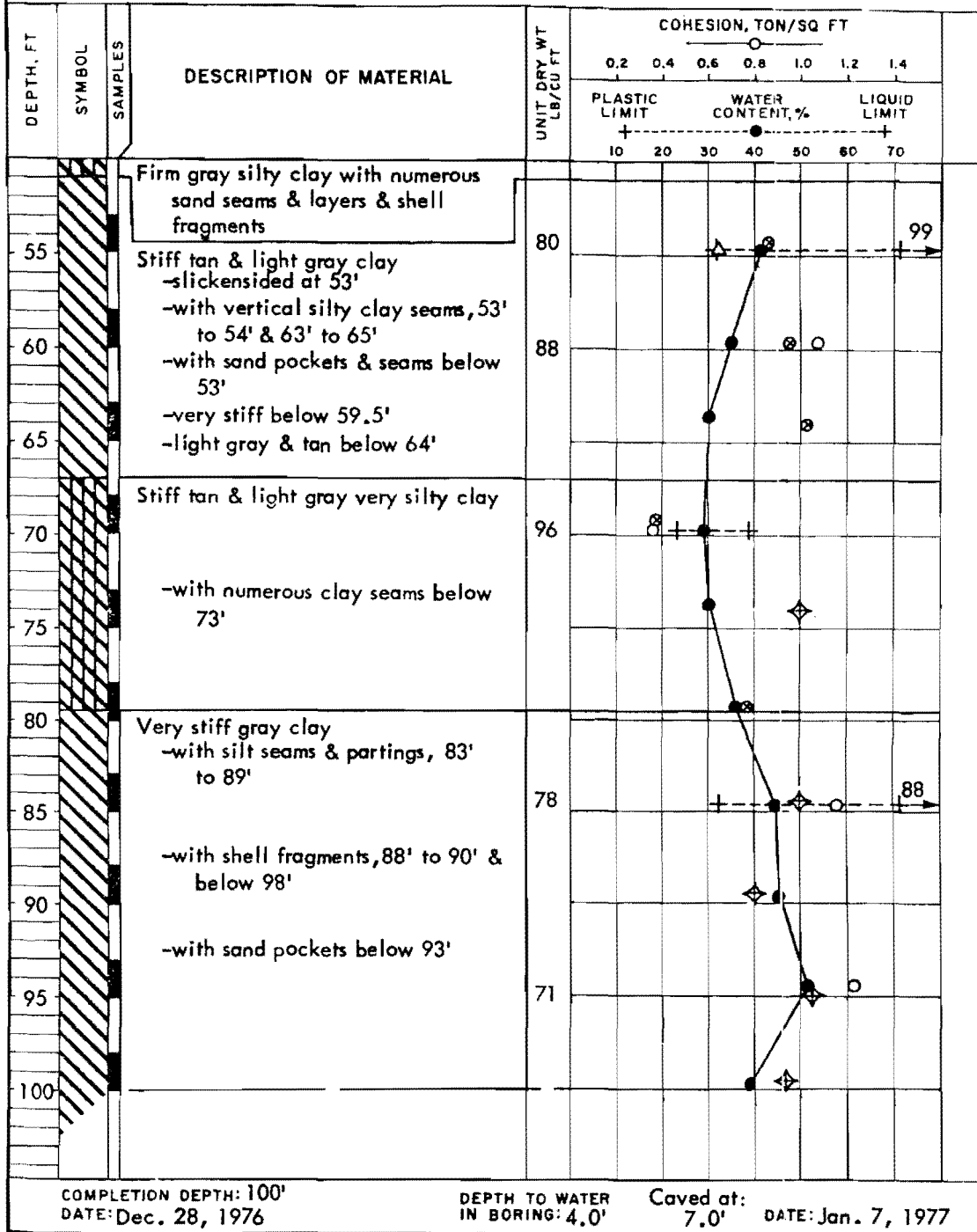
†Indicate each foot by shading for core recovery, leaving blank for no core recovery, and crossing (X) for undisturbed laboratory samples taken.
 NOTE: Refer to Foundation Exploration and Design Manual for directions in filling out this form. For distribution, forward one copy to the Bridge Division (D-6) and one copy to the Materials and Tests Division (D-9) if samples are submitted and make a note of same on I-5 copy.

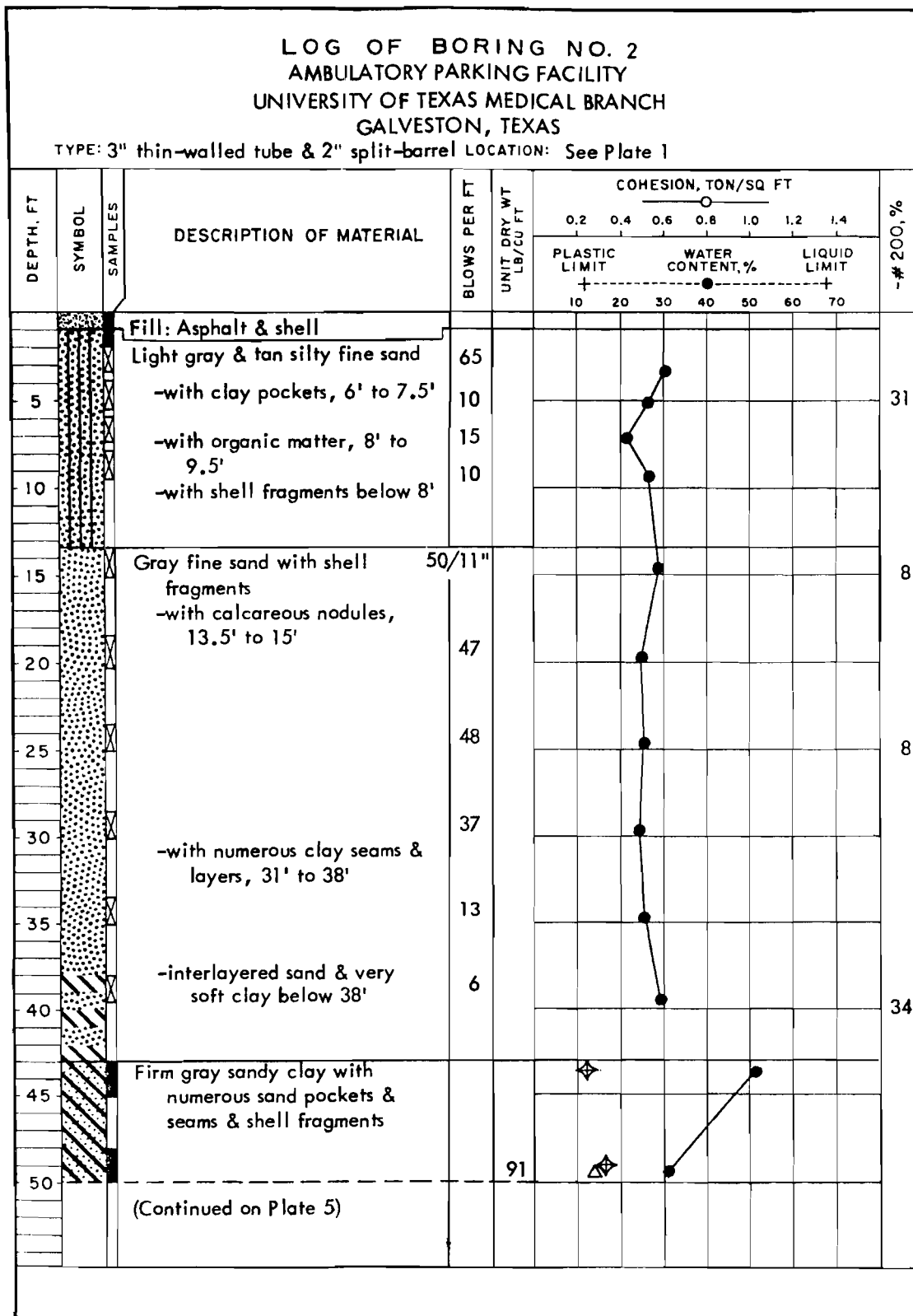
BORING LOGS

Test Site 2
Galveston, Texas

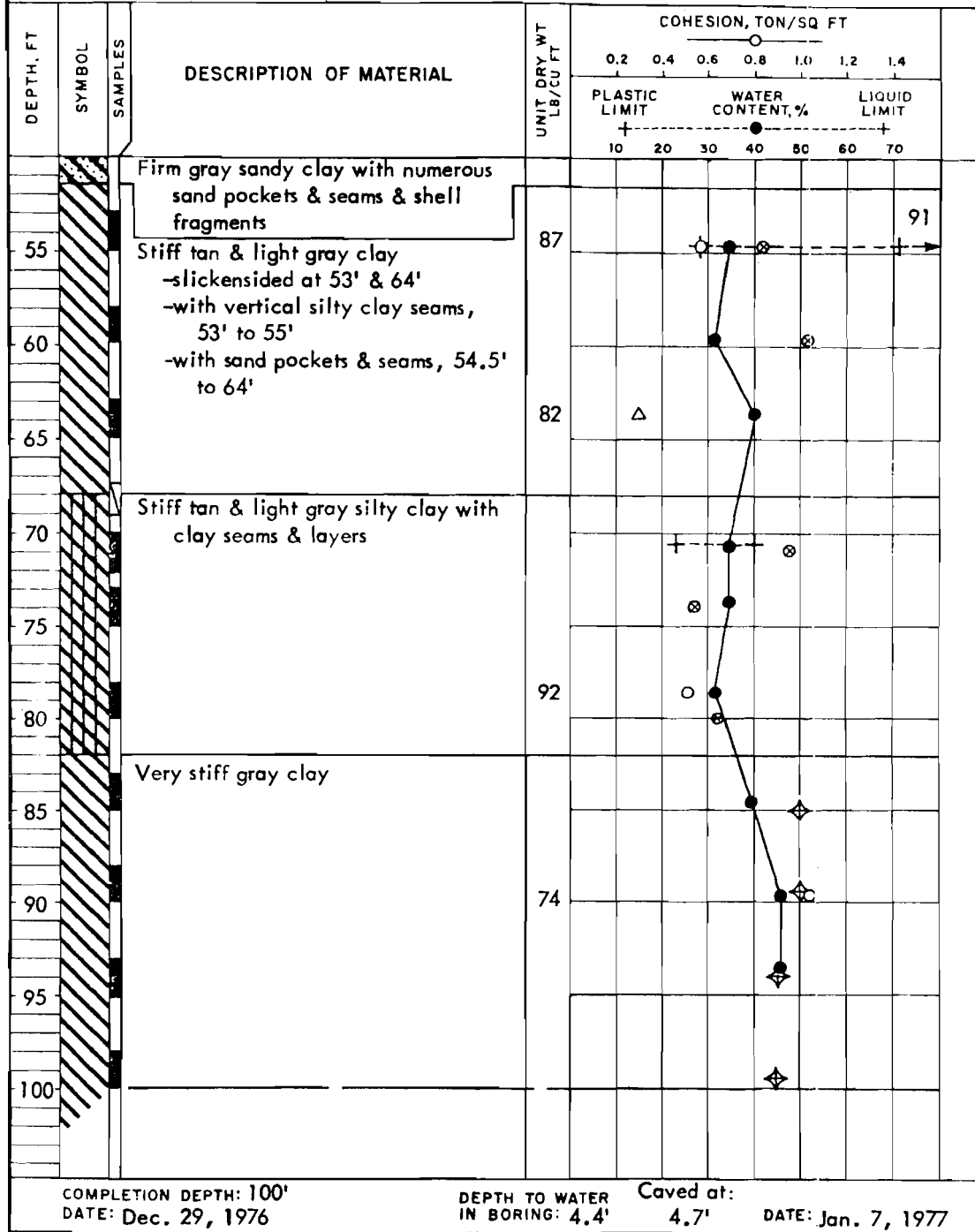


LOG OF BORING NO. 1 (continued)
AMBULATORY PARKING FACILITY
UNIVERSITY OF TEXAS MEDICAL BRANCH
GALVESTON, TEXAS





LOG OF BORING NO. 2 (continued)
AMBULATORY PARKING FACILITY
UNIVERSITY OF TEXAS MEDICAL BRANCH
GALVESTON, TEXAS



COMPLETION DEPTH: 100'
 DATE: Dec. 29, 1976

DEPTH TO WATER
 IN BORING: 4.4'

Caved at:
 4.7'

DATE: Jan. 7, 1977

BORING LOGS

Test Site 3
Eastern Site

TEST BORING REPORT

GROUND ELEVATION		DESCRIPTION OF MATERIALS	SAMPLE NUMBER	HAMMER BLOWS ON SAMPLER	PENE-TRATION (FOOT)	HAMMER BLOWS ON CASING
1.0'	1.0'	Dark brown medium fine silica sand w/slight trace roots	1	2/3	1	1
				5/6	2	2
3.0'	2.0'	Brown medium fine silica sand w/some limerock	2	7/8	3	5
4.0'	1.0'	Brown-tan medium fine silica sand w/trace limerock	3	8/8	4	7
				3/3	5	7
6.0'	2.0'	Dark brown sandy muck	4	3/4	6	5
				3/4	7	6
8.0'	2.0'	Tan medium fine silica sand w/slight trace roots	5	3/3	8	11
				2/1	9	3
10.0'	2.0'	Brown medium fine silica sand	6	1/1	10	4
				1/2	11	4
12.0'	2.0'	Tan medium fine silica sand w/some limerock & marl	7	2/2	12	6
				1/1	13	3
14.0'	2.0'	Tan medium fine silica sand w/some limerock & marl	8	1/1	14	5
				1/2	15	4
16.0'	2.0'	Tan medium fine silica sand w/some limerock & marl	9	2/2	16	7
				2/3	17	7
18.0'	2.0'	Tan limerock with silica sand;some shell	10	3/3	18	8
				1/2	19	3
20.0'	2.0'	Brown medium fine silica sand with trace shell	11	2/3	20	5

Water level: 3.7' below surface @ 11:50 am
on 12/10/80

TEST BORING REPORT

GROUND ELEVATION		Not Given.	DESCRIPTION OF MATERIALS	SAMPLE NUMBER	HAMMER BLOWS ON SAMPLER	PENE-TRATION (FOOT)	HAMMER BLOWS ON CASING
					2/2	21	4
22.0'	2.0'		Brown medium fine silica sand	12	2/4	22	7
					2/2	23	5
24.0'	2.0'		Brown medium fine silica sand	13	3/4	24	8
					3/4	25	13
26.0'	2.0'		Brown medium fine silica sand; trace limerock	14	5/5	26	15
					6/8	27	14
28.0'	2.0'		Brown medium fine silica sand	15	8/8	28	20
					5/8	29	15
30.0'	2.0'		Brown medium fine silica sand	16	10/12	30	22
					6/8	31	18
32.0'	2.0'		Tan fine silica sand	17	12/16	32	26
					7/7	33	16
34.0'	2.0'		Tan fine silica sand	18	11/12	34	28
					6/11	35	15
36.0'	2.0'		Tan fine silica sand	19	13/16	36	24
					5/5	37	20
38.0'	2.0'		Tan fine medium silica sand	20	8/8	38	22
					4/5	39	18
40.0'	2.0'		Tan fine medium silica sand	21	7/7	40	25

TEST BORING REPORT

GROUND ELEVATION		Not Given.	DESCRIPTION OF MATERIALS	SAMPLE NUMBER	HAMMER BLOWS ON SAMPLER	PENE-TRATION (FOOT)	HAMMER BLOWS ON CASING
					3/4	41	16
42.0'	2.0'		Tan fine medium silica sand	22	5/6	42	21
					3/4	43	18
44.0'	2.0'		Tan fine medium silica sand	23	7/8	44	26
					5/6	45	20
46.0'	2.0'		Tan medium fine silica sand	24	6/7	46	28
					4/5	47	22
48.0'	2.0'		Gray medium fine silica sand; trace shell	25	8/8	48	29
					4/4	49	21
50.0'	2.0'		Gray medium fine silica sand with trace shell	26	7/7	50	29
					4/5	51	28
52.0'	2.0'		Tan medium fine silica sand with some limerock	27	6/7	52	30
					3/5	53	28
54.0'	2.0'		Tan medium fine silica sand with trace limerock	28	6/8	54	25
					5/6	55	28
56.0'	2.0'		Gray medium fine silica sand with some limerock	29	9/12	56	36
					6/6	57	25
58.0'	2.0'		Gray medium fine silica sand with some limerock	30	12/13	58	38
					5/9	59	22
60.0'	2.0'		Gray medium fine silica sand with some limerock	31	11/14	60	31

TEST BORING REPORT

GROUND ELEVATION		Not Given.	DESCRIPTION OF MATERIALS	SAMPLE NUMBER	HAMMER BLOWS ON SAMPLER	PENE-TRATION (FOOT)	HAMMER BLOWS ON CASING
					6/8	61	30
62.0'	2.0'		Gray medium fine silica sand with some limerock	32	10/11	62	45
64.0'	2.0'		Gray medium fine silica sand with some limerock	33	6/12 10/13	63 64	26 41
66.0'	2.0'		Gray medium fine silica sand with some limerock	34	16/12 10/13	65 66	35 50
68.0'	2.0'		Gray fine medium silica sand with some limerock	35	12/14 21/28	67 68	45 62
70.0'	2.0'		Gray limerock with silica sand	36	11/16 26/34	69 70	51 61
72.0'	2.0'		Gray limerock with silica sand	37	11/14 16/18	71 72	53 64
74.0'	2.0'		Gray limerock with silica sand	38	12/13 15/18	73 74	50 61
76.0'	2.0'		Gray limerock with silica sand	39	8/10 18/26	75 76	58 71
78.0'	2.0'		Gray limerock with silica sand	40	10/13 21/25	77 78	75 104
80.0'	2.0'		Gray limerock with silica sand	41	8/12 16/18	79 80	82 110

TEST BORING REPORT

GROUND ELEVATION		Not Given.	DESCRIPTION OF MATERIALS	SAMPLE NUMBER	HAMMER BLOWS ON SAMPLER	PENE-TRATION (FOOT)	HAMMER BLOWS ON CASING
					6/7	81	61
82.0'	2.0'		Gray limerock with silica sand	42	10/11	82	72
					5/7	83	58
84.0'	2.0'		Gray limerock w/silica sand;slight trace marl	43	9/10	84	61
85.0'	1.0'		Gray limerock w/silica sand;slight trace marl	44	5/8	85	
					Boring Completed.		
			see page 1....				

TEST BORING REPORT

GROUND ELEVATION	Not Given.	DESCRIPTION OF MATERIALS	SAMPLE NUMBER	HAMMER BLOWS ON SAMPLER	PENE-TRATION (FOOT)	NO. BLC. E.
				2/2	1	2
				6/6	2	1
				10/10	3	1
3.5'	3.5'	Tan medium fine silica sand with limerock	1	10/9	4	1
4.0'	0.5'	Dark gray medium fine silica sand	2			
				9/10	5	2
6.0'	2.0'	Tan medium fine silica sand	3	13/15	6	2
				6/5	7	1
				5/5	8	1
9.0'	3.0'	Brown medium fine silica sand w/slight trace roots	4	4/4	9	1
				4/5	10	1
				3/4	11	1
				5/6	12	2
					13	2
14.0'	5.0'	Tan limerock with silica sand; trace marl	5		14	2
15.0'	1.0'	Tan limerock with silica sand; trace marl	6		15	3
				5/6	16	2
				11/12	17	2
					18	2
					19	3
20.0'	5.0'	Tan limerock with silica sand; trace marl	7		20	3

Water level: 4.4' below surface @ 3.20pm
Date: See Above.

TEST BORING REPORT

GROUND ELEVATION		DESCRIPTION OF MATERIALS	SAMPLE NUMBER	HAMMER BLOWS ON SAMPLER	PENETRATION (FOOT)	HAM BLOW CAP
	See Pg. 1.					
				4/4	21	13
				7/8	22	18
					23	24
					24	20
25.0'	5.0'	Tan limerock with silica sand; trace marl	8		25	22
				2/3	26	16
				6/6	27	21
					28	31
					29	36
30.0'	5.0'	Brown fine medium silica sand with slight trace limerock	9		30	38
				2/3	31	14
				5/6	32	21
					33	32
					34	41
35.0'	5.0'	Tan fine medium silica sand	10		35	54
				2/3	36	19
				6/6	37	28
					38	34
					39	38
0.0'	5.0'	Gray medium fine silica sand	11		40	46

Water level: See Pg. 1.

TEST BORING REPORT

GROUND ELEVATION		See Pg. 1.	DESCRIPTION OF MATERIALS	SAMPLE NUMBER	HAMMER BLOWS ON SAMPLER	PENE- TRATION (FOOT)	HAMI BLOW CABE
					4/5	41	1
					7/8	42	2
						43	3
						44	4
15.0'	5.0'		Gray medium fine silica sand	12		45	4
					5/5	46	1
					6/6	47	1
						48	2
						49	2
10.0'	5.0'		Gray medium fine silica sand with trace limerock	13		50	2
					4/5	51	1
					7/7	52	2
						53	3
						54	3
5.0'	5.0'		Gray medium fine silica sand with trace shell; slight trace marl	14		55	7
					6/7	56	3
					12/12	57	6
						58	4
						59	4
0.0'	5.0'		Tan medium fine silica sand with trace limerock, marl, shell.	15		60	5

Water level: see page 1...

TEST BORING REPORT

GROUND ELEVATION	Not Given.	DESCRIPTION OF MATERIALS	SAMPLE NUMBER	HAMMER BLOWS ON SAMPLER	PENE- TRATION (FOOT)	HARD BLOW/ CARP
				2/2	1	1
				6/6	2	3
				9/10	3	10
4.0'	4.0'	Tan medium fine silica sand with some limerock	1	10/12	4	14
5.0'	1.0'	Dark brown medium fine silica sand w/organics	2	4/5	5	8
				8/9	6	9
				8/8	7	10
				11/11	8	14
				7/7	9	15
10.0'	5.0'	Tan medium fine silica sand	3	5/5	10	11
				3/2	11	10
				2/3	12	10
					13	9
					14	9
15.0'	5.0'	Tan-brown medium fine silica sand	4		15	10
				1/1	16	5
				1/2	17	6
					18	5
					19	6
0'	5.0'	Tan medium fine silica sand; trace shell, limerock	5		20	8

water level: 4.1 'below surface @ 3:05 pm
Date: See Above.

TEST BORING REPORT

GROUND ELEVATION		DESCRIPTION OF MATERIALS	SAMPLE NUMBER	HAMMER BLOWS ON SAMPLER	PENETRATION (FOOT)	HAMMER BLOWS ON CASING
	See Pg. 1.					
				2/2	21	9
				4/4	22	10
					23	17
					24	24
25.0'	5.0'	Brown medium fine silica sand	6		25	26
				2/3	26	12
				5/6	27	16
					28	21
					29	26
30.0'	5.0'	Brown fine medium silica sand	7		30	34
				3/4	31	18
				8/9	32	24
					33	36
					34	39
5.0'	5.0'	Brown fine medium silica sand	8		35	51
				3/3	36	21
				5/6	37	31
					38	38
					39	42
0.0'	5.0'	Tan fine medium silica sand	9		40	51

Water level: See Pg. 1.

TEST BORING REPORT

GROUND ELEVATION		See Pg. 1.	DESCRIPTION OF MATERIALS	SAMPLE NUMBER	HAMMER BLOWS ON SAMPLER	PERCENTRATION (FOOT)	HAMMER BLOWS ON CASING
					4/4	41	20
					6/6	42	28
						43	31
						44	32
45.0'	5.0'		Gray medium fine silica sand	10		45	32
					5/6	46	20
					9/9	47	21
						48	24
						49	35
50.0'	5.0'		Gray medium fine silica sand	11		50	51
					4/5	51	41
					9/10	52	51
						53	70
						54	78
55.0'	5.0'		Gray fine medium silica sand; trace shell	12		55	91
					6/6	56	54
					12/12	57	66
						58	80
			Tan fine medium silica sand with trace limerock; slight trace marl	13		59	84
60.0'	5.0'					60	11

Water level: see page 1...

APPENDIX B

PREPARATION AND INSTALLATION OF
MUSTRAN CELLS

PREPARATION AND INSTALLATION OF MUSTRAN CELLS

Due to the proven performance of the Mustran cell in axial load tests of drilled shafts, their use is becoming quite prominent throughout the United States. Because of the increased use of Mustran cells, the following sections have been included in Appendix B.

Material List for Mustran Cell

Construction Sequence for Mustran Cell

Installation Procedure for Mustran Cell

MATERIAL LIST FOR MUSTRAN CELL

Following is a list of the materials needed for the construction of a single Mustran cell.*

MATERIALS

<u>Item No.</u>	<u>Quantity</u>	<u>Description</u>
1	1 each	top cap, steel (Fig. B.1)
2	1 each	bottom cap, steel (Fig. B.2)
3	1 each	centerpiece, steel (Fig. B.3)
4	2 each	mounting angles, steel (Fig. B.4)
5	1 each	gauge application tool set, ATS-2 (to be ordered only once)
6	2 each	strain gauge, EA-06-250TG-350
7	as needed	sandpaper, wet or dry silicon-carbide, 220 (SCP-1) and 320 (SCP-2) grit
8	as needed	cotton swabs, CSP-1
9	as needed	gauze sponges, GSP-1
10	as needed	M-bond 600 adhesive kit
11	as needed	M-coat D kit
12	as needed	M-coat G kit
13	as needed	chlorothene NU degreaser, CNU-1
14	as needed	M-prep conditioner A, MCA-2
15	as needed	M-prep neutralizer 5, MN5-2
16	as needed	Mylar JG tape, MJG-2
17	2 each	pressure pads and backup plates, GT-14 (reusable)
18	1 each	hargrave spring clamp, 1", HSC-1 (reusable)
19	as needed	stranded-tinned copper wire, red, black, green, and white, 126-BWV
20	4 each	bondable terminals, CTF-50C (solder tabs)
21	as needed	TFE teflon film, TFE-1 (reusable)

* Items 5-21 are all available from Micromasurements; Micro-measurement name and part number are given.

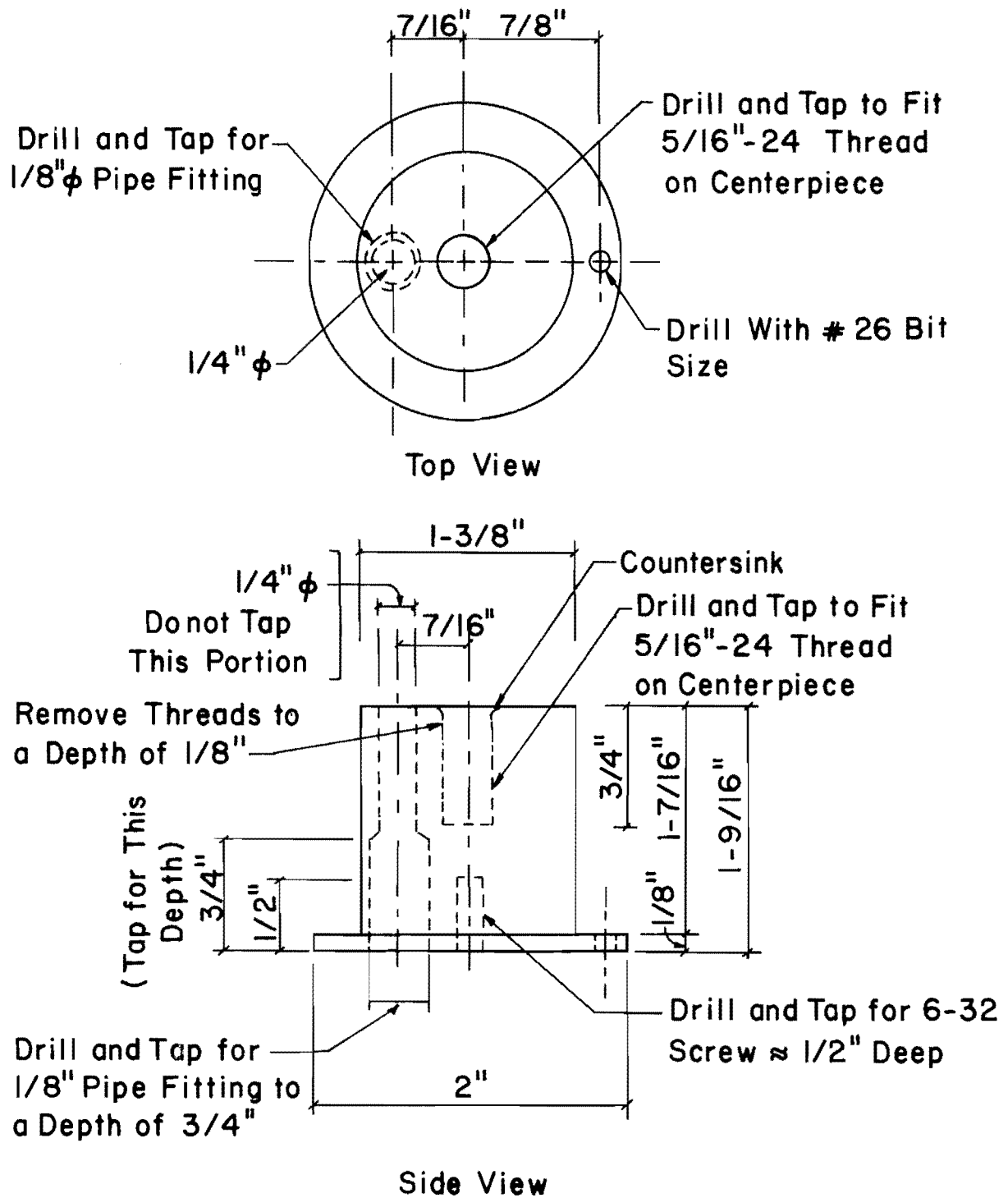


Fig. B.1 Top Cap

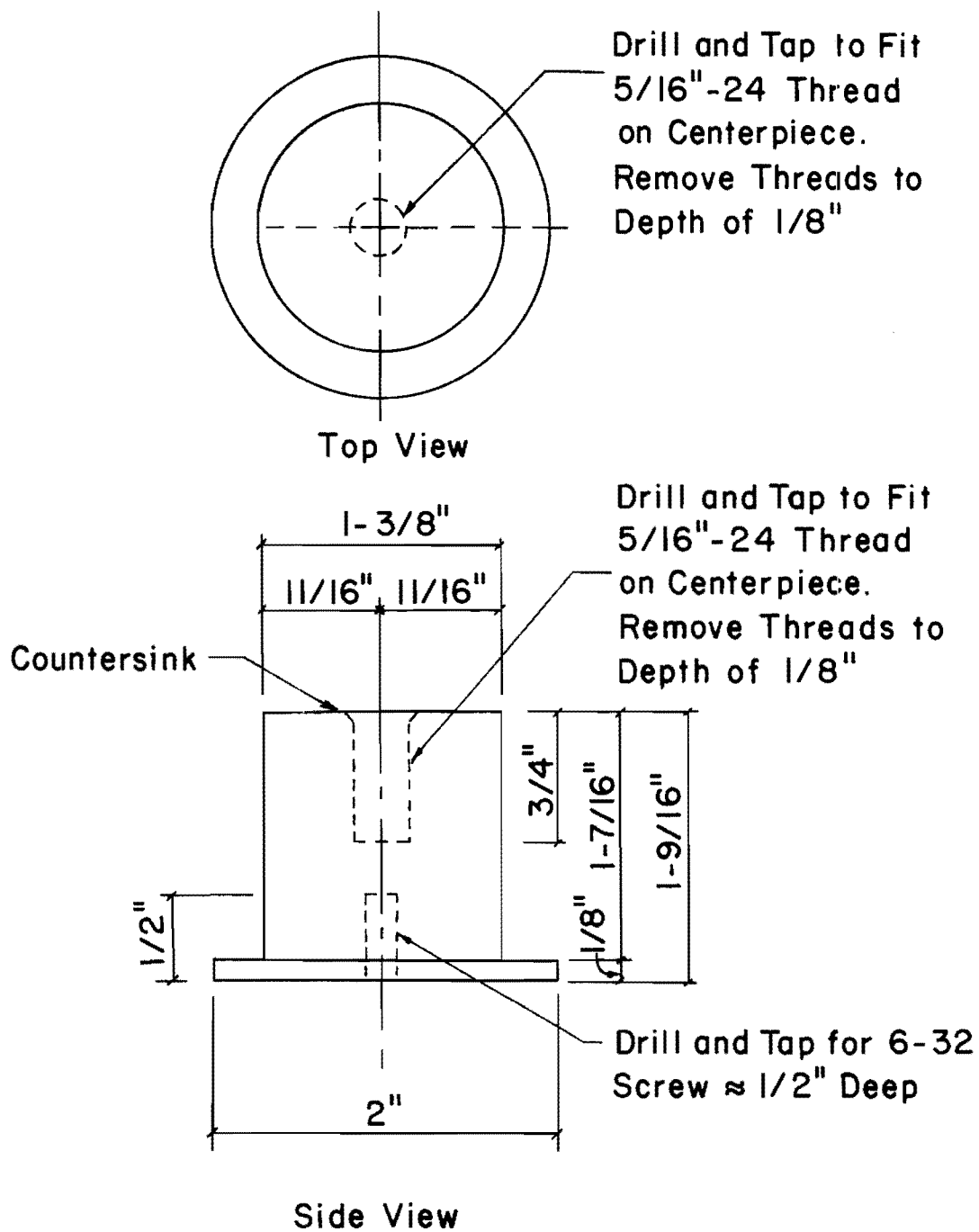


Fig B.2 Bottom Cap

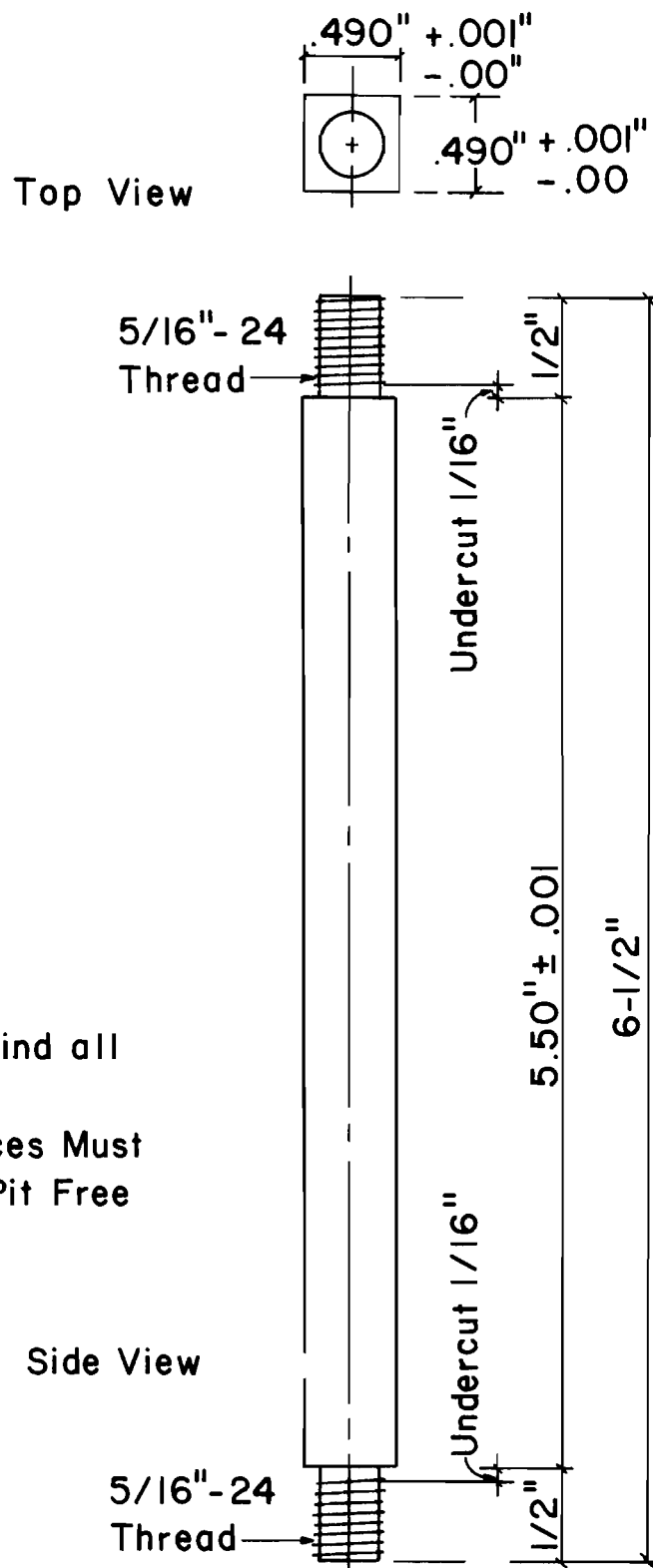
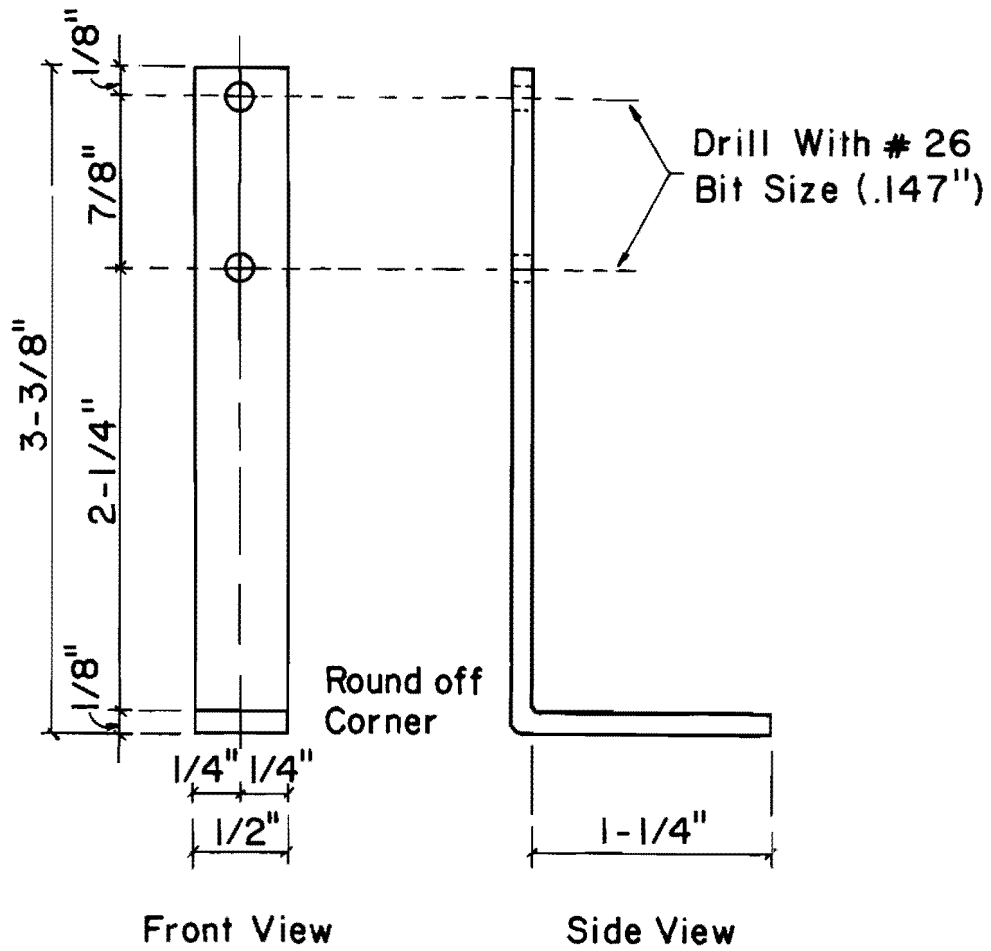


Fig. B.3 Centerpiece



Make With $1/8\text{''} \times 1/2\text{''}$ Steel Strip and Bent to Above Dimensions

Fig. B.4 Mounting Angles

<u>Item No.</u>	<u>Quantity</u>	<u>Description</u>
22	as needed	solder, low temperature
23	as needed	Belden wire, #8729, 22 AWG, stranded, 4-conductor, beldfoil sheilded plastic jacketed instrumentation cable, 0.265-inch O.D.
24	as needed	vacuum grease
25	as needed	teflon tape, 1/2-inch wide
26	1 each	radiator hose (Gates No. 1522H (24022)), 1 3/8-inch I.D., 8-inch length
27	2 each	hose clamps, radiator (ideal combo hex #5424 maximum clamp diameter - 2 inches)
28	as needed	silicone rubber sealant
29	1 each	male connector, Swagelok #B-400-1-2
30	1 each	front ferrule, Swagelok #B-403-1
31	1 each	back ferrule, Swagelok #B-404-1
32	1 each	tygon tubing, 1/4-inch I.D., 3/8-inch O.D., 1-inch length
33	as needed	Scotch cloth tape, #390, olive drab, 3-inch, or 3-inch silver duct tape
34	4 each	bolts, 6-32 with 1/2-inch thread
35	2 each	nuts, 6-32
36	1 each	male connector, Swagelok #B-600-1-4 (to be ordered only once)
37	1 each	back ferrule, Swagelok #B-604-1
38	1 each	front ferrule, Swagelok #B-603-1

CONSTRUCTION SEQUENCE FOR MUSTRAN CELL

Following is a step-by-step process for constructing a Mustran cell.

1. Inspect centerpiece; make sure it meets specifications. Check end caps by screwing onto centerpiece.
2. Choose the two best opposite sides of the centerpiece for strain gauge application.
3. Remove grease from centerpiece.

4. Mark centerpiece, vertical and horizontal scribe marks, for centering of strain gauge (both sides). Scribe marks should not go into gage area.

5. Apply M-prep conditioner and sand the centerpiece gauging area with 220 or 320 silicone (both sides).

6. Neutralize complete bar with M-prep neutralizer.

7. Clean area to be gauged with Chlorothene Nu degreaser, using a cotton swab to wipe area. (Fig. B.5 shows centerpiece after steps 1-7.)

8. Lay strain gauge and 4-terminal solder tab (solder tab will be on only one side of centerpiece) on glass plate and clean with Chlorothene Nu degreaser. Use cotton swabs.

9. Place strain gauge (and solder tab if needed) on Mylar tape so that the gauge side is against the tape. This is done by laying the gauge and tab (tab should be at vertical end of strain gauge) on the glass plate, gauge side up and putting the Mylar tape on the strain gauge and tab.

10. Position the gauge/tape assembly so the alignment marks on the gauge are in line with the alignment marks on the centerpiece. Holding the tape at a shallow angle (about 45°), place the assembly onto the centerpiece surface. If the gauge appears to be misaligned, lift one end of the tape at a shallow angle until the assembly is free, then realign. (See Fig. B.6.)

11. Once alignment is correct, lift the unanchored end of the tape at a shallow angle until gauge and terminal are free of specimen surface.

12. Tuck the loose end of tape under and press to the surface of the centerpiece so the gauge lies flat with the bonding side exposed. (See Fig. B.7.)

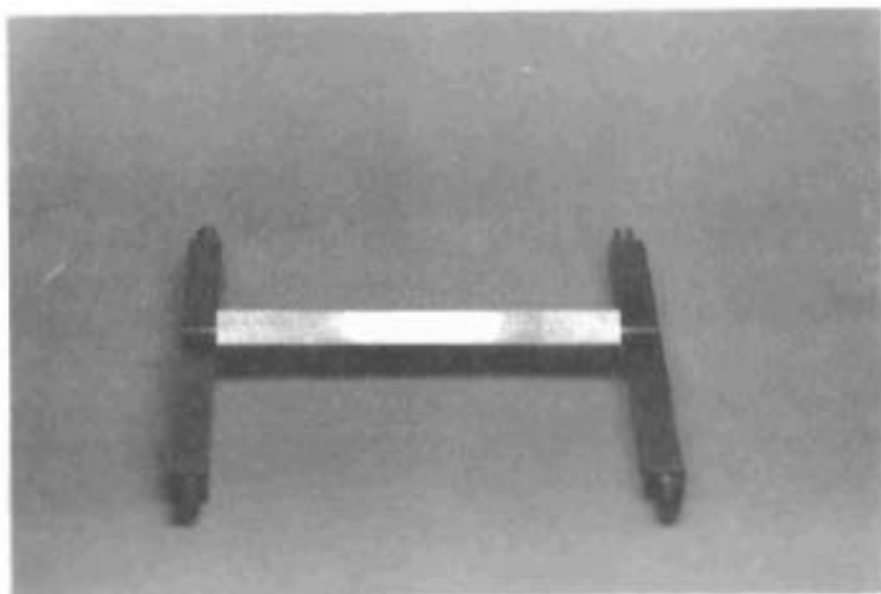


Fig. B.5 Cleaned and Scribed Centerpiece

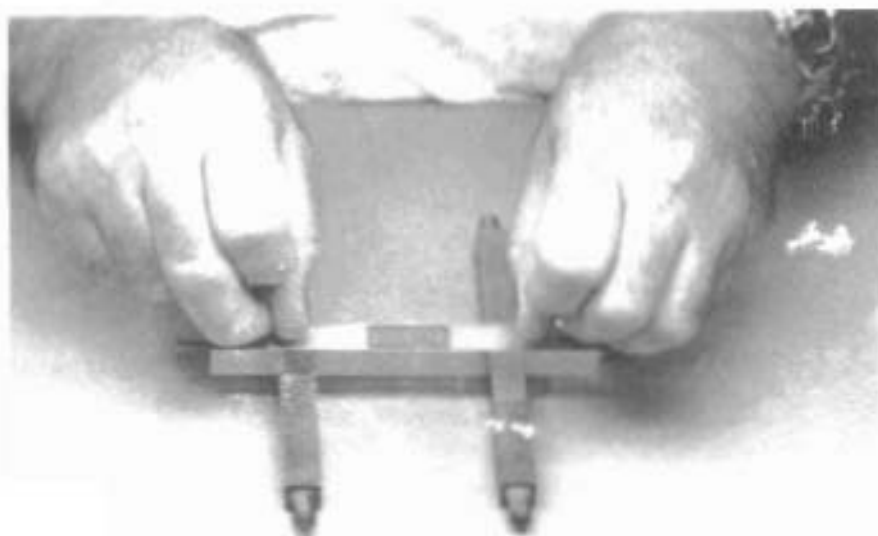


Fig. B.6 Alignment of Strain Gauge

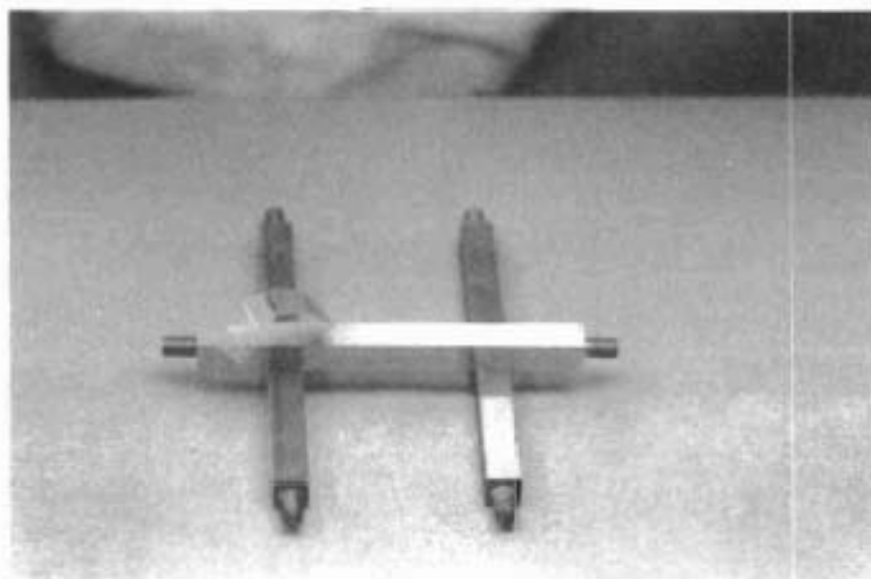


Fig. B.7 Strain Gauge and Centerpiece Ready for Application of M-Bond 600

13. Apply thin coat of M-bond 600 to back of gauge and to centerpiece gauge area. Allow this to air dry for 5 to 20 minutes. (See Figs. B.8 and B.9.)

14. Set strain gauge in place; lift tucked-over end of tape and strain gauge over the gauge area of centerpiece at approximately a 30° -angle. With a piece of teflon, slowly make a single wiping stroke over the gauge/tape assembly, bringing the gauge down over the alignment marks on the centerpiece. (See Fig. B.10.)

15. Place teflon guard (TFE teflon film) over the strain gauge and Mylar tape; tape teflon guard to centerpiece. (See Fig. B.11.)

16. Repeat steps 7-15 for opposite side strain gauge placement. Be sure that the horizontal and vertical grids on the strain gauges match on both sides.

17. Place pressure pads and backup plates over the strain gauges (teflon guards still in place).

18. Clamp the pressure pads and backup plates with the Hargrave spring clamp. (See Fig. B.12.)

19. Place entire assembly in preheated oven for temperature curing (250°F for 2 hours).

20. After temperature curing, allow centerpiece to cool gradually to room temperature.

21. Remove clamps, pressure pads and backup plates, and teflon guard.

22. Carefully peel off the Mylar tape. (Fig. B.13a and b show strain gauges on both sides of centerpiece after step 22.)

23. Check for strain-gauge bonding and for air bubbles underneath strain gauge.

24. Apply solder dots to gauge tabs and to 4-terminal solder tab. Solder wiring between the gauges (Fig. B.14). (Fig. B.15 shows centerpiece after step 24.)

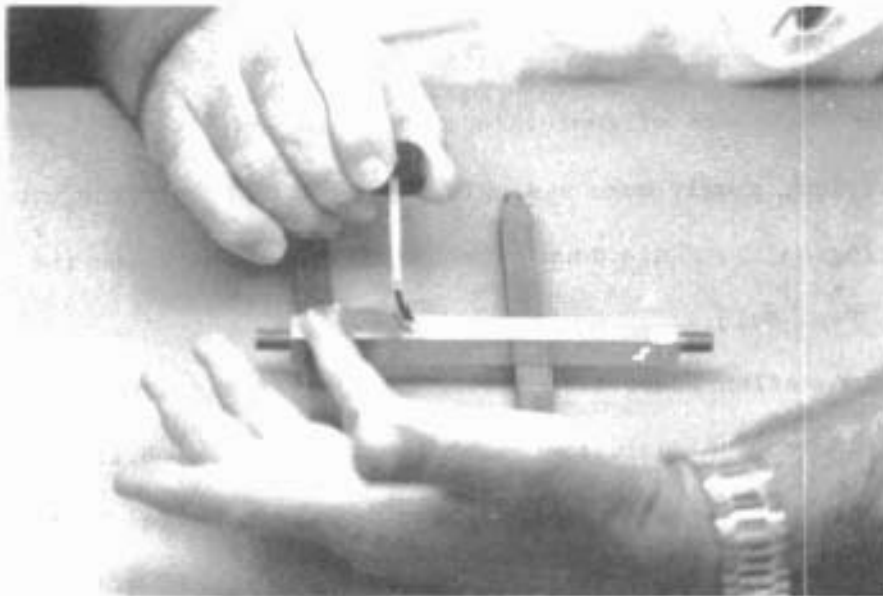


Fig. B.8 Application of M-Bond 600 to Strain Gauge

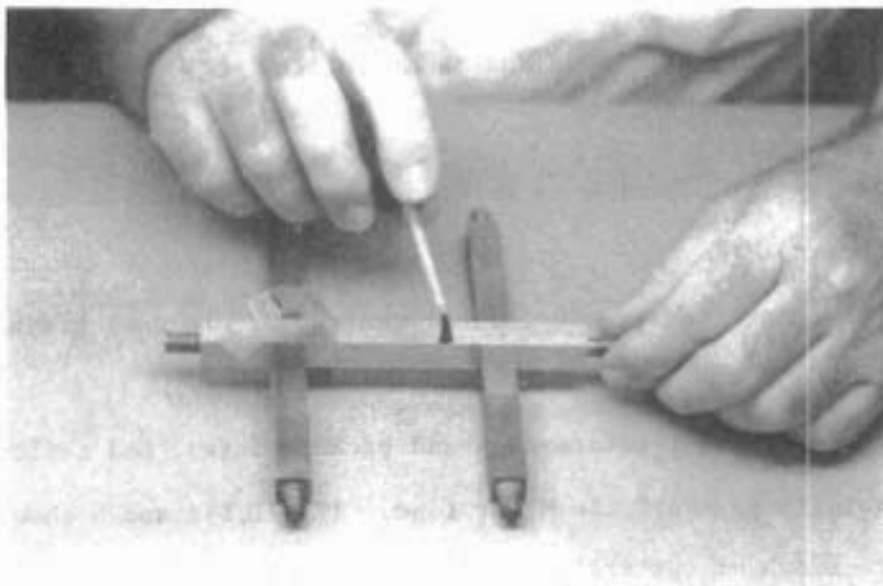


Fig. B.9 Application of M-Bond 600 to Centerpiece

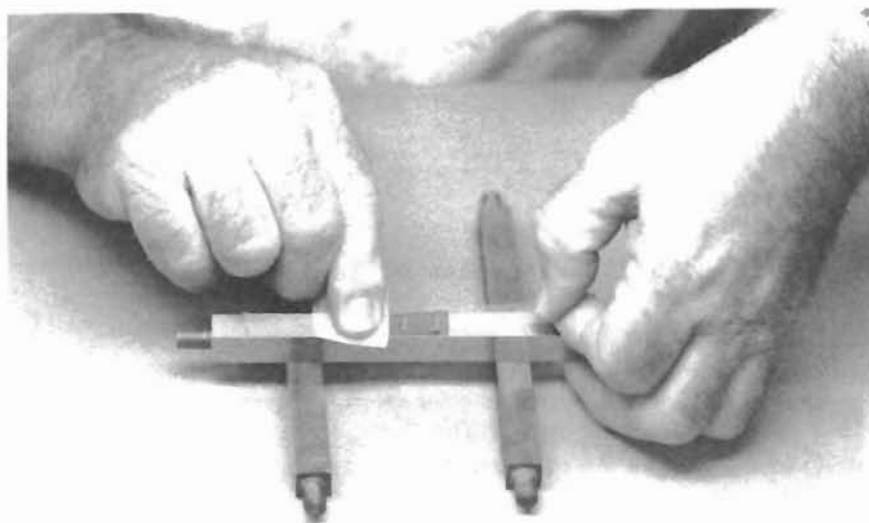


Fig. B.10 Laying of Strain Gauge

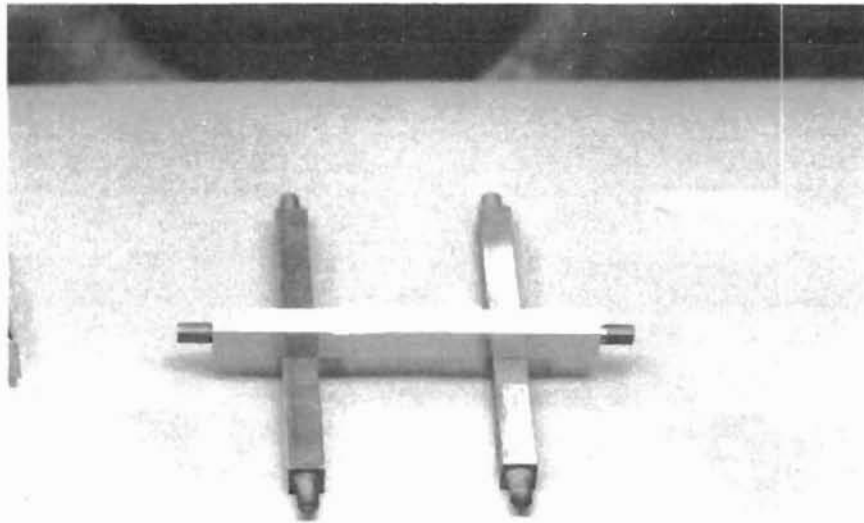


Fig. B.11 Placement of Teflon Pads

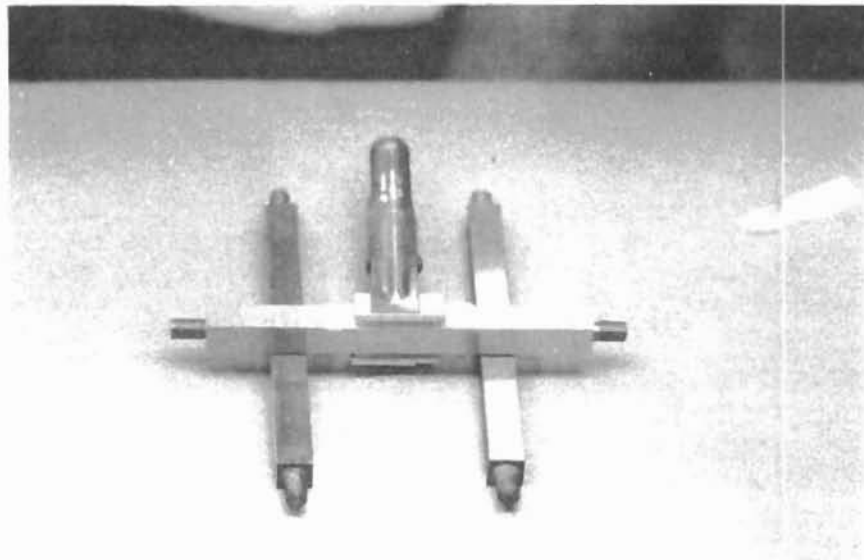
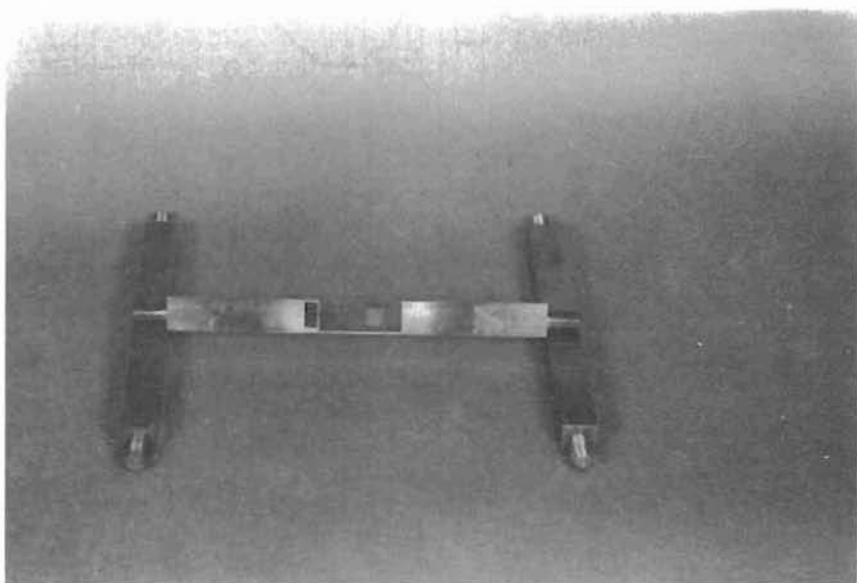


Fig. B.12 Clamp and Pressure Pads



(a)



(b)

Fig. B.13 (a) Strain Gauge on Back of Centerpiece
(b) Strain Gauge and Tab on Front of
Centerpiece

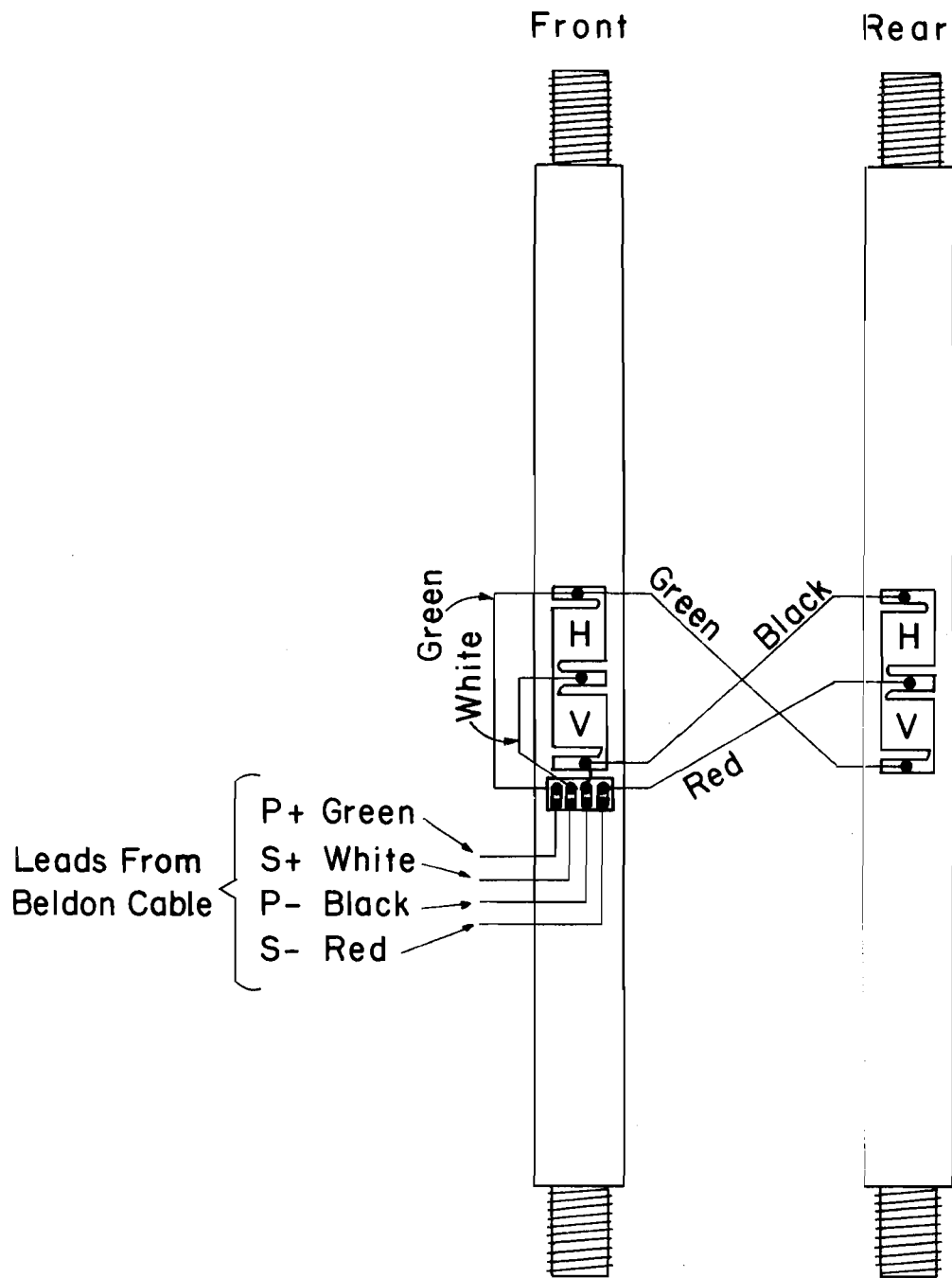


Fig. B.14. Wiring Between Gauges

25. Attach strain indicator and check gauge for balance and operation.
26. Cut Belden cable #8729 to required length and label it by using the 3-inch-wide tape and also by writing on the cable; a waterproof marker should be used.
27. Remove approximately 6 in of outer sheath at one end of the Belden cable.
28. Put the top of a Swagelok #B-400-1-2 male connector on the end of the cable where the outer sheath was removed.
29. Put back ferrule, Swagelok #B-404-1, on same end of cable.
30. Put front ferrule, Swagelok #B-403-1, on same end of cable.
31. Put teflon tape on threads of the bottom of a Swagelok #B-400-1-2 male connector.
32. Attach the bottom of the male connector to the top cap.
33. Insert the lead wires from the Belden cable through the Swagelok male connector and top cap. At this time one should be able to screw the top and bottom of the Swagelok male connector back together, with the front and back ferrules in place.
34. Securely attach top cap to centerpiece so that the top cap is on the end closest to the 4-terminal solder tab.
35. Strip approximately 1/4 in of each lead wire from the Belden cable.
36. Solder the four lead wires from the Belden cable to the solder tabs.
37. Check the wiring with portable strain indicator for balance and with OHM-meter for resistance to ground.

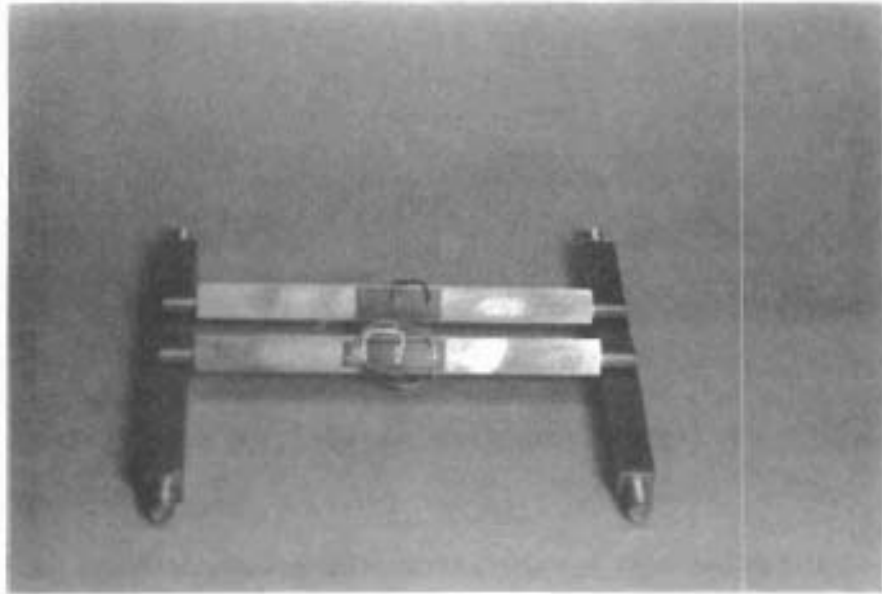


Fig. B.15 Wiring Between Gauges, Front and Back of Centerpiece

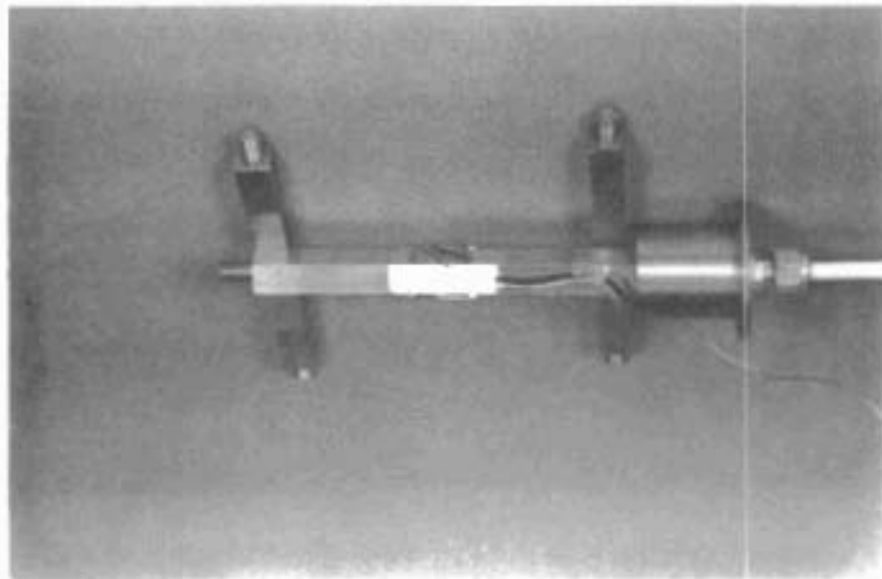


Fig. B.16 M-Coat D Applied to Centerpiece

38. Apply one coat over all wiring connections with M-coat D. Allow 30 minutes for drying (Fig. B.16).

39. Coat all gauges and exposed wiring with heavy application of M-coat G (Fig. B.17). Allow 24 hours for drying. Caution: do not coat or plug cable entrance hole through top cap.

40. Cut proper length (8 in) of radiator hose.

41. Put two hose clamps loosely on the radiator hose.

42. Apply silicone rubber sealant to both the top and bottom caps.

43. Insert the centerpiece and top cap (up to the 2-inch-diameter lip) in the radiator hose, at the same time trapping the ground wire between the top cap and radiator hose.

44. Securely attach bottom cap to centerpiece. After this point, if for any reason the Mustran cell needs to be taken apart, the radiator hose should be cut off. This is to prevent the wires from being torn loose.

45. Center the radiator hose and clamp.

46. Cut off the ground wire that is sticking out of the radiator hose.

47. Drill hole (#26 bit size) in lip of bottom cap to coincide with hole in lip of top cap.

48. Secure attaching brackets to top and bottom caps, using 4-6-32 X 1/2 bolts and 2-6-32 nuts. (Fig. B.18 shows assembled Mustran cell.)

49. Remove approximately 6 inches of outer sheath from the other end of the Belden cable.

50. Strip approximately 1/2 inch of each of the four lead wires.

51. Insert the lead wires and approximately 3 inches of the Belden cable through the 1/4-inch tygon tubing.

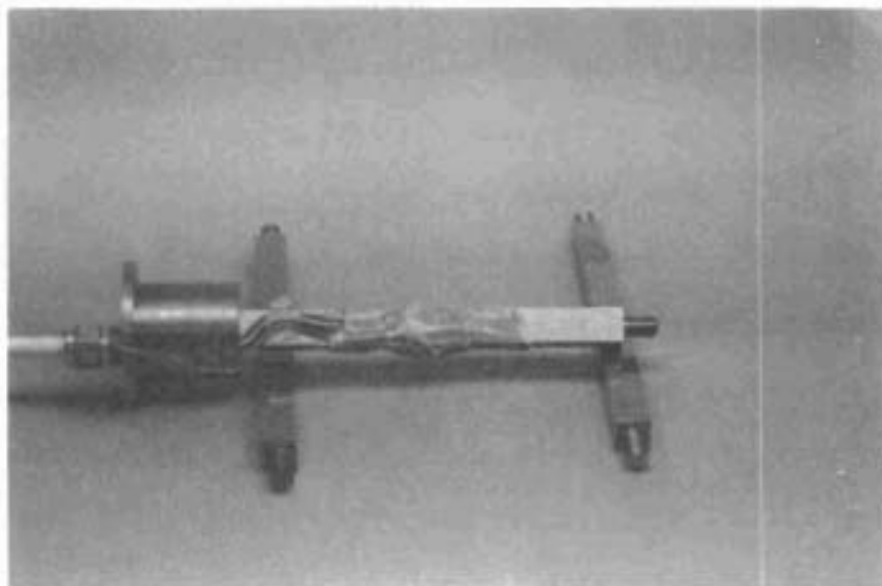


Fig. B.17 M-Coat Applied to Centerpiece

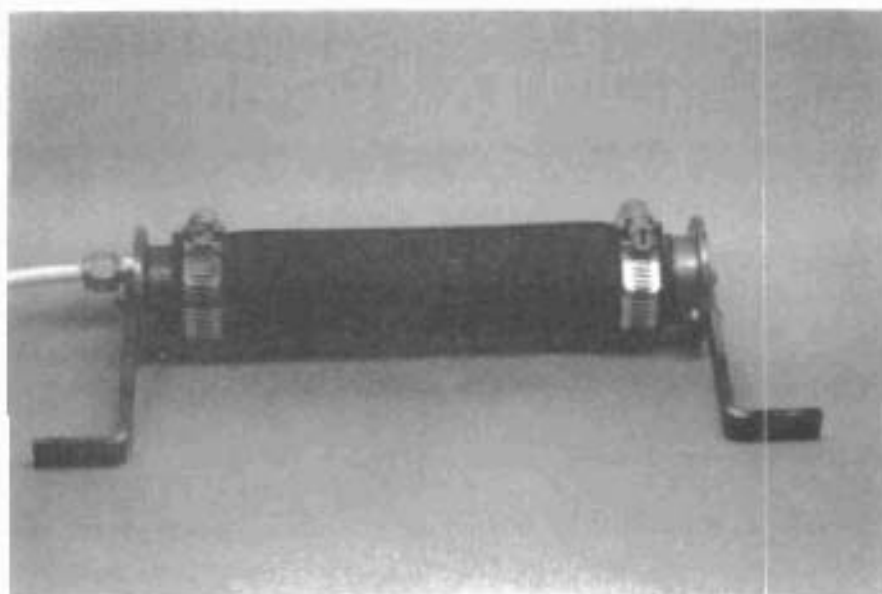


Fig. B.18 Assembled Mustran Cell

52. Put the top of a Swagelok #B-600-1-4 male connector on the tygon tubing (bottom of male connector is in manifold).

53. Put the back ferrule, Swagelok #B-604-1, on the tygon tubing.

54. Put the front ferrule, Swagelok #B-603-1, on the tygon tubing.

PROCEDURE FOR MUSTRAN CELL INSTALLATION

The following is a set of instructions for installing Mustran cells on a reinforcing steel cage.

1. After unpacking the cells, check them with a portable strain indicator to see if they will balance and with an Ohm-meter for resistance to ground, which should be infinite.

2. Measure the length of the reinforcing cage.

3. Mark off the placement depths of the Mustran cells.

4. Starting at the bottom of the reinforcing cage, mount the Mustran cells at the placement depths that were marked off. (The bottom level and the top level should both contain at least four Mustran cells.)

5. Cells should be mounted so that the end with the Swagelok fitting, the top cap, will be pointing to the bottom of the drilled shaft.

6. Mounting should be done so that any level of 2 or 4 that the cells should be approximately 180° or 90° apart. (See Fig. B.19.)

9. String the cable out on the interior of the reinforcing cage and out the top of the reinforcing cage. After four levels of cells have been installed, two cells on each of the four rebars being used, the cable should be taped to the rebars for the complete length of the shaft.

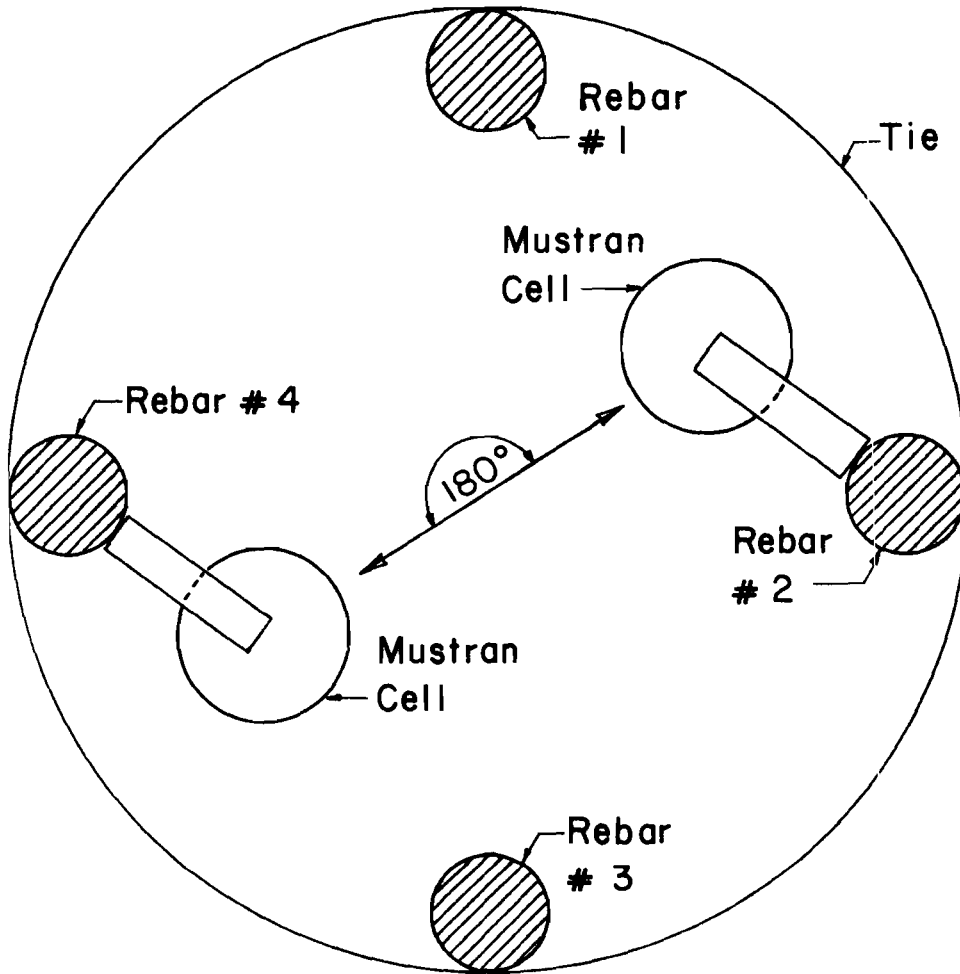


Fig. B.19 Mounting of Mustran cells

10. Repeat steps 5-9 for mounting the rest of the cells. Note: After the bottom level of four cells, levels containing two cells should be alternated from one axis to the other. An example of this using the numbering in Fig. B.19, cells at one level are mounted on reinforcing bars 1 and 3; at the next level they are mounted on bars 2 and 4.

11. After all Mustran Cells have been mounted and the cable taped up, the loose ends of the cable should be connected to the manifold.

12. Hose clamps that are clamping the Mustran cell to the reinforcing cage should be checked to make sure they are tight.

13. Hose clamps that are clamping the radiator hose on the Mustran cell should be tightened as much as possible. Caution: if tightened too much, the hose clamp will break.

14. Pressurize the manifold to 20 psi.

15. Take a soap solution and check manifold connections and the Mustran cells for leaks.

16. If any Swagelok fittings leak at the connection between the top and bottom of a Swagelok fitting and tightening the top does not eliminate it, carefully loosen the top part and put some silicone rubber sealant around the ferrules. Then tighten the fitting back together. Do not, under any circumstances, loosen the bottom part of the Swagelok fitting that is attached to the Mustran cell top cap.

17. Silicone rubber sealant should be put around the end of the tygon tubing that is on the outside of the manifold. This will prevent the tygon tubing from being blown out when the pressure is turned up.

18. A final measurement of the position of the Mustran cells should be made, measuring from the top of the reinforcement cage.

19. Before the reinforcement cage is placed in the excavation, the pressure should be turned up to the "final" pressure and checked for leaks. ("Final" pressure is approximately equal to depth of excavation. Example: excavation is 60 ft; "final" pressure equals 60 psi. "Final" pressure should never be lower than 20 psi.)

20. The manifold should be attached to the reinforcement cage approximately 15 feet from the top of the cage so that the cables are hanging fairly straight. The pressure should be at the "final" pressure.

21. As the reinforcing cage is being lowered into the excavation, the lowering of the cage should stop when the manifold is in a position that it can be removed from the cage.

22. Once the manifold is removed, the cage is lowered the rest of the way into the excavation. The manifold should be walked out away from the excavation as the cage is lowered.

23. This step is applicable only if there is a casing to be removed. The cables and the manifold should be put inside the reinforcement cage and the manifold attached to the cage when the concrete is within approximately two feet of the surface or when the contractor decides to pull the casing. After the casing is pulled, the manifold should be removed and cleaned.

24. After the concreting has been completed, a measurement from the ground surface to the top of the reinforcement cage should be made.

25. The "final" pressure should be kept on the system for at least four days. After this the pressure may be set at one-half the "final" pressure, but not less than 20 psi, of the test.

APPENDIX C

TYPES OF INTERNAL INSTRUMENTATION FOR USE
IN DRILLED SHAFTS FOR MEASUREMENT OF
AXIAL LOADS AS A FUNCTION OF DEPTH

APPENDIX C. TYPES OF INTERNAL INSTRUMENTATION FOR USE
IN DRILLED SHAFTS FOR MEASUREMENT OF
AXIAL LOADS AS A FUNCTION OF DEPTH

The making of Mustran cells and their use are described in some detail in this report for the purpose of making information available to any potential uses. The cells are not patented and may be constructed and used by anyone. However, there are other types of instrumentation that can be used successfully. Several of these were discussed in detail by Barker and Reese (1969) and only a brief presentation is made here.

Telltales. A telltale is a bar that is placed in a tube that is cast in the shaft. When a load is applied, the tube will strain but the bar, if installed properly, will not change in length. Thus, with the bar as a reference, an ordinary dial gauge can be used to obtain the shortening in a shaft from the top of the shaft to the bottom of the bar. If several telltales are installed in a test shaft, the downward movement of various points along the shaft can be obtained almost directly. Differentiation of the deformation curve will yield the strain in the shaft. The internal load can then be obtained if the axial stiffness of the shaft is known.

Weldable Strain Gauges. A strain gauge is manufactured by Micro-Measurements, P. O. Box 27777, Dept. TR, Raleigh, North Carolina 27611, that can be fastened directly to a rebar by use of a special welding tool. The gauges are made in the factory with a protective copper tube over the lead wires from the gauge to the end of the wire. Thus, each gauge is waterproofed. The gauge can be read with an ordinary strain indicator.

Bar Strain Gauge. A device is manufactured by Jido Seigyo Giken Co., Ltd., 5-10-14, Kamiidedai, Ohta-ku, Tokyo 145, Japan, that employs a linear variable differential transformer in a strain gauge that will replace a section of a rebar. The rebar is cut, the special gauge about 17.5 in. in length is welded into place, and lead wires are brought to the top of the drilled shaft.

Removable Extensometer. The Laboratoire Central des Ponts et Chaussees, Paris, has developed a special extensometer that can be placed in a drilled shaft and removed after the load test is completed. One or more pipes, approximately 2 in. in inside diameter, are cast from top to bottom of the shaft. After the concrete has set and before the test is started, the extensometer is lowered into the pipe. The extensometer consists of a series of "blockers" that are connected by thin metal tapes on which strain gauges are attached. The blockers can be activated with compressed air so that they expand and engage the inside of the pipe. The lower blocker is expanded, the system is loaded at the ground surface so that the metal tapes are prestressed to an acceptable degree, and then the other blockers are expanded. As a load is applied to the top of the shaft, the prestress in the tape is reduced and the strain from point to point along the shaft is obtained.

Other Devices. A number of other devices or systems can be employed. Two of these devices are used in Europe and have not been marketed in the U.S. to any extent; they are the vibrating wire strain gauge and the Gloetzl cell. Each of these devices can be embedded in concrete and used to obtain the distribution of load.

Some investigators have used load cells to extend across the entire cross section of the shaft. The cells are expensive, time-consuming to install, and

construction difficulties can result. Also, a rebar cage cannot be employed with such load cells.

APPENDIX D

CONSTRUCTION SITUATIONS WHERE CASING
WOULD BE DIFFICULT TO REMOVE

APPENDIX D. CONSTRUCTION SITUATIONS WHERE CASING
WOULD BE DIFFICULT TO REMOVE

There are a large number of circumstances in the construction of drilled shafts that would lead to the sticking of a casing (personal communication from Mr. Glyen Farmer). Short descriptions of some of these instances are given in the following paragraphs.

The most common situation is where the casing has to be seated into a strong formation. Some bedrock where casing would be used will have a high compressive strength, perhaps more than 1000 psi. The bond on the outside of the casing can in turn be high, leading to a large tensile force that would be needed to withdraw the casing. The contractor should make some trials during the initial phases of construction so that the casing is seated no more than necessary.

Another undesirable situation occurs when a hole is drilled through sand or other cohesionless soil and when an obstruction is encountered in the drilling that causes the auger to be displaced. Thus, the drilled hole will not be plumb and straight. When the casing is installed it will bear against the side of the excavation. The pulling resistance will, of course, be increased over that of normal construction.

As noted in Chapter 1, in most instances the excavation is usually made with drilling fluid prior to placing a casing. After the placing and seating of the casing, the slurry is removed from inside the casing so that the excavation can be advanced in the dry to the design depth. If a seal has not been made properly, the drilling fluid in the annular space behind the casing

will flow into the excavation, allowing the soil behind the casing to collapse. Thus, the pulling resistance will be increased.

The last problem to be mentioned relates to improperly designed concrete. If there is a pour requiring a large volume of concrete, if the haul from the mix plant is long, if the weather and concrete materials are hot, the concrete can partially harden during the pouring operation. In such a case the pulling resistance will be increased by the extra frictional resistance of the concrete inside the casing. This problem can be solved by the proper design of a concrete mix and by good inspection procedures.

Leaving casing in place can be avoided in many cases if the contractor has a service crane of sufficient capacity on the job. Some contractors have available service cranes of only 40-ton capacity and others have cranes of 100-ton capacity or larger. Obviously, the larger crane is more effective in pulling the casing.

However, if there is great difficulty at a given site in removing the casing even when good construction procedures are employed, consideration should be given to the use of the slurry displacement method of construction.

REFERENCES

1. American Petroleum Institute, API Recommended Practice for Planning, Designing, and Constructing Fixed Offshore Platforms, American Petroleum Institute, January 1980.
2. Arias, Robert P., "Evaluation of Drilled Shaft Integrity by Non-Destructive Methods," Master's thesis, University of Texas at Austin, Civil Engineering, December 1977.
3. Barker, W. R., and L. C. Reese, "Instrumentation for Measurement of Axial Load in Drilled Shafts," Research Report 89-6, Center for Highway Research, The University of Austin, November 1969.
4. Barker, W. R., and L. C. Reese, "Load-Carrying Characteristics of Drilled Shafts Constructed with the Aid of Drilling Fluids," Research Report 89-9, Center for Highway Research, The University of Texas at Austin, August 1970.
5. Coyle, Harry M., and Reno R. Castello, "New Design Correlations for Piles in Sand," Journal of the Geotechnical Engineering Division, ASCE, Vol. 107, No. GT7, July 1981.
6. Engeling, Don, and L. C. Reese, "Behavior of Three Instrumented Drilled Shafts under Short-Term Axial Loading," Research Report 176-3, Center for Highway Research, The University of Texas at Austin, 1974.
7. Fuller, F. M., and H. E. Hoy, "Pile Load Tests Including Quick-Load Tests Methods, Conventional Methods, and Interpretation," Highway Research Record Number 333, Pile Foundations, Washington, D.C., 1970, pp. 74-86.
8. Meyerhof, G. G., "Bearing Capacity and Settlement of Pile Foundations," Journal of the Geotechnical Engineering Division, ASCE, Vol. 102, No. GT3, March 1976.
9. O'Neill, Michael W., and L. C. Reese, "Load Transfer in a Slender Drilled Pier in Sand," ASCE Spring Convention and Exhibit, Preprint 3141, Pittsburgh, PA., 1978.
10. Quiros, Gerardo W., and L. C. Reese, "Design Procedures for Axially Loaded Drilled Shafts," Research Report 176-5F, Center for Highway Research, The University of Texas at Austin, 1977.

11. Peck, Ralph B., W. E. Hanson, and T. H. Thornburn, Foundation Engineering, second edition, John Wiley & Sons, New York, 1973.
12. Reese, Lymon C., and S. G. Wright, "Construction Procedures and Design for Axial Loading," Drilled Shaft Manual, Vol. I., U. S. Department of Transportation, Offices of Research and Development, Washington, D.C., July 1977.
13. Touma, Fadlo, and L. C. Reese, "The Behavior of Axially Loaded Drilled Shafts in Sand," Research Report 176-1, Center for Highway Research, The University of Texas at Austin, 1972.